Renewable and Sustainable Energy Reviews 92 (2018) 62–94

Contents lists available at ScienceDirect

Renewable and Sustainable Energy Reviews

journal homepage: www.elsevier.com/locate/rser

Methods of heat transfer intensification in PCM thermal storage systems: Review paper

Maher Al-Maghalseh[a,b,*], Khamid Mahkamov[b]

[a] College of Engineering, Palestine Polytechnic University, P.O. Box 198, Hebron, Palestine
[b] Faculty of Engineering and Environment, Northumbria University, Newcastle, UK

ARTICLE INFO

Keywords:
Phase change materials
Latent heat storage
Thermophysical properties
Heat transfer Intensification methods

ABSTRACT

This paper presents a comprehensive review of significant studies that are relevant to thermal energy storage technologies using phase change materials (PCMs). The review focuses on the techniques applied to enhance the performance of thermal storage systems and the methods used to analyse the heat transfer problems in PCMs. In addition, this paper reviews the published results and discussions on the heat transfer intensification methods including application of fins, filling materials, nano-fluids, nano-particles, microencapsulation and the thermal conductivity enhancement method. Furthermore, the experimental and mathematical methods to enhance the thermal conductivity of PCMs are summarised, and the methods used to determine the nanofluid dynamic viscosity in recent investigations are also listed and discussed. The focus of this review is to provide a solid basis for the identification of the optimal design for the various heat transfer applications using PCM.

1. Introduction

The rapid utilisation of fossil fuels has resulted in a considerable increase in the level of greenhouse gases. Carbon dioxide emissions amount to approximately 347 billion tons since 1751 [1]. Therefore, significant efforts are being made by scientists to reduce consumption of fossil fuels and to generate energy from natural renewable sources, such as wind, sunlight, geothermal as well as hydropower. Solar energy, given that it is abundant and freely available, is one of the most promising renewable energy resources. The International Energy Agency has estimated that solar power will produce 21% of the world's electricity by 2050 [2]. However, there are several problems associated with the utilisation of the solar energy: the intensity of the solar radiation varies with location, time of the day and the seasons and depends on the local weather conditions (clear or cloudy sky). Owing to this, it is a sensible engineering solution to store solar energy in various forms including electrochemical storage and thermal energy storage systems (TESS) [3].

Thermal energy storage systems can be classified into several main groups, namely thermochemical storage, sensible heat storage and latent heat storage, or a combination of these storage systems [4]. Thermochemical heat storage involves chemical reactions taking place in the storage vessel. In sensible storage systems, the heat is stored by increasing the temperature of a single-phase storage medium, while latent heat systems store the energy as a result of the phase transition of the materials at constant or near constant temperature. A number of research studies have highlighted that latent heat storage systems utilizing a phase change material (PCM) are perhaps the most effective heat storage technique as they provide a very high energy density during the melting and solidification processes compared to the conventional sensible heat energy storage systems. This means that a latent heat storage system using a PCM requires a much smaller volume of materials to store a certain amount of energy.

Castelln and Solé [5] provided an overview of design methodologies for liquid–solid PCM storage systems. This paper summarised and highlighted the most common methodologies for designing the PCM storage systems. They classified these methodologies in six types: (1) empirical correlations and characterizing parameters, (2) dimensional analysis and correlations, (3) effectiveness-NTU, (4) Log Mean Temperature Difference (LMTD), (5) Conduction Transfer Functions (CTF), and (6) numerical models. However, dimensionless correlations and effectiveness-NTU are the most common and straight-forward methods and the ones that offer more possibilities for general solutions in the design methodology. A considerable amount of literature relating to the heat transfer enhancement of PCMs for thermal energy storage applications was reviewed by Ibrahim et al. [6]. This article comprehensively reviewed the recent development of several techniques for enhancing the heat transfer in the latent heat thermal storage systems. The most important finding of this study is that the extended surfaces such as fins and heat pipe are mainly used to increase the heat transfer

* Corresponding author at: College of Engineering, Palestine Polytechnic University, P.O. Box 198, Hebron, Palestine.
E-mail address: maherm@ppu.edu (M. Al-Maghalseh).

https://doi.org/10.1016/j.rser.2018.04.064
Received 16 September 2016; Received in revised form 26 March 2018; Accepted 14 April 2018
1364-0321/

area, while high conductive materials/particles are used to increase the thermal conductivity of the PCM.

A considerable amount of literature has been reviewed by Khan et al.[7] about PCMs in solar absorption refrigeration systems. This paper provides an overview of PCMs and their enhancement methods for absorption refrigeration system. Also, this article comprehensively reviews latent heat thermal storage system, suitable materials selection for the storage system, PCM enhancement techniques used in the thermal storage system, and cost analysis of the storage systems. Further, it highly describes the design approaches for thermal storage systems, challenges faced and solutions in the design, heat propagation, PCM behaviour and effect on the system. Concluding remarks on improving the system output by selecting materials according to the material heat balance, dissipation, and operating temperature. Recent work by Safari et al. [8] has reviewed the supercooling of Phase Change Materials in thermal energy storage systems. The paper discusses in details the design techniques of supercooled heat storage systems, the thermal energy storage of supercooled liquids, degree and measurement of supercooling, factors that influence the degree of supercooling and their effect on output capacity. Applications including solar thermal storage was discussed in details.

A considerable amount of literature has been reviewed by Cunha and Eames [9] for the PCM thermal storage system with the melting temperature range between 0 and 250 °C. The results of this study indicate that the organic compounds and salt hydrates are the most interesting PCM materials for the applications with the temperature range below 100 °C. Eutectic mixture with Urea seems useful for the applications around 100 °C, and eutectic mixture of inorganic salt hydrates is the most attractive for the temperature range between 130 and 1250 °C. A mixture of sodium and potassium appear to be promising for the application with temperature range around 170 °C. The study also assessed the design of latent heat storage systems, heat transfer enhancement methods, and the potential applications of the systems. In their review of heat transfer techniques in PCM thermal storage systems, Tay et al. [10] compared between the traditional methods of non-transportable PCMs, focusing on the disadvantages of these techniques. The study also presented three methods of transportable PCM systems. These are: PCM slurries (PCS), direct-contact PCM systems and dynamic PCM systems. This review paper presents the different heat transfer enhancement techniques reported in the literature. It also summarises the research conducted on phase change storage systems where the PCM is moved in the storage system.

Zhou et al. [11] presented a critical review of thermal storage systems using PCMs. The paper analysed in details the selecting of PCM and its heat transfer characteristic, the optimization methods of heat transfer during the charging process, and the design method of heat transfer systems. Moreover, an experimental and numerical study was carried out to evaluate the effectiveness of $NH_4Al(SO_4)_2{\cdot}12H_2O$ as a new inorganic phase change material (PCM) in the solar thermal storage systems. The most obvious finding to emerge from this study is that the system employed with new PCM was more effective in low-density residential buildings. Muhammad [12] presented a review on the heat transfer enhancement method for parabolic trough solar plants thermal storage systems. The study was conducted in order to evaluate and find the commercially available PCM and the best way for intensifying the heat transfer in the system. He found that three commercially - available PCMs are suitable in the operating temperature range of parabolic trough plants. These are $NaNO_3$, KNO_3/KCL, and KNO_3. Also, he confirmed that aluminium fins are the most promising in the temperature range of 250–330 °C.

Furthermore, a detailed review of energy storage systems using PCMs was carried out in [13–16].

The main objective of this study is to review existing methodologies, experiments and numerical models for the enhancement of heat transfer in thermal storage systems utilizing PCMs. This review will provide a solid basis for the identification of the optimal design for the various heat transfer applications utilizing PCMs. The literature survey is constructed according to the thermal storage systems geometry (spherical, rectangular, and cylindrical) and configurations (encapsulation, backed bed, and shell-and-tube). Furthermore, the reviewed studies were classified according to the research method (experimental, numerical models or both), type of the PCM used, melting temperature range, heat transfer fluid type, PCM processes (charging or discharging), dimensions of the storage system, and heat transfer parameters. Finally, heat transfer intensification methods are discussed, including the use of fins, fins materials and geometry, filling materials, nano-fluid, nano-particles, microencapsulation and thermal conductivity enhancement.

This paper presents results of the literature review on thermal energy storage technologies as well as the latent heat thermal energy storage (LHTES) using PCMs. The paper discusses the outcomes of previous studies on the design and configuration of thermal storage systems, methods of heat transfer intensification, and the experimental testing and mathematical simulation of systems with PCMs.

2. Encapsulated and packed bed thermal storage systems

Recent developments in the field of thermal energy storage systems using PCMs have led to renewed interest in encapsulated thermal storage systems (ETSS) and packed bed storage systems. Such systems have the advantage of a higher storage density with higher efficiency, and a large number of published papers describe relevant performance analyses. In these works, the following aspects were investigated: storage systems designs and their configurations, the PCM materials used, the heat transfer enhancement methods deployed and the flow and heat transfer processes during both the charging and discharging processes. A number of the published articles describing the heat transfer in thermal storage systems using PCM capsules have been summarised by Regin in [17]. A large pool of published literature was also discussed in an extensive review of the research carried out on packed bed thermal storage systems. A recently published article by Gracia and Cabeza [18] offered probably the most comprehensive revision of the several numerical models of PCM packed bed systems. The paper discussed in details the characteristics, parameters, correlations and limitations of the different methodologies. The main findings for the presented modules were evaluated and highlighted. The study by Jacob and Bruno [19] offered a comprehensive review about the shell materials used in the encapsulation of PCM for high temperature thermal storage system application. The study identified several materials that have potential to encapsulate high temperature PCMs. These materials include: steel (carbon and stainless), nickel (and nickel alloy), sodium silicate, silicon dioxide, calcium carbonate and titanium dioxide. Abokersh et al. [20] conducted a review study on the solar domestic water heating system using PCM. The study discussed in details the heat transfer characterises of domestic solar heating systems, the heat transfer enhancement methods and applications.

Another study by Miliána et al. [21] reviewed the encapsulation methods for phase change materials for thermal storage system. They mainly focused on inorganic phase change material and the effect of their thermophysical properties. A detailed review of the types of encapsulated inorganic PCMs, classification of encapsulation methods, improvement of thermal conductivity methods, and properties of the encapsulated materials have been performed. Concluding summaries on the basis of the approach to the use of encapsulation inorganic PCM in solar thermal storage systems have been made. Regin et al. developed a numerical model to analyse and predict the thermal performance of packed bed cylindrical latent heat thermal storage systems [22]. The storage container was filled with spherical capsules filled with paraffin wax. These were in the flow of the heat transfer fluid. Fig. 1 presents the layout of this system.

The inlet temperature of the heat transfer fluid, the phase change temperature range and capsule sizes were discussed by the authors. The results of the study show that the solidification time was longer than the

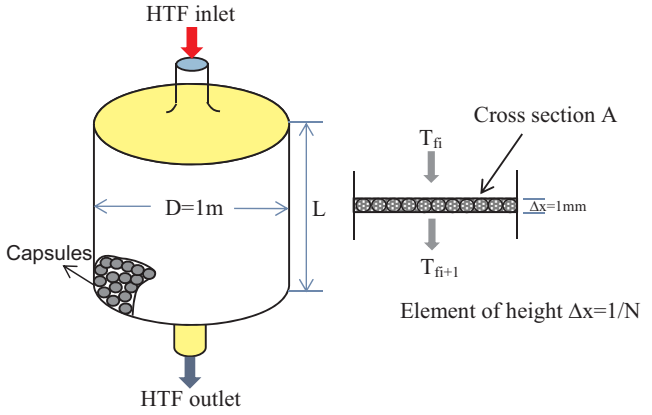

Fig. 1. Layout of the storage system [22].

duration of the melting process. This was due to the very low value of the heat transfer coefficient during the solidification process because of the high thermal resistance of the solidified layer, which formed on the inner wall of the capsule. With the increase in the inlet heat transfer fluid temperature, the time to reach the melting point and the charging time were reduced. Similarly, for higher mass flow rates of the heat transfer fluid, the time interval needed to complete the charging process was shorter. The second major finding was that the capsule size had a significant effect on the charging and discharging processes. Smaller capsules provided higher storage rates, and a shorter time was needed to reach the melting point. These findings were consistent with those of Zeinab et al. [23], who numerically investigated the thermal performance of a cylindrical packed bed thermal storage unit filled with PCMs in spherical capsules.

Cho and Choi [24] experimentally investigated the thermal characteristics of storage systems with paraffin in spherical capsules during the freezing and melting processes. The influence of two factors were investigated; namely, the Reynolds number and the inlet temperature. The temperature distribution in the storage tank and inside the spherical capsules was measured during both processes. It was found that the temperature on the capsule surface was lower than that inside the capsule during the freezing and melting processes due to the difference between the heat removal rate and the solidification heat release rate. Moreover, the phase-change period during the freezing and melting processes decreased as the Reynolds number increased, even with a reduced inlet temperature. Another significant finding was that the phase-change period for the capsule in the first layer was shorter than that for the capsule in the seventh layer, and the phase-change period in the centre of the capsule was longer than that in the capsule edge. The reason for this is that the porosity at the edge of the tank is greater than that at the centre. Bedecarrats et al. [25,26] also experimentally investigated the thermal behaviour of the system with spherical PCM capsules randomly filling up a cylindrical storage tank. The obtained results were used to explain the temperature distribution and the duration of solidification and melting processes in spherical capsules.

The thermal characteristics of a packed bed thermal storage system with spherical capsules were also investigated numerically and experimentally by Ismail and Henríquez [27]. This study concentrated on the effect of the working fluid entry temperature and its mass flow rate as well as the capsule temperature during both the charging and discharging processes. Moreover, capsules made of different materials were also investigated, and the numerical results corroborated the findings of the experimental work. Singh et al. [28–31] developed a mathematical model to predict the thermal performance of packed bed storage systems using a computer code written in the C++ language. Different shapes and sizes of thermal storage systems were studied, and the computational model predicted the temperature distribution, thermal energy stored in the unit and the energy consumption. Wang et al. [32] conducted an experimental study of the charging process in cylindrical heat storage capsules filled with multiple PCMs. Two cylindrical capsules made of three coaxial red copper tubes were horizontally immersed in the water tank. One of these was filled with three different PCMs: stearic acid, sliced paraffin and lauric acid. The other tube was filled with sliced paraffin only. The experiment results showed a significant enhancement of the charging process using the multiple PCM (MPCM) capsule compared to that using a single PCM (SPCM). Moreover, the complete melting time in the MPCM capsule was significantly decreased, namely by 37–42%. In addition, the melting process time in the MPCM capsules was shorter by 15–25% in the charging process.

The isothermal phase change of a PCM encapsulated in a storage tank was analysed mathematically and experimentally by Zivkovic and Fujii [33]. A computational model was developed using the enthalpy method to simulate the transient performance of the isothermal phase change process. The reason for this was that such a method did not require an explicit treatment of the boundary conditions in the phase change system. Both cylindrical and rectangular containers were investigated. The volumes of the containers as well as the convective heat transfer area for both types were selected to be equal. It was demonstrated that the melting time increased gradually with the increasing volume of both types of containers. However, the melting time of the rectangular container was much shorter compared to that of the cylindrical container with the same volume and heat transfer area. The use of a rectangular container for the encapsulation of PCMs was subsequently recommended.

Tan et al. [34] experimentally investigated the buoyancy and natural convection phenomena during the melting process of a PCM inside a spherical capsule. These results were validated with a numerical solution obtained using the CFD software FLUENT. The most interesting finding was that the conductive heat transfer dominated during the early stage, whereas, the buoyancy-driven convection became more prominent as the liquid fraction volume increased. However, the molten PCM ascended upwards to the upper regions of the sphere due to the natural convection. Consequently, the upper regions of the sphere melted first, followed by the other regions. Another interesting finding from the computational results was that the temperature distribution fluctuated chaotically at some points inside the sphere, due to the existence of the unstable fluid layer at these points. The findings of this study supported observations in a previous research by the same author [35,36].

Koizumi [37] experimentally examined the heat transfer on an isothermally heated sphere placed in a uniform, downwardly directed flow using a micro-foil heat sensor (HFS). This study dealt with the opposing flow mixed convection, where the direction of the free flow was opposite to that of the forced flow. Two situations were analysed and discussed. In the first case, isothermal spheres were used, made of 3 mm thick copper with an outer diameter of 50 mm, while in the second case, solid PCM capsules were used, which were made of 1 mm thick glass with an outer diameter of 50 mm. The spherical capsules were filled with *n-Octadecane* as a PCM. Fig. 2 depicts schematics of these two cases.

In this study, three types of air flow patterns with a Grashof number (Gr) of 3.3×10^5 were investigated. These were chaotic flow at Reynolds number (Re) < 240, two-dimensional steady separated flow at $240 \leq Re \geq 500$ and three-dimensional unsteady separated flow at $Re > 500$. The time average local Nusselt number (Nu) was obtained using the following formula:

$$\overline{Nu} = \frac{hd}{k} = \frac{qd}{(T_w - T_f)k} \quad (1)$$

The measurements of the Nusselt number for the three types of patterns are illustrated in Fig. 3. The dashed line shows the experimental results for the pure forced convection found by Yuge [38].

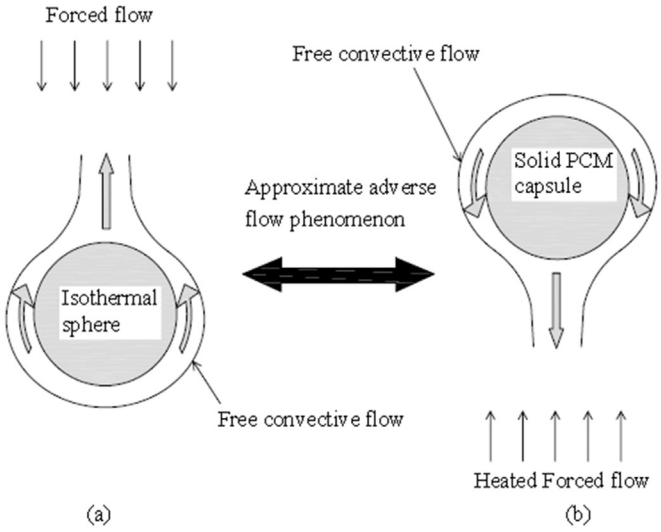

Fig. 2. Schematic drawing of the opposing flow mixed convection. (a) Isothermal sphere and (b) solid PCM capsule [37].

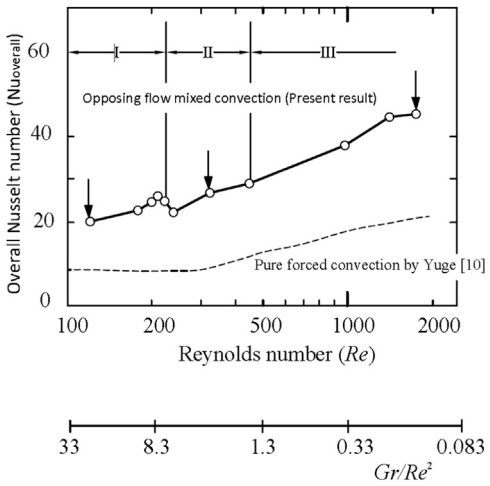

Fig. 3. Nusselt Number vs Reynolds number [37].

The experimental results show that, in the case of the chaotic flow at $Re < 240$, the Nusselt number around the sphere is 10% higher than that for the pure forced convection, while it is greater by factor of two in the case of $Re \geq 500$. Moreover, the results were validated using the numerical results of Jia and Gogos [39], and a very good agreement between the numerical and experimental results were obtained. Additionally, the experiments investigated the influence of copper plates inserted inside the solid PCM capsule. The study found a significant improvement in the latent heat storage rate by the solid PCM when the copper plate was inserted inside the spherical capsule.

A study in [40] addressed the transient thermal response of a packed bed of spheres containing a PCM. The authors presented a computational model which analysed both isothermal and non-isothermal melting behaviour, axial thermal dispersion effects and intraparticle conditions (Biot number) effects. In order to validate the results, an experiment was conducted on a cylindrical bed filled with high-density polypropylene spheres. Data from the computational model was compared with the experimental results. The results showed good agreement for the temperature distribution and energy stored in the system. On the other hand, the study provided an opportunity to explain the heat transfer, isothermal melting and phase trajectory melting processes under a variety of conditions, such as a varying Reynolds number. Khalil et al. [41] experimentally investigated the thermal performance of a packed bed thermal storage system containing spheres of different sizes. The study examined the effect of the Reynolds number and particle size on the heat transfer in the system. The results indicated that the heat transfer improved significantly when porous media were used and when the flow Reynolds number was increased. Correlations were proposed between the Nusselt and Reynolds numbers for the cases with and without the porous material. The Nusselt number in the case of using the porous material was:

$$Nu_D = 17.30\left(\frac{D}{d}\right)^{-0.77} Re_D{}^{0.235}\left(\frac{D}{d}\right)^{0.3} \quad (2)$$

For $2167 \leq Re_D \leq 19400$ and $3.54 \leq D/d \leq 14.16$.

The Nusselt number as a function of the Reynolds number for the case without the porous material was

$$Nu_D = 0.042\, Re_D{}^{0.76} \quad (3)$$

For $2778 \leq Re_D \leq 19400$ and $1.5 \leq P_r \leq 3.4$.

Nsofor and Adebiyi [42] also experimentally investigated the heat transfer and natural convection phenomena in a packed bed thermal storage system at high temperature conditions. Heat transfer correlations were proposed by expressing the Nusselt number as a function of the Prandtl and Reynolds numbers and comparisons were carried out with the existing correlations derived previously for similar storage media.

The heat transfer and pressure drop characteristics of a backed bed thermal storage system were experimentally investigated by Varun et al. [43]. The storage tank was filled with large cylindrical elements with various horizontal and vertical orientations. Significant correlations were derived to calculate the Nusselt number and friction factor as a function of the Reynolds number. Therefore, these correlations could be accurately used in predicting the performance of solar thermal energy storage systems in the form of large cylindrical elements.

The efficiency of the effective thermal conductivity of latent heat storage capsules was evaluated numerically by Shiina and Inagaki [44]. The uniform and non-uniform heat transfer around the cylindrical surface was observed. In this study, water, octadecane, Li_2CO_3 and NaCL were selected as PCMs, and copper, aluminium and carbon steel were used as the porous media. The PCM injected inside the capsule had the following dimensions: an outer diameter of 6.6 mm, an inner diameter of 6 mm and a thickness of 0.3 mm. Acrylic resin and copper were used as the capsule walls. Moreover, air, helium and water were used as the heat transfer fluid HTF. Fig. 4 shows the results obtained for the melting time as a function of the effective thermal conductivity of two composite PCMs of octadecane and Li_2CO_3 at $Re = 7500$ and with helium as HTF.

It can be seen that the melting time is reduced when the effective thermal conductivity is increased. Furthermore, the melting time of the PCM in the case of the acrylic wall is much longer compared to that of the copper wall. It can be seen that, unlike the PCM with the high thermal conductivity, the influence of the effective thermal conductivity on the melting time is greater for the PCM with the low thermal conductivity.

Hawlader et al. [45] conducted a numerical and experimental study of the thermal energy storage involving an encapsulated PCM. The study investigated the effect of the encapsulation ratio, hydrophilicity, and energy storage on the thermal performance of PCM capsules. It was concluded that using the PCM capsule increases both the thermal energy charging and discharging capacity. In addition, the capsule maintained its original geometrical profile and the energy storage capacity after 1000 thermal cycles.

Large volumes of published papers describe the role of heat transfer and phase change processes in packed bed thermal storage systems. Further published results about the packed bed thermal storage systems are summarised in Table 1. The papers were classified according to thermal storage system geometry and dimension, methods of investigation, PCM materials, HTF type, charging or discharging

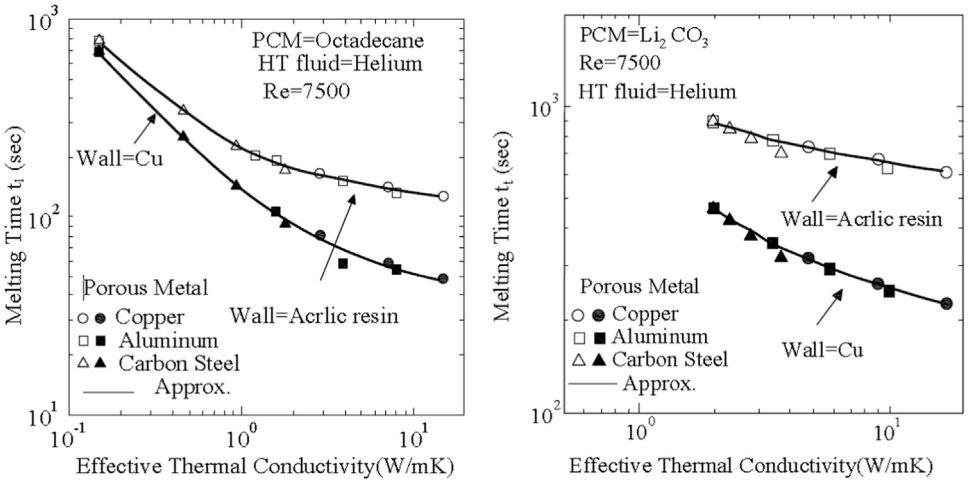

Fig. 4. Melting time for composite PCMs of octadecane and Li_2CO_3 [44].

processes, and parameters range.

3. Cylindrical PCM container storage systems

Cylindrical PCM containers have been classified in three types [15]. In the first type, the PCM fills the shell and the HTF flows through a single tube (Fig. 5a); this is called the pipe model. In the second type, the PCM fills the tube and the HTF flows parallel to the tube (Fig. 5b); this is called the cylinder model. The third type is called the shell and tube model (Fig. 5c). This contains several parallel tubes, and the HTF flows through the tubes while the PCM fills the space around them.

3.1. Pipe model

Jian et al. [66] developed a numerical model to predict the transient thermal behaviour during the charging and discharging processes of a latent thermal storage unit involving a triplex concentric tube with the PCM filling the middle channel. Mellouli et al. [67] numerically investigated the effect of heat transfer enhancement and heat storage performance in a metal hydrid-phase change material tank. In addition, the effect of HTF fluid type and mass flow rate on the storage performance was discussed and evaluated. A simple numerical method, called the temperature and thermal resistance iterations, was used in the numerical calculation. The data from the numerical model was then compared with the experimental results and a good agreement was observed. Ho and Chen [68] also developed a numerical model for the melting of ice around a horizontal isothermal cylinder. The model's results were compared with experimental data published by White in [69], and a good agreement was found. It was concluded that the melting process of ice is strongly affected by the changing recirculation occurring in the molten water. Another numerical model of melting around a horizontal pipe was developed by Rieger et al. [70]. The numerical solution was obtained for Rayleigh numbers (Ra) up to1.5×10^5, Stefan numbers in the range of ($0.005 \leq Ste \leq 0.08$) and for ($Pr = 50$). It was found that the natural convection is the dominant process in the heat transfer mechanism throughout almost the entire melting process.

Dimaano and Watanabe [71] studied the charging and discharging processes of a latent heat storage system with a capric and lauric acid mixture with a melting point of 18–19.5 °C. A vertical cylindrical storage unit involving a copper tube filled with the PCM was employed in the study. The temperature distribution in both radial and axial directions was experimentally measured, as was the heat stored during the charging and released during the discharging process. Bareiss and Beer [72] carried out an experimental and mathematical investigation of a horizontal cylindrical tube filled with PCMs. A photographic technique was used to evaluate the melting and solidification fraction. Furthermore, both $C_{18}H_{38}$ *n-Octadecane* and C_9H_{10} p-xylene were used as PCM. The numerical and experimental results were compared and an excellent agreement between them was observed. However, the validity of the analytical model was limited to the following conditions:

$$Ste\ \rho^* \frac{Ra}{\mathrm{Pr}\ Ar} < 1.4 \tag{4}$$

Ismail and Abugderah [73] developed a fixed grid one-dimensional numerical model using the control volume finite difference method. The model predicts the transient behaviour of the thermal storage system of a vertical tube type. The influence of several parameters were investigated, including the Reynolds and Stefan numbers, phase change temperature range, system length, outer radius and time periods. It was noted that both Reynolds and Stefan numbers had a significant effect on the system performance whereas there was no considerable influence of the phase change temperature range. Another interesting finding was that the tube's outer radius and system length both noticeably affected the system performance. Al-Maghalseh [74] conducted a numerical study to study the effect of natural convection heat transfer in latent heat thermal storage systems. Four different dimensional models were simulated using Fluent/ANSYS for rectangular storage system with a horizontal HTF pipe. The results show that the natural convection has a significant effect on the temperature distribution inside the storage system as well as the total melting time of the PCM.

Sari and Kaygusuz [75] experimentally evaluated the thermal behaviour of a eutectic mixture of lauric and stearic acid as a PCM in a system with two vertical concentric pipes. The key experimental parameters were the Reynolds and Stefan numbers. It was demonstrated that these two parameters had more effect on the total PCM melting time than on the total solidification time. This is due to the convection phenomena occurring during the melting process which improved the melting rate, whilst the thermal resistance during the solidification process decreased the solidification rate. On the other hand, the Reynolds number had more effect on the heat transfer coefficient during the melting process than solidification, whilst the Stefan number had more effect on the solidification than melting.

The same authors then conducted a series of experimental studies on a latent heat storage system involving a vertical double pipe [76–80]. The phase change stability and the thermal characteristics of several PCMs during the solidification and melting processes were investigated. Stearic, palmitic, lauric, myristic and fatty acids were used as PCMs in the storage system and the influence of the transition time, temperature range, expansion of the solid-liquid interface and heat flow rate on the phase change stability were investigated. It was found that stearic, palmitic and myristic acids are all suitable for domestic solar water

Table 1
Heat transfer and phase change process studies in packed bed thermal storage systems.

No	Author	Geometry	Methods	PCM	HTF	Process	Parameters range	Dimensions
1.	Regin et al. [22]	Cylindrical storage/ spherical capsule	Numerical Modelling	Paraffin wax	Water	Charging and discharging	Charging: $T_i = 50°C$, $70 < T_{HTF} < 82°C$, $0.0398 < \dot{m}_f < 0.1592 Kg/s$. Discharging: $T_i = 70°C$, $50 < T_{HTF} < 35°C$, $0.0398 < \dot{m}_f < 0.1592 Kg/s$.	Tank: D = 1 m, L = 1.5 m, Sphere, D = 1 mm.
2.	Cho and Choi [24]	Acryl storage/ spherical capsule	Experimental	*n*-tetradecan ($C_{14}H_{30}$) n-hexadecane ($C_{16}H_{34}$)	Water	Charging and discharging	Re = 8,12 and 16. Charging, $T_{init} = -7, -4$and $-1°C$, $T_{inlet} = 10°C$. Discharging, $T_{init} = 10°C$, $T_{inlet} = -7, -4$and $-1°C$	Tank: D_i = 220 mm, thickness = 10 mm, H = 173 mm
3.	Chen [46,47]	Cylindrical storage/ spherical capsule	Experimental and numerical	Water/ice	Alcohol	Charging process	$2 < \dot{m}_f < 5 Ipm$, $-20 < T_i < -10°C$	Capsule: D = 34 mm, porosity $0.365 < \varepsilon < 0.61$
4.	Silva et al. [48]	Rectangular	Experimental and numerical	Paraffin wax	Air	Charging and discharging	$\dot{m}_f$:0.005488 kg/s , $T_{HTF} = 19.3°C$, heat flux (q):480 W/m^2	Tank: H = 813 mm, L = 623 mm
5.	Zeinab et al. [23]	Cylindrical storage/ spherical capsule	Numerical Modelling	Paraffin wax	Water	Charging and discharging	Charging, $T_{init} = 50°C$, $70 < T_{HTF} < 82°C$, $0.0398 < \dot{m}_f < 0.16 Kg/s$. Discharging, $T_{ini} = 70°C$, $50 < T_{HTF} < 35°C$, $0.0398 < \dot{m}_f < 0.16 Kg/s$.	The porosity of the bed is 0.4
6.	Bedecarrats et al. [25,26]	Cylindrical storage/ spherical capsule	Experimental	Water/ice	Chilling fluid	Charging and discharging	Charging, $T_{HTF} = -6°C$, Flow rate = 1.3 m^3/h. Discharging, $T_{HTF} = 5°C$, Flow rate = 1.1 m^3/h	Tank: D = 0.95 m, H = 1.42 m. Sphere: D_o = 77 mm, thickness = 2 mm
7.	Bilir and İlken [49]	Cylindrical spherical storage	Numerical Modelling	Water/ice	–	Discharging process	$0.01 < Ste < 0.5$, $1 < Bi < 50$.	
8.	Ismail and Henríquez [27]	Cylindrical/spherical capsule	Experimental and numerical	Water/ice	Ethylene glycol	Charging and discharging	$T_{initial} = 20°C$. $0.5 < \dot{m}_f < 1.5 m^3/h$, $-15 < T_{inlet} < -3°C$,	Tank: D = 0.92 m, L = 1.54 m.
9.	Ismail and Henríquez [50]	spherical capsule	Numerical Modelling	Water/ice	Ethanol	Discharging process	$0.01 < Ste < 0.5$, $1 < Bi < 100$, $-25 < T_{HTF} < -5°C$, $5 < T_{init} < 35°C$,	Capsules: D = 20, 40, 100, 140, 200, 300 and 400 mm. thickness = 0.1 m
10.	Ismail [51]	Cylindrical storage/ spherical	Numerical Modelling	Stone/ steel	Water/air	Charging and discharging	$0.5 < \dot{m}_f < 1 kg/s$, $0.3 < \varepsilon < 0.5$,	particle D = 25–50 mm,
11.	Singh et al. [28–30]	Cylindrical	Numerical	–	Air	System performance	$T_{inlet} = 40°C$.	Tank: D = 0.95 m, H = 6 m.
12.	Farid and Husian [52]	Cylindrical	Experimental and numerical	Paraffin wax	Air	Charging and discharging	$0.007 < \dot{m}_f < 0.014 Kg/h$, $28 < T_{init} < 70°C$, $T_{HTF} = 75°C$	Tank: (D = 31.8 mm, L = 335 mm)
13.	Kousksou et al. [53]	Cylindrical/spherical capsule	Experimental and numerical	Water/ice	Chilled glycol	Charging process	$T_i = 6°C$, $-8 < T_{HTF} < -3.5°C$, $1 < \dot{m}_f < 2.5 m^3/h$.	Tank: D = 0.95 m, L = 1.42 m. Sphere: D = 77 mm,
14.	Wang et al. [32]	Cylindrical/ spherical capsule	Experimental	Stearic acid/ sliced paraffin/ lauric acid	Water	Charging process	$T_{inlet} = 70 - 72.5°C$, $\dot{m} = 1.5 m^3/h$	Tank volume 200 l
15.	Eames et al.[54]	Spherical	Experimental	Water/ice	Chilled water	Charging and discharging	$-9.5 < T_{HTF} < -4.4°C$, $\dot{m}_f = 0.1 m/s$.	Spheres: D = 8.14, 7.00 and 6.27 cm
17.	Zivkovic and Fujii [33]	Cylindrical and rectangular/spherical capsule	Experimental and numerical	calcium chloride hexahydrate	Air	Charging process	$T_{inlet} = 60°C$, $T_{initial} = 15$ °C, Heat transfer (q) = 16 W/m^{2}K	Tank L = 100 mm, W = 100 mm, H = 20 mm.
18.	Hirata et al. [55]	Rectangular capsule	Experimental and numerical	Octadecane/ ice	–	Discharging process	$T_{init} = (T_{melting} - 2)$ °C, $0.0287 < Ste < 0.251$	
19.	Tan et al. [34]	Spherical capsule	Experimental and numerical	Paraffin wax *n-Octadecane*	–	Charging process	$T_{subcool} = 1°C$ $T_{surface} = 40°C$	Sphere D = 101.66 mm, thickness = 1.5 mm
20.	Tan and Chan [35]	spherical capsule	Experimental	n-hexadecane	Water	Discharging process	$T_{initial} = 8$, 2and0 °C $T_{surf} = 13$, 8and3 °C	
21.	Tan [36]	Spherical capsule	Experimental	*n-Octadecane*	Water	Charging process	$T_{init} = 1$ °C, 10 °Cand20 °C $T_{surfac} = 35$ °C, 40 °Cand45 °C	Sphere D = 101.66 mm, thickness = 1.5 mm
22.	Khodadadi and Zhang [56]	Spherical container	Numerical Modelling	Paraffin wax	–		$0.008 < Ste < 0.0533$ T_{init}ambient	Sphere $20 < D < 100 mm$
23.	Fomin and Saitoh [57]	Spherical capsule	Numerical Modelling	*n-octadecane*	–	Charging process	$0.1 < Ste < 0.5$	
24.	Koizumi [37]	Spherical capsule	Experimental	*n-Octadecane*	Air	Charging process	$T_{inlet} = 321°C$ $1500 < R_e < 1800$	Sphere D = 55 mm, thickness = 3 mm

(*continued on next page*)

Table 1 (*continued*)

No	Author	Geometry	Methods	PCM	HTF	Process	Parameters range	Dimensions
25.	Saito et al. [58]	Cylindrical capsule	Experimental and numerical	Gelled sodium sulphate decahydrate	Water	Discharging process	$5\times10^{-4} < cooling\ rate < 1.6\times10^{-3}$°C, $0.00926 < Ste < 0.0926$, $26 < T_{initial} < 34$°C	Capsule: D = 24.3 mm, L = 1220 mm.
26.	Besley and Ramanarayanan [40]	Cylindrical storage/ spherical capsule	Experimental and numerical	Paraffin wax	Air	Charging process	Re = 260	Tank: D = 20.3 cm, H = 30.5 cm. Sphere: D = 2.1 cm.
27.	Khalil et al. [41]	Cylindrical storage/ spherical capsule	Experimental	–	Water	Charging process	$2167 < R_e < 19400$	Tank: D = 42.5 mm, L = 0.5 m, thickness = 5.5 mm
28.	Yagi [59]	Spherical capsule	Experimental and numerical	AaCl, KNO_3	Nitrogen gas	Charging and discharging	$2.33\times10^{-3} < \dot{m}_f < 4.67\times10^{-3}m^3/s$, $300 < T_{HTF} < 900$°C,	Sphere: D = 40 mm.
29.	Nsofor and Akiyama [42]	Cylindrical storage and spherical capsule	Experimental	–	Gas	Charging process	T = 400 °Cto1000°C $100 < \dot{m}_f < 610 kg/h$	Tank: D = 0.61 m, L = 0.61 m. Pellet D = 18.3 mm, L = 18.3 mm.
30.	Benmansour et al.[60]	Cylindrical storage/ spherical capsule	Experimental and numerical	Paraffin wax	Air	Charging and discharging	$T_{inlet} = 70$°C $560 < R_e < 1120$	Tank: D = 0.2 m, thickness = 1 mm, H = 0.6 m. Sphere: D = 31.8 mm.
31.	Katayama et al. [61]	Cylindrical capsule	Experimental and numerical	Naphthalene	Water	Charging and discharging		Capsule :(D = 30 mm, L = 300 mm)
32.	Shiina and Inagaki [44]	Cylindrical capsule	Numerical Modelling	Water/O-ctadecane/ Li_2CO_3/ NaCL	Air/helium/ water	Charging process	Re = 300, 3000 and 7500, $T_{HTF} - T_{final} = 5$ °C , $T_{init} - T_f = -5$ °C	Capsule D = 6.6 mm, thickness = 0.3 mm
33.	Varun et al. [43]	Cylindrical storage/ Cylindrical capsule	Experimental	N/A	Air	Charging process	$700 < Re < 1300$	Tank: D = 0.6 m, L = 1.25 m. Cylindrical elements: D = 0.06 m , L = 0.12 m
34.	Wei et al.[62]	Cylindrical storage/ spherical capsule	Experimental and numerical	Paraffin wax	Water	Discharging process	$0.3 < \dot{m}_f < 1.2m^3/h$ $40 < T_{initial} < 105$°C	Tank: L = 303 mm, W = 103 mm, thickness = 175 mm, Sphere: D = 2–5 mm
35.	Arkar and Medved [63]	Cylindrical storage/ spherical capsule	Numerical Modelling	Paraffin (RT20)	Air	Charging and discharging	For charging: $108 < \dot{m}_f < 215m^3/h$. For dis charging: $76 < \dot{m}_f < 166m^3/h$	Tank : (D = 340 mm, L = 1.52 m). Sphere D = 50 mm)
36.	Lacroix [64]	Parallelepedic capsule	Numerical Modelling	*n*-Octadecan	–	Discharging process	$0 < cooling\ rate < 5$, $0.00926 < Ste < 0.0926$	Tank: L = 75 mm, $25 < W < 225$, H = 30 mm
37.	Assis et al.[65]	Spherical shell	Experimental and numerical	Paraffin wax	Air	Charging process	$T_{initial}$: 23 °C, wall temperature varies from 2 to 20 °C > T_m	Spheres D = 40, 60 and 80 mm

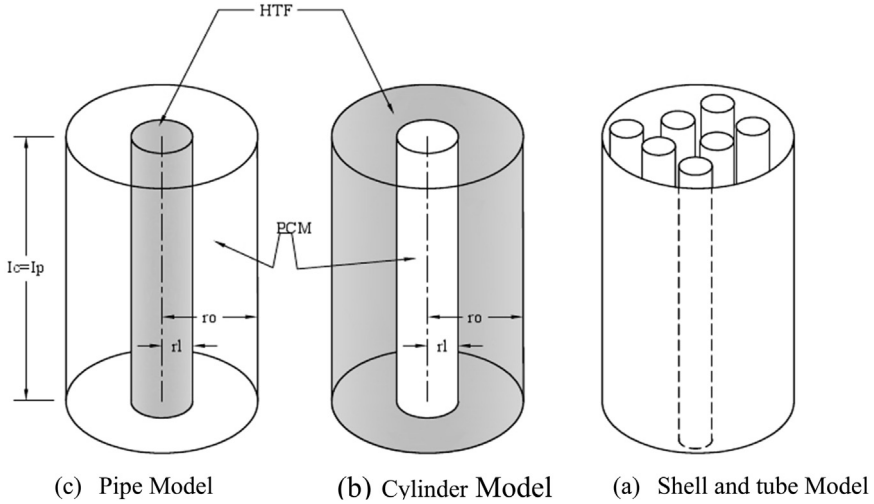

Fig. 5. Cylindrical PCM containers [15].

heating storage systems because they do not exhibit any subcooling, while lauric acid is suitable as an energy storage material for space heating and greenhouses applications. Khillarkar et al. [81] carried out a numerical study to examine the free convection of a pure PCM during melting in tube geometries of two different configurations: a square external tube with a circular tube inside, and a circular tube with a square tube inside. The effects of heating the inside wall, the outside wall or both walls, as well as of the Raleigh number on the system performance were described. The results indicated that the rate of melting is lower at the bottom part compared to the top part due to the buoyancy force acting during the melting of the PCM. Furthermore, in both cases, the effect of heating the inside walls and outside walls was the same as heating both walls until an interaction occurred between the two zones.

3.2. Cylinder model

Shmueli et al. [82] conducted a numerical investigation into melting PCMs in vertical circular tubes. The effects of various parameters in the numerical model on the results were examined, including a detailed study of the effects of pressure-velocity coupling and pressure discretization schemes. PISO vs. SIMPLE and PRESTO vs. Body-Force-Weighted schemes were examined, and no difference was found in the results using PISO and SIMPLE. On the other hand, there were considerable differences between results using the PRESTO and Body-Force-Weighted schemes. Furthermore, the term describing the magnitude of the mushy zone in the momentum equation was analysed and it was concluded that an optimum value of the specific constant C, should be used for this term.

Jones et al. [83] conducted an experimental and numerical study of the melting of a moderate-Prandtl-number material (n-eicosane) in a cylindrical enclosure heated from the sides. A multiblock finite volume method and enthalpy method were deployed in the numerical calculations for a range of values of the Stefan number and the numerical data was validated against the experimental information. A good agreement was observed between both methods for Stefan number values of up to 0.1807. Fang et al. [84] numerically studied the heat transfer Stratified water storage (SWS) using PCM. In this study, they provide an index of effective energy storage ratio to characterize the effective energy storage capacity of the system. The methods were compared with experimental work for the validation purpose. The study further shows that the heat transfer enhancement in the fluid side may enhance the energy storage ratio. Regin et al. [85] conducted a theoretical study of the latent heat thermal storage using a horizontal cylindrical capsule filled with paraffin wax as a PCM. The effects of various parameters on the melting performance were considered. The numerical modelling was conducted using the finite difference approach and fixed approach based on the enthalpy method. The model was validated by comparing the theoretical results to experimental data and an acceptable agreement was found between these two data sets.

The enthalpy-temperature relationship is presented below for the four regions during the melting processes (Fig. 6): the solid phase, solid-solid phase change below the melting point, solid-liquid phase and liquid phase.

$$H = C_{ps}T + \frac{L_p}{(a1 + a2)}(T - T_{(p-a1)}), \quad T_{(p-a1)} < T < T_{(p+a2)} \tag{5}$$

$$H = C_{ps}T + T_p, \quad T_{(p+a2)} \le T \le T_{(m-e1)} \tag{6}$$

$$H = C_{pl}T + L_p + \frac{L}{(e1 + e2)}(T - T_{(m-e1)}), \quad T_{(m-e1)} < T < T_{(m+e2)} \tag{7}$$

$$H = C_{pl}T + L_p + L, \quad T \ge T_{(m+e2)} \tag{8}$$

The PCM's thermal conductivity, k, in the interface phase was expressed as:

$$k = k_s + \left(\frac{k_l - k_s}{(\Delta T)_m}\right)(T - (T_{m-e1})), \quad T_{(m-e1)} < T < T_{(m+e2)} \tag{9}$$

The stored energy in a unit volume of the PCM was expressed as:

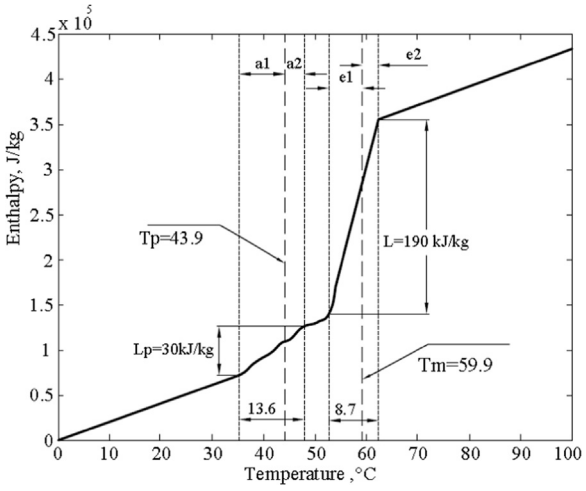

Fig. 6. Enthalpy temperature relationship [85].

$$E = \int_{T_o}^{T_{p-a1}} \rho_s C_{ps} dT + \int_{T_{p-a1}}^{T_{p+a2}} \rho_s C_{ps} dT + \rho_s L_p + \int_{T_{m-e1}}^{T_{m+e2}} \rho_l C_{pl} dT + \rho_l L + \int_{T_{m+e2}}^{T_f} \rho_l C_{pl} dT \quad (10)$$

The melting of particle-laden slurry in a cylinder was numerically and experimentally investigated by Sun et al. [86]. A particle-diffusive model and the enthalpy method were used in the numerical analysis. This study was later validated with results by Jones et al. [83]. It was found that the melting behaviour of the slurry with a lower particle loading ($\phi = 5\%$) was similar to the melting of pure wax. Indeed, a strong influence of convection was observed in both cases. On the other hand, the natural convection was reduced as the particle loading increased and the melting process was then dominated by conduction. Nevertheless, one major drawback of the diffusive flux model is that the model is not sufficiently adequate to describe the melting of slurries with various particle loadings.

The melting of a PCM in a latent heat thermal energy storage having a hollow cylinder form was studied semi-analytically by Zhang and Faghri using the integral approximation method [87]. The results were then validated using findings by the same authors in [88]. The structure of the thermal storage system in both studies was similar but the earlier study adopted a structure without external radial fins. It was demonstrated that the laminar forced convection heat transfer never reached the fully developed state, even with the application of a very long tube. Pahamli et al. [89] numerically studied the thermal characteristics of the double pipe heat exchanger with PCM. The numerical model was compared with the published study of [90] for the validation purpose and a very good agreement was found between them. They studied the effects of the inlet HTF parameters and downward movement of inner pipe on the melting processes of the PCM. The results show that the inner pipe downward movement significantly enhances the natural convection heat transfer inside the PCM and hence accelerates the melting processes. Furthermore, the inlet temperature of the HTF has a considerable effect on the melting process and highly reduced the total melting time. On the other hand, there was a slight effect of the HTF mass flow rate on the total melting time.

Cabeza et al. [91] experimentally examined the PCM behaviour in cylinders at the top of a water tank. Several configurations with two, four and six PCM modules were investigated (see Fig. 7). Commercial aluminium bottles filled with PCMs were used as PCM modules. Several PCMs were investigated: paraffin, sodium acetate trihydrate and fatty acids. It was found that this technique provides long periods of the storage time as well as increases the energy capacity and density.

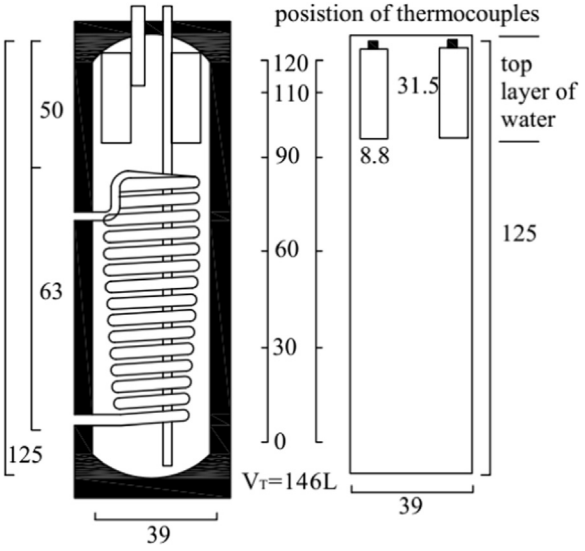

Fig. 7. Water tank with PCM modules of different configurations [91].

Wu and Lacroix [92] numerically analysed the natural convection in a melting PCM in a vertical cylindrical capsule heated from below. The model was created using the finite-difference method. They compared their numerical predictions with the numerical and experimental results in [93–95], and reported that the heat transfer rate at the top surface was dominated by conduction, but was decreased to zero as melting progressed and the natural convection developed fully. On the other hand, they also observed that the most intensive heat transfer took place at the bottom surface of the capsule.

Rieger and Beer [96] examined the effect of the natural convection flow on the heat transfer during the melting process of ice inside an isothermal horizontal cylinder. They numerically predicted the overall and local heat transfer coefficients, temperature fields, interface positions and flow pattern. Moreover, they compared their numerical results with experimental data and reported that the heat transfer was enhanced at the lower part of the ice body at wall temperatures less than 8 °C because of the density effect, whilst for the wall temperature exceeding 8 °C, the ice body moved downwards. The same procedures were applied by Rieger et al. in [97] to investigate the heat transfer during melting *n-Octadecane* as a PCM inside a horizontal tube.

Tay et al. [98] carried out an experimental investigation of a tube-in-tank thermal storage unit during the freezing and melting process of salt hydrate as a PCM. The HTF circulated inside the tube and the PCM was contained in the cylindrical tank. Three different experiments with different configurations were carried out. The first was conducted in a tube which was 5.46 m in length in a cylindrical tank, whilst the second configuration used two tubes with lengths of 5.61 and 6.01 m. The third experiment was conducted on four tubes with lengths of 5.95, 6.05, 5.79 and 6.04 m.

Temperature distributions, average effectiveness and solidification and melting times were analysed. The experimental measurements were compared to numerical results by Tay et al. in [99], with a good agreement demonstrated between the two sets of data. The numerical model was developed using ANSYS code and a three-dimensional CFD model was created in order to analyse the transient heat transfer during the melting and solidification process. It can be concluded from the results that the CFD model can accurately predict the performance of the thermal storage system and can also be used to optimize its design. Saraswat et al. conducted both an experimental and a numerical study in order to investigate the melting process of paraffin wax in a semi-cylindrical storage system [100]. The authors concluded that understanding the melting process and the natural convection phenomena inside the storage would help the design of efficient thermal storage systems.

Saitoh and Hirose numerically investigated the natural convection heat transfer inside a horizontal circulator cylinder capsule packed with a PCM during the melting and solidification process for high Rayleigh numbers [101]. The model predicted the formation of the transient solid-liquid interface, solid-liquid temperature, streamlines, isotherms and heat stored. The numerical results were validated through a comparison with those of Pannu et al. in [102] and, in general, considerable quantitative and qualitative differences were found. It is interesting to note that the natural convection controlled the melting heat transfer inside the capsule and also that the thermal instability occurred at the bottom portion of the capsule.

Sparrow and Broadbent experimentally examined the melting process in a phase change medium contained in a vertical tube [103]. The experimental results were compared with a numerical solution and a good agreement was observed. It was demonstrated that the rates of melting and heat transfer are significantly affected by the natural convection inducing the fluid flow in the liquid molten zone. The experimental measurements of the energy transferred and stored in the liquid molten zone were higher than those predicted by the numerical model.

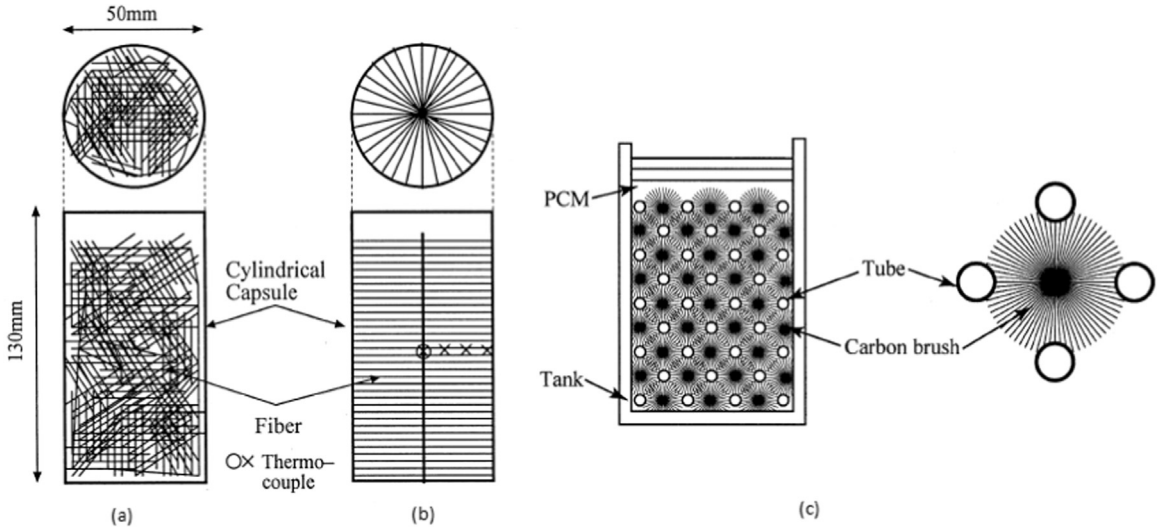

Fig. 8. Configurations of the carbon fibres [104–106].

3.3. Shell and tube model

Fukai et al. carried out an experimental and numerical investigation on the effects of a carbon-fibre brush on the thermal conductivity in a thermal energy storage system [104–106]. Several techniques for the thermal conductivity enhancement using carbon-fibre brushes were investigated. These include: randomly oriented carbon fibres packed in a cylindrical capsule (Fig. 8a), a carbon fibre brush packed in a cylindrical capsule (Fig. 8b) [104], a carbon fibre brush/PCM composite inserted around tubes (Fig. 8c) [105] and carbon fibre on the shell side [106]. The findings of such studies indicated that the type of the brush had a significant effect on the thermal conductivity enhancement. The randomly oriented fibres had little effect on the magnitude of the thermal conductivity. In addition, the transient thermal response in the brush/PCM composite was improved as the diameter of the brush increased. However, the response did not improve when the diameter of the brush was greater than the distance between the tubes due to the increased thermal resistance near the tube wall. The heat exchange rate during both the charging and discharging processes was significantly improved when brushes inserted around the tube were used.

Hamada et al. also experimentally and numerically studied two heat transfer enhancement mechanisms using carbon-fibre chips and carbon brushes packed into a shell-and-tube thermal storage system [107]. For the experimental investigations, four steel tubes were vertically placed in a cylindrical container made of acrylic resin and insulated using glass wool. Carbon-fibre chips with a diameter of 10 μm and length of 5 mm were packed in the container. The PCM *n-Octadecane*, with a thermal conductivity of 0.34 W/m K, was used to fill the container. Fig. 9 illustrates the experimental apparatus.

Three types of the fibre were used, namely those with low, medium and high levels of thermal conductivity (k_f = 5, 190 and 500 W/m K respectively). The control volume method was used in the numerical model, and the computational domain is illustrated in Fig. 10. The mathematical and experimental data were then compared and it was found that the carbon-fibre chips significantly improved the heat transfer rate in the PCMs. However, taking into account the effect of the thermal resistance near the heat transfer surface, the overall heat transfer for the carbon brushes was higher than that for the carbon-fibre chips.

Trp studied the transient heat transfer in a shell-and-tube thermal storage system in an experimental and numerical study [108,109]. He developed a mathematical model based on the non-isothermal phase transition and implemented as a FORTRAN computer code. The numerical results were validated with experimented data and it was concluded that heat transfer from the HTF to the PCM was low due to the large Prandtl numbers of the HTF. Therefore, a large amount of heat was carried downstream with the HTF, whilst a small amount of heat was transferred to the PCM upstream. The same author numerically investigated the effects of several geometrical parameters and different HTF operational conditions on heat transfer during both the melting and solidification processes by measuring the transient temperature distribution of the HTF, PCM and tube wall [110]. Gasia et al. experimentally investigated the effect of the dynamic melting within a cylindrical shell-and-tube heat exchanger [111]. Four different PCM flow rates were tested during the experiment. Results showed that the melting time and the effectiveness were significantly improved when the PCM flow rate was twice the HTF flow rate. The study has identified that dynamic melting is an effective technique for enhancing the heat transfer during the melting process of PCM.

Lacroix developed a numerical model using an enthalpy-based method [112]. The model predicted the transient behaviour of a shell-and-tube storage unit with circulating HTF inside the pipe and with PCM on the shell side. The model was validated by comparison with experimental data and the effects of several thermal and geometric parameters on heat transfer were investigated. It was found that the shell radius, mass flow rate and inlet temperature must be selected carefully in order to optimize the storage unit performance.

Morcos experimentally analysed both the charging and discharging processes in a thermal energy storage involving a shell-and-tube unit [113]. Two types of PCMs were investigated, namely paraffin wax and asphalt. Experimental measurements of the temperature distribution, heat stored during charging and heat released during discharging were compared for these different storage substances. Ezan et al. experimentally investigated the effect of natural convection and several design/flow parameters on the charging and discharging processes for ice in a shell-and-tube design [114]. It was found that the natural convection dominated the heat transfer mechanism after a short period in which the conduction was the main mode of heat transfer. Furthermore, the flow rate, inlet temperature, shell diameter and thermal conductivity of the tube material had considerable effects on the charging and discharging processes. Jin et al. [115] developed a numerical model for charging and discharging PCM heat transfer based on energy asymmetry. The model was validated with the experimental results and a great agreement was achieved between them. They found that the melting temperature range and the solidifying temperature range were the main reasons for the energy asymmetry, as well as the supercooling problem during the cooling process. However, the results of symmetrical model were compared with asymmetrical model and it was found

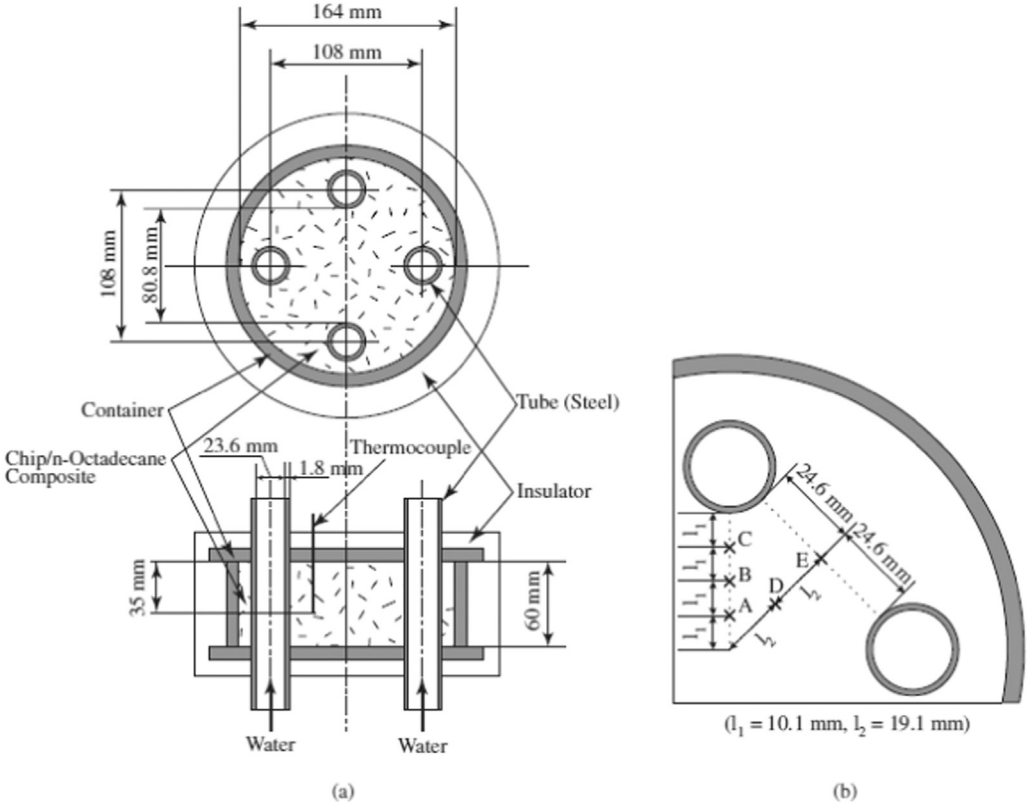

Fig. 9. Experimental apparatus [107].

that the asymmetrical model was more accurate and was close to the experimental processes.

Akgün et al. carried out an experimental investigation on the charging and discharging processes of paraffin as a PCM [116,117]. They used a novel tube-and-shell configuration which was oriented vertically. The key experimental parameters investigated were the HTF inlet temperature and Reynolds number. It was concluded that increasing the inlet temperature results in a decrease in the total melting time, whilst the Reynolds number had no significant influence. The PCM started to melt in the lower region close to the inner wall, and the molten PCM ascended radially outwards to form a conical shape of the molten region as a result of the natural convection currents. A large number of studies considered the enhancement of heat transfer using fin configurations. A summary of some of these studies are presented in Table 2. The studies tableted are contrasted in terms of a number of parameters including system geometry and dimension, methods of investigation, HTF type, process and PCM materials.

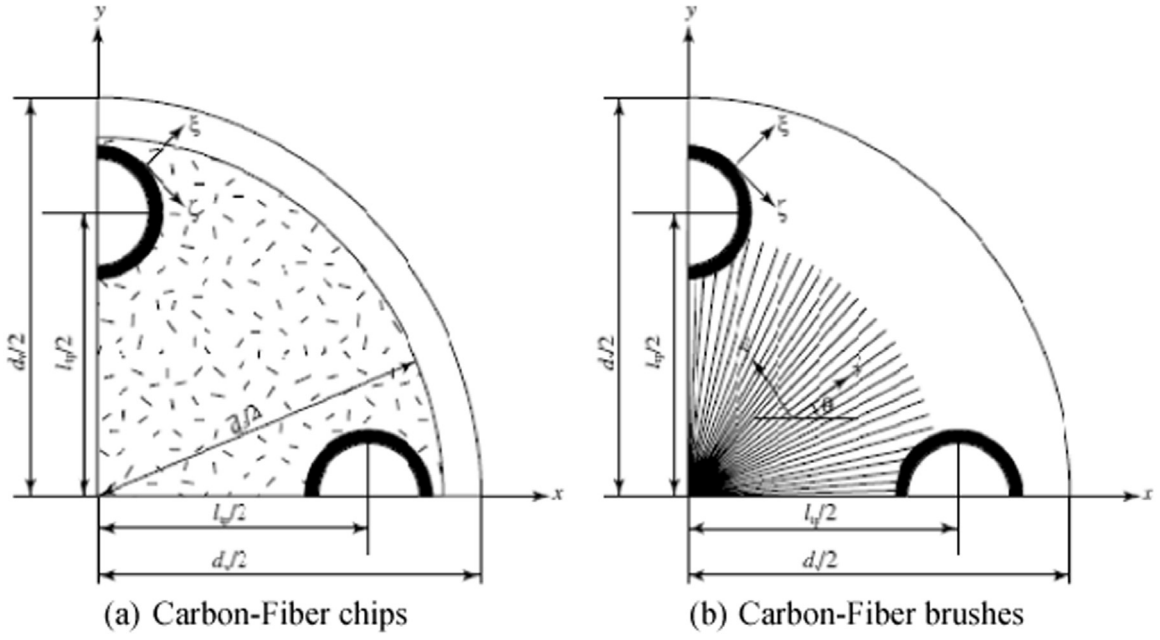

Fig. 10. Computational domain [107].

Table 2
Results of studies on the shell and tube thermal storage systems with PCMs.

No	Author	Geometry	Methods	PCM	HTF	Process	Parameters range	Dimensions
1.	Jian [66]	Pipe model	Experimental and numerical	n-Hexacosane	Water	Charging and discharging	Charging process: T_{HTF} = 58°C	300 < L < 3100mm 15 < Di < 90mm 17 < Do < 94mm
2.	Ho and Chen [68]	Pipe model	Numerical	Ice	-	Charging process	T_i = 4, 6, 8, 9, 10°C	Cylinder: D_i = 25.4 mm
3.	Rieger et al. [70]	Pipe model	Numerical	Ice	-	Charging process	Ra = 1.5× 10^5, 0.005 ≤ Ste ≤ 0.08 , Pr = 50	-
4.	Dimaano and Watanabe [71]	Pipe model	Experimental	capric and lauric acid	Water	Charging and discharging	Charging: $\dot{m}$ = 1.67 ×$10^{-5}m^3$/s 30 < Ti < 39.8°C Discharging: $\dot{m}$ = 2.51 ×$10^{-5}m^3$/s, Ti = 2.1°C	Tube: D = 30 mm, thickness = 0.1 mm, L = 420 mm) Cylinder: (D = 56 mm, thickness = 10 mm, L = 345 mm)
5.	Bareiss and Beer [72]	Pipe model	Experimental and numerical	n-Octadecane and p-xylene		Charging and discharging		Tube: (D = 60 mm, thickness = 1 mm, L = 40 mm)
6.	Sarı and Kaygusuz [75–80]	Pipe model	Experimental	Stearic, palmitic, lauric, myristi and fatty acids	Water	Charging and discharging	Investigate the effect of flow operation conditions	Tube: : (D = 50 mm, L = 350 mm) Cylinder: (D = 120 mm, L = 200 mm)
7.	Khillarkar et al. [81]	Pipe model	Numerical	octadecane		Charging process	0.0432 < F_o < 0.432, 2.844 ×10^6<Ra< 2.844 ×10^7	-
8.	Lu et al.[118]	Pipe model	Numerical	Molten salt	-	Charging and discharging	T_s = 300 K, Inlet velocity = 1 m/s, T_o = 453 K	Pipe (D_i = 0.008 m, D_o = 0.01 m, L = 2 m)
9.	Ismail and Abugderah [73]	Vertical tube type	Numerical			Charging and discharging	100 < Re < 2200 , 0.1 < Ste < 0.6, 0.75 < Do < 2.5	-
10.	Shmueli et al. [82]	Cylinder model	Experimental and numerical	Rubitherm GmbH	-	Charging process	-	Cylinder: (D = 30 and 40 mm)
11.	Jones et al. [83]	Cylinder model	Experimental and numerical	n-Eicosane	Water	Charging process	T_{wall} = 45, 55and70°C, T_s = 32°C, Re=5.45 ×10^6, 1.31 ×10^7and2.72×10^7, Ste = 0.1807, 0.3265and0.0836	Cylinder: (D = 31.9 mm, thickness = 5.97 mm, L = 59.8 mm)
12.	Regin et al. [85]	Cylinder model	Experimental and numerical	Paraffin wax	Water	Charging process	0.04 < Ste < 0.24 T_{HTF} = 75 °C	Cylinder: D_i = 76 mm, thickness = 2 mm, L = 100 mm)
13.	Sun et al. [86]	Cylinder model	Experimental and numerical	n-Eicosane	Water	Charging process	T_{HTF} = 70 °C Ti = 35.5 °C	Cylinder: D_i = 63.8 mm, D_o = 69.5 mm, L = 59.8 mm
14.	Zhang and Faghri [87]	Cylinder model	Numerical modelling	n-Octadecane	Water	Charging process	0.25 < Fo < 4	
15.	Cabeza et al. [91]	Cylinder model	Experimental	Paraffin, sodium acetate trihydrate and fatty acids	Water	Charging process		Cylinder module : (D = 8.8 cm, H = 31.5 cm) Tank : (D = 39 cm, H = 125 cm)
16.	Wu and Lacroix [92]	Cylinder model	Numerical modelling	-	-	Charging process	Ste = 0.1 Ra= 10^5and10^6	-
17.	Rieger [96,97]	Cylinder model	Experimental and numerical	Ice/ n-Octadecane	-	Charging process	10^5<Ra<10^6	Cylinder tube: D_i = 32 mm, thickness = 1 mm, L = 40 mm
18.	Tay et al. [98,99]	Cylinder model	Experimental and numerical	Salt hydrate	Nano-fluid	Charging and discharging	$\dot{m}$ = 0.013, 0.019, 0.024and 0.026kg/s	Cylinder tank: D = 290 mm, H = 330 mm
19.	Saitoh and Hirose [101]	Cylinder model	Numerical modelling	Paraffin, Ice/ n-Octadecane	-	Charging and discharging	P_r = 54.6, R_a = 15800, 426400, 3411000, and 2914000 ΔT = 7 K and 13 K	Cylinder capsule: D = 0.01, 0.02, 0.03, 0.0448 and 0.06 m
20.	Sparrow and Broadbent [103]	Cylinder model	Experimental and numerical	Paraffin		Charging process	Ste = 0.0387, 0.0971, and 0.248	Cylinder: D_i = 5.08 cm, thickness = 0.152 cm, L = 39.4 cm
21.	Hasan [119]	Cylinder model	Experimental	Palmitic acid	Water	Charging and discharging	Ti = 40 °C, $\dot{m}$ = 0, 1, 2, 3.2, *and* 5.1 *kg/min*, T_{HTF} = 40. 65. 71. *and* 75 °C	Cylinder tube: D_i = 40 mm, thickness = 1.5 mm, L = 550 mm
22.	Yang and Tao [120]	Cylinder model	Numerical modelling	-	-	Charging process	R_a = 10^3–10^6	Slot width = 0–0.5, r_0/r_i = 2.6
23.	Fukai et al. [104–106]	Shell-and-tube	Experimental and numerical	Paraffin wax	Water	Charging and discharging	Charging: 55<T_{HTF}<60 °C Discharging: −35<T_{HTF}< − 38 °C HTF velocity = 0.015, 0.03 and 0.08 m/s	Cylindrical: D = 50 mm, H = 130 mm. Brush: D = 10 μm, L = 5 and 200 mm. Tube D_i = 8 mm, D_o = 9.5 mm

(*continued on next page*)

Table 2 (*continued*)

No	Author	Geometry	Methods	PCM	HTF	Process	Parameters range	Dimensions
24.	Hamada et al. [107]	Shell-and-tube	Experimental and numerical	n-Octadecane	Water	Charging process	$Ti = 18$℃ HTF velocity = 0.35 m/s $T_{HTF} = 23$ ℃	Tube: $D_i = 23.6$ mm, $D_o = 25.4$ mm.Shell: D = 164 mm, L = 60 mm
25.	Trp [108–110]	Shell-and-tube	Experimental and numerical	RUBITHERM RT30	Water	Charging process	$\dot{m} = 0.017$ kg/s $13 < T_{inlet} < 45$ ℃	Inside tube: ($D_i = 0.033$ m, $D_o = 0.035$ m, L = 1 m) Outside tube: : ($D_i = 0.128$ m, $D_o = 0.133$ m, L = 1 m)
26.	Lacroix [112]	Shell-and-tube	Experimental and numerical	n-Octadecane	Water	Charging process	$0.03 < \dot{m} < 0.07$ kg/s $32 < T_{inlet} < 47$℃ $Ti = 9.5$℃	Inside tube: $D_i = 0.0127$ m, $D_o = 0.0158$ m, L = 1 m Outside tube: $D_i = 0.0258$ m, L = 1 m
27.	Morcos [113]	Shell-and-tube	Experimental	Paraffin wax and Asphalt	Water	Charging and discharging	$10 < \dot{m} < 55$ kg/h $62 < T_{inlet} < 95$℃ $Ti = 25$℃	Inside tube: $D_i = 026.64$ mm, $D_o = 33.4$ mm, L = 1 m) Outside tube: $D_i = 52.5$ mm,$D_o = 60.33$ mm, L = 1 m)
28.	Ezan et al. [114]	Shell-and-tube	Experimental	Ice	Water, Ethylene, and Glycol	Charging process	Tube material: s. steel and copper. $\dot{m} = 2, 4$ and 8 l/min $Ti = -5, \ -7.5, \ -10, and -15$℃	$D_i = 15$ mm, $D_o = 25$ mm, L = 0.4 m
29.	Akgün [116,117]	Shell-and-tube	Experimental	Paraffin P24–44 Paraffin P46–48 Paraffin P56–58	Water	Charging and discharging	Charging process: $T_{HTF} = 60$, 65, 70 and 75 ℃ $\dot{m} = 2, \ 6$ and 8 kg/s Charging process: $T_{HTF} = 20$ ℃ $\dot{m} = 2, \ 6$ and 8 kg/s	Tube diameter = 28 mm Cylindrical Storage (D = 94.67 mm, L = 465 mm) Storage geometry with a shell angle: (upper D = 133.4 mm, lower D = 56 mm)
30.	Hendra et al. [121]	Shell-and-tube	Experimental and numerical	Mikro	Water	Charging and discharging	Ti = 300 K	Tube diameter: 0.015 m Container diameter: 0.2625 m
31.	Ismail and Gonçalves [122]	Shell-and-tube	Numerical modelling	n-Eicosane	Water	Discharging process	$0 < Bi < 50$, $1 < R^* < 6$ $10 < T_{inlet} < 35$℃	
32.	Castell et al. [123]	Shell-and-tube	Experimental	Hydrate salt	-	Charging process		Pipe: (Di = 0.008 m, L = 5.46 m) Tank: (Di = 0.29 m, H = 0.35 m)

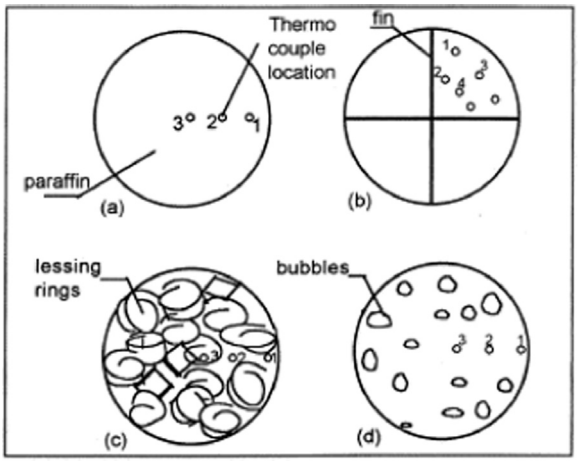

Fig. 11. The cross section of tube storage units with different configurations: (a) plain tube (b) with internal longitudinal fins (c) Lessing rings (d) bubbles [128].

4. Methods used for heat transfer intensification

The low values of thermal conductivity in PCMs resulted in a large number of studies on the enhancement of heat transfer during the solidification and melting of PCMs. Various techniques were tested to enhance the heat transfer performance and melting and solidification processes in PCM latent heat thermal storage systems. This section presents a review of these methods and provides information on their advantages and disadvantages.

4.1. Intensification using fins

Fins or extended surfaces can be used to provide an additional heat transfer surface in the thermal system and thus increase the heat transfer rate. A range of fin geometries were extensively studied by a number of researchers. Abdulateef et al. conducted an extensive review on the enhancement of the thermal performance of LHTES systems through the use of additional heat-transfer surface [124]. The study was meant to assess the effects of extended surfaces geometrical dimensions, dimensionless numbers, and fin location through numerical and experimental studies on the thermal characteristics of the PCM-latent heat thermal storage systems. It was found that the highest enhancement was achieved by using the longitudinal fins. Further, the heat enhancement factor was effectively dependent on increasing the numbers and dimensions of fins. Liu et al. experimentally studied the enhancement of PCM thermal conductivity by using copper fins with a spirally twisted configuration [125]. The experimental results showed that the fin design had a profound effect on both the conductive and natural convective heat transfer. It was also observed that finer fins are more effective than large fins in enhancing the melting process if an equal amount of fin material is used. Furthermore, it was concluded that changing the fin width could lead to a more significant enhancement of the PCM's thermal conductivity.

In [126], Stritih investigated the heat transfer enhancement in a thermal storage unit with a finned surface during both solidification and melting processes. The storage unit was made as a rectangular box with an inlet and outlet, while water was used as the HTF. The other part of the system was a heat exchanger with 32 rectangular fins. The exchanger was filled with RUBITHERM RT paraffin as a PCM. The heat transfer and natural convection phenomena were investigated and compared with those of the storage unit without fins. Experimental correlations were presented for the fin effectiveness as a function of Stefan (*Ste*) and Fourier numbers (*Fo*) and the Nusselt number (*Nu*) as a function of the Rayleigh number (*Ra*):

$$\eta_f = 1 \times 10^{7*}(Ste.\ Fo)^2 - 1719.4*(Ste.\ Fo) + 0.7813 \quad (11)$$

$$Nu = 8 \times 10^{-12} Ra^{1.0392} \quad (12)$$

It was found that for low Fourier numbers, the fin effectiveness was less than 1. The reason for this was that the natural convection, which was dominant in the melting process, was suppressed due to the presence of fins. In the solidification process, the fin effectiveness varied from 0.4 to 3.06 depending on the Stefan and Fourier numbers. An experimental study with numerical modelling of the solidification process of a PCM inside a cylindrical vertical tube and using internal longitudinal fins was performed by Velraj et al. [127]. The experimental results showed that the surface heat flux increased significantly with an increase in the number of fins. The effect of the radius of the tube on the surface heat flux was also investigated. It was found that for a tube of small radius, the surface heat flux initially increased, but after a certain period of time, it became lower than the corresponding case with a tube of large radius. The reason for this is that in the smaller tube, the thickness of the solidification layer is greater. Therefore the conductive resistance of the solidification layer becomes higher than in the case in which the tube radius is smaller. The solidification process for cases with and without fins was also compared. It was found that the complete solidification time for the tube with fins was approximately 1/n-th (n is the number of fins) in the case of the tube without fins. A numerical model was developed to investigate the effect on the heat transfer of different tube wall and fin thicknesses. The calculations were conducted for a tube with a radius of 0.03 m, and it was demonstrated that there was no reduction in the heat transfer until the tube wall and fin thicknesses were reduced to 0.0015 m.

In [128], the same authors studied different heat enhancement techniques for the thermal storage units shown in Fig. 11; namely internal longitudinal fins inside a plain cylindrical storage tube filled with paraffin; the same tube filled with Lessing rings of 1 cm in diameter with a small amount of water in the tube, which was then evacuated using a vacuum pump after adding the molten paraffin. The vacuum was maintained such that the saturation temperature of the water inside the tube was nearly equal to the melting temperature of paraffin. It was found that the total solidification time was significantly reduced to the one-quarter value by using fin compared with the plain tube and to one-ninth when Lessing rings were used. (Fig. 12)

Kayansayan and Acar conducted a numerical and experimental study of the solidification of ice in a cold thermal storage system with a horizontal finned tube [129]. The effects of the HTF inlet temperature, flow rate, fin density and fin size were investigated. The numerical model was validated with comparison to experimental data and the numerical model was also tested against the results of Lacroix in [130], who developed his own mathematical model for the melting process with the same geometrical and flow parameters. Kayansayan and Acar used water as the HTF and *n-Octadecane* (n-$C_{18}H_{38}$) as the PCM, while the latter study used ethyl-alcohol as the HTF and ice as the PCM. The comparison was carried out for a tube with 12 fins and a working fluid of the same Peclet numbers of 75.4, 754 and 7540. Fig. 13 shows the effect of the flow rate on the molten fraction and HTF exit temperature. In general, a good agreement was observed and the results demonstrated that increases in the flow rate, HTF inlet temperature and the number of fins led to an increase in the heat transfer rate and the amount of energy stored in the system.

Ismael et al. presented a numerical model of the solidification process around a vertical axially finned tube immersed in a PCM and the model results were compared with experimental data [131]. The study was designed to determine the effect of the fin length, thickness and number, the aspect ratio of the annular space and the difference between the phase change temperature and the wall temperature of the tube. The numerical results were supported by the findings of the experimental work, and these indicated that as the fin length increases, the complete solidification and the solidified mass fraction are reduced

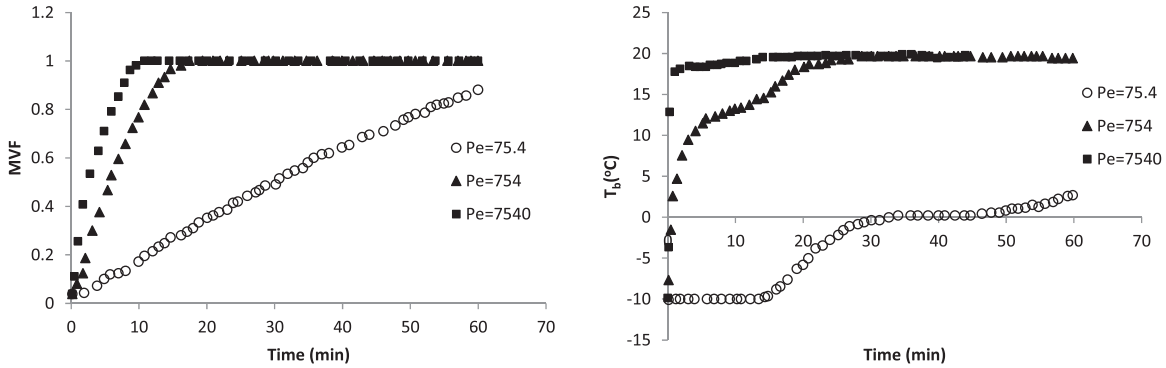

Fig. 12. A comparison of numerical results on the effect on the HTF exit temperature and molten fraction in [129] and [130].

significantly. An increase in the fin thickness as well as the number of fins resulted in an increase in the solidified mass fraction and a reduction in the solidification time. The results also demonstrated that an increase in the aspect ratio of the annular space resulted in an increase in both the solidification time and the solidified mass fraction, whilst an increase in the temperature difference resulted in a reduction in the solidification time and the solidified mass fraction.

Zhang and Faghri developed theoretical methods to study the heat transfer enhancement in a latent heat thermal energy storage unit using tubes with internal longitudinal fins (Fig. 13a) and external radial finned tubes (Fig. 13b) [88,132]. The most interesting finding was that the use of internal fins provided stronger effect of enhancing the melting heat transfer for transfer fluids at low Reynolds numbers. Another important finding for the externally finned case was that the tube wall temperature and Nusselt number were increased significantly when the thickness of the wall increased, but the latter had no significant effect on the molten liquid volume. On the other hand, the fin height had a significant impact on the molten volume fraction (MVF). Youssef et al.[133] conducted both experimental and numerical studies on the PCM heat exchanger with spiral-wired tubes. The PCM heat exchanger was designed to be connected with heat pump for hot water circulation. 3D CFD model was developed for the validation purpose. The results show that there is an excellent agreement between the experimental and numerical results. Further, the study investigated the effects of the inlet Heat Transfer Parameters (HTF) parameters on the charging and discharging process of the PCM. The results show that the inlet HTF parameters can significantly affect the heat transfer inside the heat exchanger.

Castell et al. experimentally investigated the natural convection phenomena for a cylindrical model of the system with external vertical fins [134]. The model consisted of a PCM placed in the middle upper part of a cylindrical water tank. Experimental correlations between the Nusselt number and the Rayleigh number were proposed.

Agyenim et al. studied different aspects of the enhancement of the heat transfer in a medium temperature thermal storage system using both circular and longitudinal fins [135]. It was reported that longitudinal fins achieved a sufficient enhancement of the heat transfer, and that the average temperature was higher than in the control and circular finned systems. The circular fins did not provide a noticeable improvement of heat transfer during sensible heat absorption even though they increased the heat transfer area. Abdulateef et al. experimentally and numerically studied the impact of two-types of extended surfaces incorporating a PCM [136]. Two types of external fins, namely the longitudinal and triangular were examined. The effects of fins type on the heat transfer enhancement and energy storage capacity were compared and evaluated. The results showed that fins configurations improved the heat transfer in the thermal storage system. Further, the triangular fins have been considered the most efficient way for reducing the total melting time. Shatikian et al. conducted a numerical study of the melting of a PCM in a heat storage system with internal fins and a horizontal base [137,138]. He reported that the melting process and heat flux were affected by changes in the geometry of the system and the boundary conditions. In addition, it was found that the Nusselt number and melting fraction depended on a combination of dimensionless numbers, such as the Fourier (*Fo*), Stefan (*Ste*) and Rayleigh (*Ra*) numbers:

$$Nu = 5 + \frac{4}{(Fo^{*}Ste^{*}Ra_{lf}^{-1/4}Ra_{lb}^{1/6}) + 0.015} \quad (13)$$

Sparrow et al. experimentally examined the enhancement of the conduction and convection heat transfer during the solidification process in a thermal storage unit with a vertical tube with external fins [139]. It was found that the conduction enhancement for fins was less than the area ratio of the finned and unfinned tubes, whilst the enhancement in the natural convection was very nearly equal to the area ratio. On the other hand, the degradation in the heat transfer due to the

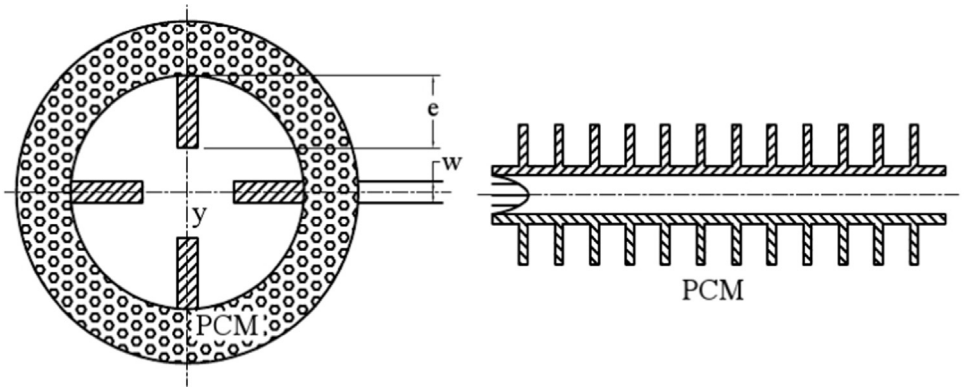

Fig. 13. Schematic of internally and externally finned tubes deployed in [88] and [132] .

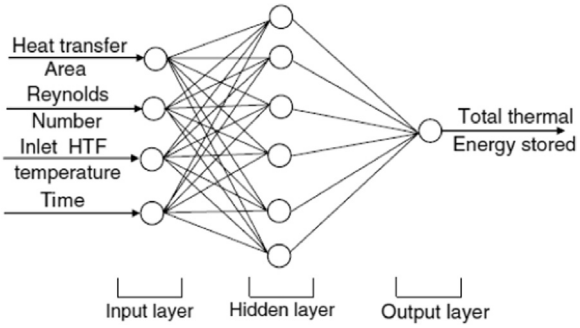

Fig. 14. A three layer feed-forward back propagation neural network for heat transfer analysis [140].

natural convection increased with time and this degradation was greater for lower values of the temperature difference across the frozen PCM layer. Using an artificial neural network (ANN), Ermis et al. analysed the heat transfer in a latent heat thermal storage system with a finned tube [140]. ANN modelling was used to predict the amount of heat transfer through the PCM around the finned tube. The four network input parameters considered (Fig. 14) were the heat transfer area, Reynolds number, HTF inlet temperature and time, whereas the output parameter was the total thermal energy stored. The hidden node was modified to minimize the errors in the output values, and the ANN was validated by comparison with experimental data. Very good agreement was achieved for both laminar and turbulent flows.

Kazemi et al. [141] numerically investigated the influence of the longitudinal fins angle on the heat transfer enhancement during the charging process of the PCM thermal storage systems. The study presented 3 different fins configurations. These are bare tube case, double-fins, and triple-fins. It can be found from the results that the fins did not have a significant effect on the natural conviction on the system. Also, when the number of fins increase, the heat transfer area also increased and then the total melting time reduced. The best enhancement was found in the cases with fins angle compared to other cases. Eftekhar et al. experimentally studied the enhancement in the heat transfer in a thermal storage system with a heated and cooled horizontal finned-tube [142]. The heat transfer and natural convection effect at the liquid-solid interface were investigated, and correlations were obtained from the experimental data for the Nusselt number and the volumetric rate of liquid produced. These correlations, which are presented below, were validated with results in [143] and the agreement between the two sets of data was found to be satisfactory:

$$\overline{Nu} = 0.0270\, f_s^{-1} (Ra/Ste)^{1/3} \tag{14}$$

where

$$\overline{Nu} = f_c^{2/3} \left(\frac{\overline{h_e} L_c}{k} \right) \tag{15}$$

$$f_s = \frac{S}{(S_f + S_p)} \tag{16}$$

$$f_c = \frac{(\overline{T_w} - \overline{T_u})}{(\overline{T_w} - T_m)} \tag{17}$$

The following heat transfer correlation equation was derived by Bathelt and Viskanta in [143]:

$$\overline{Nu} = 0.0178\, (Ra/Ste)^{1/3} \tag{18}$$

The volumetric rate of liquid produced can be described as

$$\frac{dV}{dt} = 0.0270 f_c^{-2/3} \left(\frac{Ra}{L_c^3 Ste} \right)^{1/3} \left(\frac{k}{\rho L} \right) (S_f + S_p)(\overline{T_w} - T_m) \tag{19}$$

where S_f is the area of vertical fins, S_p is the area of heated bottom plate, T_w is the mean wall temperature, T_m is the melting temperature and S is the area of solid liquid interface.

A theoretical model was derived by Padmanabhan and Murthy in [144] to study the phase change occurring in a cylindrical annulus with axial fins on the inner tube. The theoretical model was based on the finite-difference method. It was concluded that the melt/frozen fraction could be estimated using the following formula, which was recommended for engineering design purposes:

$$VF = 1.1275\, (Fo{*}Ste{*}T_f)^{0.624} (N)^{0.028} (L)^{-1.385} (W)^{-0.049} \tag{20}$$

where N is the number of fins, L is the fin length and W is the fin thickness

Tan et al. experimentally and numerically studied the impact of the configuration of spiral aluminium fillers on the PCM's melting performance in a fin type latent heat storage system [145]. A two-dimensional simulation domain was designed using Fluent 6.3 software for both fin type and fine-spiral fillers slab (Fig. 15). The numerical results were validated with experimental data, and a good agreement was observed. It was also found that the aluminium spiral fillers have a strong influence on the PCM's melting behaviour. The heat conduction increased due to the rise in the induction area as a result of adding the spiral fillers, whilst the natural convection was reduced.

Agyenim et al. experimentally studied the melting and solidification processes in a shell-and-tube design with longitudinal fins used to

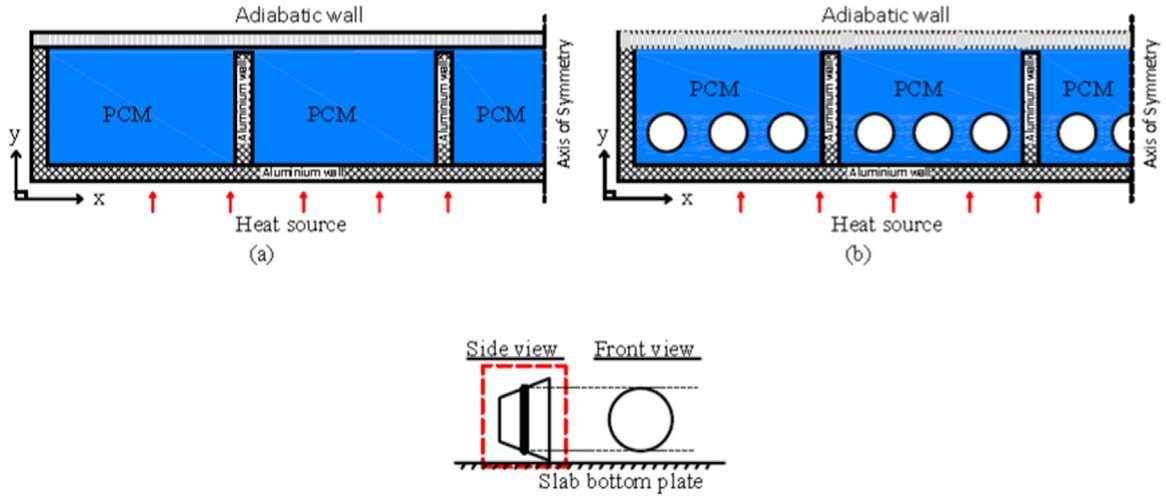

Fig. 15. Two-dimensional simulation domain [145].

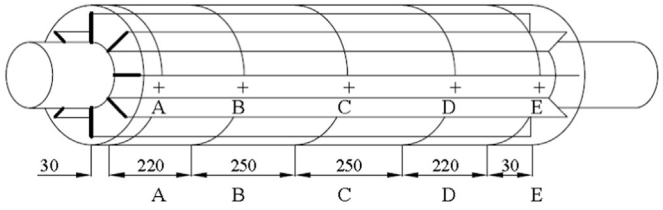

Fig. 16. Schematic diagram of a shell and tube system [146].

power a LiBr/H_2O absorption cooling system (Fig. 16) [146]. The experiments were carried out for different values of the charging mass flow rate and inlet HTF temperatures. The temperature gradients in the axial, radial and angular directions during the charging process were recorded. The results demonstrated that the optimal parameters for charging the LiBr/H_2O absorption system were as follows: a mass flow rate of 30 kg/min and an inlet temperature of 140 °C.

Choi and Kim experimentally investigated the heat transfer characteristics of magnesium chloride hexahydrate ($MgCl_2{\cdot}6H_2O$) in circular finned and unfinned systems [147]. It was found that the molten fraction in a 5-finn tube was 25% greater than that in the unfinned tube. However, the molten fraction in the 10-finned tube was similar to that in the 5-finned tube which meant that the additional surface in the 10-finned tube did not have the desirable effect on the molten fraction. Heat transfer correlations were obtained for the amount of energy storage in terms of Fourier, Stefan and Reynolds numbers:

For the unfinned-tube systems,

$$\frac{Q}{Q_{max}} = 7.42 \times 10^{-4} Fo^{0.96} Ste^{1.07} Re^{0.48}, \quad Re \leq 8000 \tag{21}$$

For the 5-finned-tube systems,

$$\frac{Q}{Q_{max}} = 10.10 \times 10^{-4} Fo^{0.92} Ste^{0.94} Re^{0.45}, \quad Re \leq 8000 \tag{22}$$

For the 10-finned-tube systems,

$$\frac{Q}{Q_{max}} = 24.90 \times 10^{-4} Fo^{0.85} Ste^{1.07} Re^{0.40}, \quad Re \leq 8000 \tag{23}$$

The thermal characteristic during the solidification process of a triplex-tube heat exchanger with longitudinal/triangular fins was experimentally and numerically investigated by Abdulateef et al. [148]. The effect of flow rate on the heat transfer was experimentally analysed and evaluated. The results indicated that the flow rate can accelerate the solidification process and reduce the total solidification time. Furthermore, the study developed a numerical model to study the effects of extended surfaces, namely the longitudinal and triangular fins in several configurations. It was found that the internal, internal-external, and external triangular significantly improved the heat transfer compared to longitudinal fins configuration.

A summary of some of recent publications on heat transfer enhancement using fins are presented in Table 3. A variety of parameters, such as methods of investigation, PCM material, fins geometry, dimension and materials, charging or discharging processes, parameters range and HTF type, are used to compare the individual studies.

4.2. Intensification of the heat transfer using filling materials

Another technique widely used to increase the heat transfer surface in thermal systems is incorporating filling materials, such as graphite materials and porous media (metal foams and matrix materials).

4.2.1. Graphite materials

Pincemin et al. experimented with graphite flakes combined with salts or eutectics as PCMs at melting temperatures of 200–300 °C [151]. Graphite was added to improve the thermal conductivity and storage capacity of the PCM. Three different types of graphite were used: natural graphite flakes (Fig. 17a), expanded natural graphite (Fig. 17b) and ground expanded natural graphite (Fig. 17c). A significant enhancement of the thermal conductivity was found to be up to a factor of 14 with an effective conductivity of 9 W/m K and a factor of 10 for an the effective conductivity of 6 W/m K. In addition, no significant changes were found in the phase change temperature, but a reduction in the phase change temperature variation was observed.

Zhao and Wu studied experimentally the intensification of heat transfer in a high temperature thermal storage system using metal foams and expanded graphite filled with a PCM [152]. It was found that the application of both metal foams and expanded graphite significantly enhanced the heat transfer during both the charging and discharging processes, the complete freezing and melting times were reduced and the effect of metal foams was greater than that of expanded graphite. Another interesting finding was that the heat transfer was significantly enhanced in the solid regions due to the increase in the conduction heat when using metal foams and expanded graphite, but these materials suppressed the natural convection effect in the liquid region. Py et al. theoretically and experimentally studied the performance of a composite PCM made of paraffin saturated with compressed expanded natural graphite (CENG) [153]. They concluded that the composite thermal conductivity can be improved by up to 70 W/mK depending on the CENG density and shape. CENG also significantly suppressed the natural convection in the melted PCM region.

Zhang and Fang studied the behaviour of a paraffin/expanded graphite composite PCM [154]. Expanded graphite with an average particle size of 300 μm and an expansion ratio of 200 ml/g was used in the study. The thermal performance of the composite was compared with that of paraffin, and the results showed that the phase change temperature and latent heat remained the same for both of these materials. On the other hand, the time needed to reach the required temperature during the melting process was reduced by 27.4% for the composite PCM compared to paraffin. It can also be seen in Fig. 18 that the total solidification time for the composite PCM was reduced by 56.4% compared to paraffin. The heat transfer rate in the composite PCM was higher than that of paraffin due to the improved thermal conductivity.

The same method of enhancing the thermal conductivity was adopted by Xiao et al. for paraffin using a thermoplastic elastomer poly composite [155]. The thermal storage performance of the composite was compared with that of paraffin, and it was reported that the heat transfer rate in the composite increased significantly with the rise of the mass of expanded graphite during the solidification process. This was due to the increase in the thermal conductivity of the composite. In the case of melting, the heat transfer rate was reduced due to the weaker natural convection, which plays a significant role during melting. The most interesting finding was that the composite PCM with a paraffin content of 80% had the same phase transition as pure paraffin. Sarı and Karaipekli obtained similar results from the experimental study of the melting process in a composite PCM made of paraffin (n-docosane) with expanded graphite (EG) [156]. The effect of the mass fraction of EG on the thermal storage characteristics was investigated. The results indicated a strong relationship between the mass fraction of EG and thermal conductivity. The continuous introduction of EG resulted in an increase in the thermal conductivity, thereby reducing the complete melting time. On the other hand, for all EG mass fractions, the latent heat capacities were roughly the same and very close to that of paraffin. The composite PCM made of 10% EG and 90% of paraffin was recommended for LHTES applications due to its stable properties.

In an effort to improve the thermal conductivity of static acid, Karaipekli et al. [157] used expanded graphite (EG) and carbon fibre (CF) and compared the results with those reported in [104,155,158–161]. They discovered a linear relationship between the thermal conductivity and the mass fractions of EG and CF additions:

$$k = 0.0841 M_f + 0.2194 \quad (\textit{for Expanded Graphite}) \tag{24}$$

Table 3
Results of studies on heat intensification using fins.

No	Author	Fin geometry	Fin material	Methods	PCM	HTF	Process	Parameters investigated	Dimensions
1.	Liu et al. [125]	Rectangular fins	Copper	Experimental	Stearic acid	–	Charging process	Effect of fin size and pitch on the heat transfer	Tube: D_i = 46 mm, L = 550 mm
2.	Stritih [126]	Rectangular	Steel	Experimental and numerical	Paraffin	Water	Charging and discharging	Effects of fins on heat transfer enhancement	Fins: H = 0.5 m, L = 0.12 m, thickness 1 mm. Rectangular Storage: H = 0.5 m, L = 0.12 m, W = 0.65 m.
3.	Velraj et al. [127]	Rectangular internal longitudinal fins	Aluminium	Experimental	Paraffin RT60	–	Discharging process	Effect of fin number and tube radius on heat flux and solidification fraction	Rectangular fins: H = 27 mm, L = 300 mm, thickness 1.5 mm. Cylindrical tube: D_i = 54 mm, L = 600 mm, D_o = 60 mm.
4.	Kayansayan and Acar [129]	Annular fins	Copper	Experimental and numerical	Ice	Ethyl-alcohol	Discharging process	Effect of HTF inlet temperature, flow rate, fin density, and fin size	Horizontal section: (L = 57 cm, W = 50 cm, H = 42 cm) Tube: (D_i = 20 mm, L = 492 mm, D_o = 30 mm)
5.	Lacroix [130]	Annular fins	Copper	Theoretical model	N-Octadecane	Water	Charging process	Effect of shell radius, mass flow rate, inlet temperature.	Inner tube: D_i = 12.7 mm, L = 1 m, D_o = 15.8 mm. Outer Tube: D_i = 25.8 mm, L = 1 m. Annular fins: Do = 25.6 mm.
6.	Ismail et al. [131]	Vertical axially finned	–	Experimental and numerical modelling	Paraffin	Water	Discharging process	Effect of fin length, thickness and, number, aspect ratio of the annular space and the temperature difference between phase change temperature and the wall temperature of the tube	Fins length: 0.087, 0.196, 0.348 mm. Aspect ratio: 2.481 Fins number: 2, 3, 4 and 5 The angular half-width of the fin: 0.55, 0.45 and 0.36
7.	Zhang and Faghri [132]	Internal fins	–	Numerical modelling	–	–	Charging process	Effect of internal longitudinal fins on heat transfer	Fins thickness W = 0.05
8.	Zhang and Faghri [88]	External radial finned	–	Numerical modelling	–	–	Charging) process	Effect of external radial fins on the heat transfer	
9.	Castell et al.[134]	External vertical fins		Experimenta	Sodium acetate trihydrate	Water	Natural convection phenomena during solidification process	Effect of fins on natural convection phenomena	Cylindrical Tank: D = 440 mm, H = 450 mm. Cylindrical model: D = 88 mm, H = 315 mm. Fins: H = 310 mm, L = 20 and 40 mm.
10.	Agyenim et al. [135]	Circular and longitudinal fins	Copper	Experimental	Erythritol	Silicon oil	Charging and discharging	Effect of circular and longitudinal fins on the heat transfer of medium temperature thermal storage system	Fins number: 8 Fin thickness: 0.001 m Fin pitch: 0.04 m Circular fin diameter: 0.134 m Longitudinal fin length: 0.95 m
11.	Shatikian et al. [137,138]	Internal longitudinal fins	Aluminium	Numerical	Paraffin wax	–	Charging process	Effect of fins on the melting process and heat flux	0.15 < Fins thickness < 1.2 mm, 5 < fins high < 10 mm, 0.5 < PCM store between fins < 4 mm
12.	Sparrow et al. [139]	External vertical fins	Styrofoam	Experimental	Paraffin (n-eicosane)	–	Discharging process	Effect of fins on natural and conduction heat transfer	Storage unit: D = 15.2 cm and H = 11.5 cm.
13.	Ermis et al. [140]	Internal fins	Bronze	Experimental and numerical modelling	Water/ice	Ethyl-alcohol	Charging and discharging	Effect of fins and flow parameters on the phase change process using artificial neural network	Fin: L = 440 mm, thickness = 3 mm. Tube: D_i = 10 mm, D_o = 15 mm, L = 570 mm. Tank: W = 420 mm, L = 570 mm, H = 500 mm.
14.	Eftekhar et al. [142]	Vertical fins		Experimental	P116 paraffin wax	Water	Charging process	Effect of fins on the enhancement of heat transfer and natural convection	Storage unit: H = 53.5 mm, L = 61.5 mm and W = 56 mm.
15.	Padmanabhan and Murthy [144]	Axial fins	Copper	Numerical	N-Eicosane	Water	Charging and discharging	Phase change process of specific storage unit	Dimensionless fin thickness = 0.1 Dimensionless fin length = 1.5
16.	Tan et al. [145]	Fins and Spiral Fillers	Aluminium	Experimental and numerical	Paraffin wax	–	Charging process	Effect of spiral fillers on melting performance	Spiral fillers diameter = 12 mm

(*continued on next page*)

Table 3 (*continued*)

No	Author	Fin geometry	Fin material	Methods	PCM	HTF	Process	Parameters investigated	Dimensions
17.	Ismail and Lino [149]	Radial rectangular fins	Copper	Experimental	Water	Ethanol	Discharging process	Effect of radial fins and turbulence promoters on heat transfer	Tank: 700 × 500 × 500, thickness= 10 mm. Tube: D_i = 12.25 mm, D_o= 18.35 mm, L= 1 m.
18.	Saha and Dutta [150]	Plate fins		Numerical	N-Eicosane	–	Charging process	Effect of aspect ratio and applied heat flux on the thermal performance of the heat sinks	Heat sink: (L= 20 mm, H= 2 mm) Fin thickness= 0.2, 2.2, 4.2, 6.2, 8.2, 9.2, and 9.9 mm. Fin height= 2.7, 3.1, 5, 10, 20, 25, 30, 35, and 40 mm.
19.	Agyenim et al. [146]	Longitudinal fins	Copper	Experimental	Erythritol	Silicon oil and water	Both charging and discharging	Effect of mass flow rate and inlet temperature of HTF on the thermal behaviour of PCM system	Shell, D_o = 154 mm Tube, D_o = 54 mm
20.	Choi and Kim [147]	Circular fins	Stainless steel	Experimental	Magnesium chloride hexahydrate	Air	Charging (melting) process	Effect of circular fins on heat transfer characteristics	Shell; D_i = 55 mm, H= 140 mm and thickness= 2.5 mm

$$k = 0.0659M_f + 0.2831 \quad (for\ Carbon\ Fiber) \tag{25}$$

Zhang et al. also studied the influence of graphite powders on the thermal conductivity of mixed shape-stabilized PCMs [162]. The study found that the thermal conductivity of the composite PCM could be increased up to 20 times. Beyond this value, the mechanical robustness of the composite deteriorated. Furthermore, the authors developed a correlation for the effective thermal conductivity as a function of the graphite mass fraction and this correlation showed a good agreement with experimental data:

$$k = -333.3\,X^4 + 213.3\,X^3 - 31.97\,X^2 + 2.187X + 0.15 \quad (0 \le X \le 0.2) \tag{26}$$

Mills et al. used a graphite matrix to form a paraffin/graphite composite [163]. The graphite matrix was made of flake graphite which can be obtained from stacked sheets of carbon. The thermo physical properties of the composite were investigated, and their experimental results were compared with correlations published by other authors in [153,164,165] with a good agreement. It was found that the PCM mass fraction was decreased for higher bulk densities, while the thermal conductivity of the composite PCM increased anisotropically.

4.2.2. Intensification of heat transfer using porous media, metal foams and matrix materials

Mesalhy et al. numerically investigated the influence of a porous matrix (with different values of thermal conductivity and porosity) filled with a PCM in two concentric cylinders [166]. The finite element approach was used, and in order to validate the numerical model, the free convection during the melting process of pure PCM was investigated. The numerical results were compared to those by Khillarkar et al. [81] and were found to be in a good agreement. The results demonstrated that a decrease in the porosity resulted in an increase in the melting rate as well as in the convection flow of liquid PCM fractions due to the reduction in the matrix permeability. Furthermore, decreasing the porosity reduced the storage capacity of the PCM due to the reduction in the PCM quantity. On the other hand, using a solid matrix with high thermal conductivity and porosity resulted in a significant heat transfer enhancement in the PCM storage. Hoogendoorn and Bart also developed a mathematical model to study the effects of metal matrix structure on the temperature transition range of melting/solidification in paraffinic materials [167]. It was demonstrated that the mathematical model provided a good agreement with the experimental results.

Phanikumar and Mahajan carried out both an experimental and a numerical analysis of the natural convection inside high porosity metal foams heated from below [168]. The numerical model was validated with experimental data and with the results of Beckermann et al. [169]. The effect of several metal foams (aluminium, carbon and nickel) on the heat transfer enhancement was examined, and it was found that using metal foams led to a significant enhancement in heat transfer. On the other hand, the effect of Darcy and Rayleigh numbers on the heat transfer was also reported, and it was demonstrated that local thermal non-equilibrium effects became significant at high Darcy and Rayleigh numbers. Sasaguchi et al. proposed a numerical model for the solidification of pure water in porous media placed around a single cylinder and two cylinders [170]. The model was used to study the effect of the natural convection on the solidification process for the system with and without porous media. Furthermore, the effects of the initial water temperature as well as the number of cylinders on solidification were studied. The model was validated with experimental results and an excellent agreement was found. It was concluded that both the initial temperature of water and the number of cylinders had considerable effects on the solidification process. Their next paper examined the effect of the position of the cylinder on the solidification process [171]. The results demonstrated that the position of the cylinder had a significant influence on temperature distribution, average Nusselt number

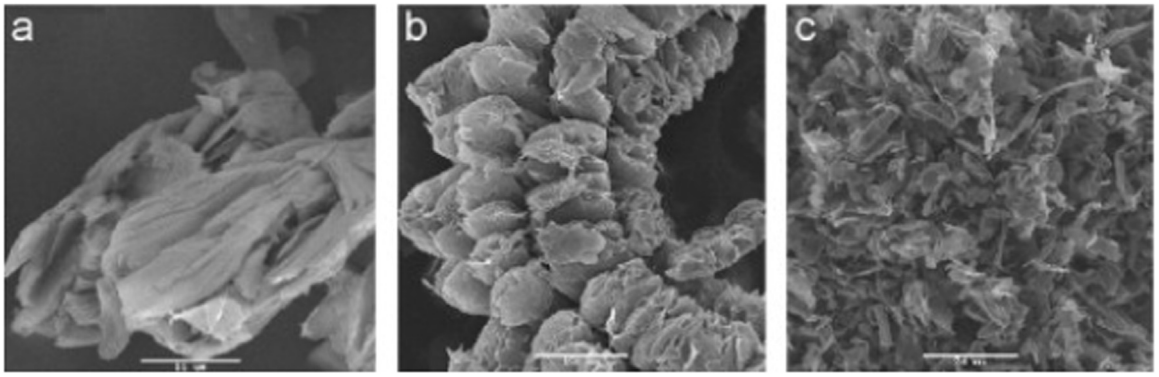

Fig. 17. Tested graphite [151].

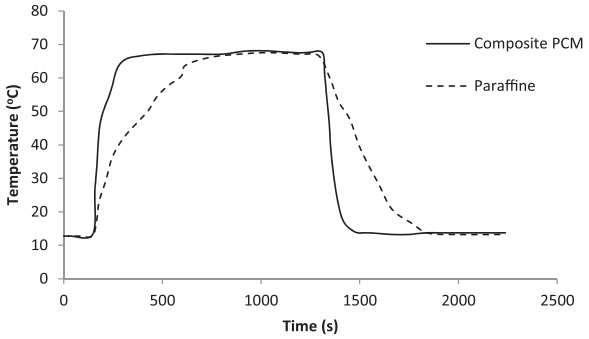

Fig. 18. Temperature variation during the melting and solidification process [154].

over the cylinder surface and the cooling rate of the water.

Bhattacharya et al. conducted both an analytical and experimental analysis of the physical properties of high porosity metal foams [172]. The effect on the thermal conductivity, permeability and internal coefficient of high porosity were investigated, and the theoretical model was validated with experimental data which demonstrated an excellent agreement. A metal fibre was used (Fig. 19), and it was concluded that the thermal conductivity depended on the porosity and the ratio of the cross-section of the fibre to the intersection area. The permeability increased with the increase of pore diameters and the porosity of the medium.

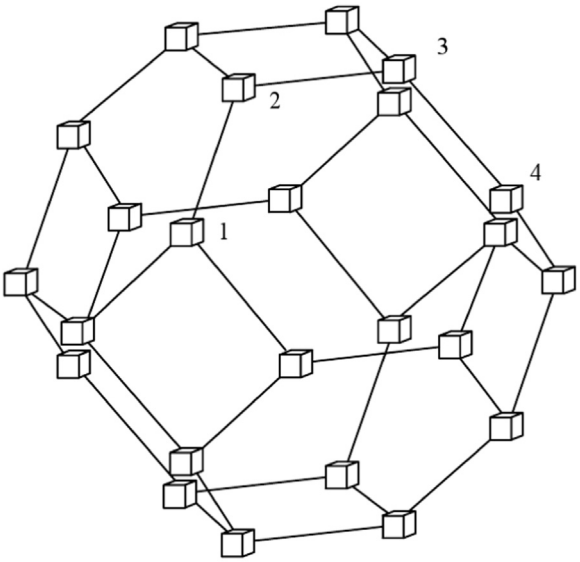

Fig. 20. Foam structure [173].

Boomsma and Poulikakos developed a three dimensional numerical model to evaluate the effective thermal conductivity of a fluid saturated

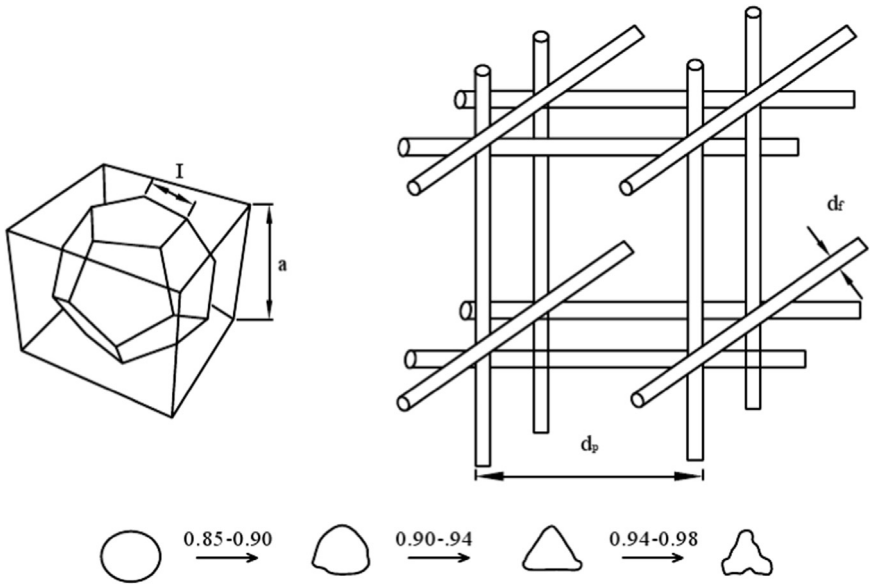

Fig. 19. Open cell representation of the metal foam and a schematic of the fibre cross-sections at different porosities [172].

metal foam [173]. The foam structure was represented as cylindrical ligaments attached to cubic nods at their centres as shown in Fig. 20. An aluminium foam with a porosity of 95% was used as the foam metal, whilst air and water were used as fluids. The model was validated with the experimental data by Calmidi and Mahajan [174] and a good agreement was observed. It was concluded that changing the fluid conductivity slightly increased the effective thermal conductivity, which demonstrated that the heat conductivity of the solid phase determined the overall effective thermal conductivity.

Calmidi and Mahajan numerically modelled and experimented with the forced convection in high porosity metal foams [174,175]. Experiments were carried out with the aluminium metal foam saturated with air and water as the fluid medium. The numerical results were compared to experimental data by Hunt and Tien [176], and it was demonstrated that the enhancement effect of the thermal dispersion was very small for the foam-air compound due to the high conductivity of the solid matrix, whilst for the foam-water, the thermal dispersion was very large. Erk and Duduković numerically modelled and experimentally analysed the heat storage in a phase change regenerator consisting of *n-Octadecane* retained by capillary force in a porous silica support [177]. CO_2 was used as the HTF in the phase change regenerator. The experiment measured the outlet temperature and compared it with the predicted value, and the results indicated the presence of a significant amount of heat losses. As much as 50% of the energy stored in the experimental unit could be lost to the surroundings via the end plates. Moreover, predictions of the net front movement were compared quantitatively with the experimental data, showing a reasonable agreement in 60% of the volume of the bed. Weaver and Viskanta experimentally investigated the freezing of distilled water in saturated porous media [178]. Spherical glass balls with diameters of 1.59 and 6 mm were used as the porous media, and their permeabilities were calculated to be 1.6×10^{-9} and 2.85×10^{-8} m^2 respectively. It was concluded that the porous media had a significant effect on the natural convection during the solidification process, inhibiting the fluid motion.

Beckermann and Viskanta carried out both an experimental and a numerical analysis of the phase change of a fluid inside a vertical rectangular enclosure filled with glass beads as a porous matrix [179]. Numerical results were compared to experimental data and a good agreement was demonstrated. It was concluded that the porous media had a considerable effect on the natural convection in the melt fraction as well as on the conduction in the solid fraction. Ji et al. [180] developed a numerical model to study the thermal process of rectangular thermal storage system with PCM heated from one side. The influences of fins with the inclined angle of 0, + 15, + 30, -15, and -30 were investigated. The results indicated that the fins with inclined angle of -15 have a higher effect on the heat transfer process and total melting time compared to the others. On the other hand, the effects of fin length and heat flux input on the PCM melting process were also studied. It was found that the fins' length with tilted fins has a considerable effect on the heat transfer processes.

Zhao and Lu produced a general model for heat transfer performance in metal foam filled pipes [181,182]. Detailed information on the velocity and temperature distributions were obtained using the Brinkman-extended Darcy momentum model and a two-equation heat transfer model. The results indicated that the metal foam significantly increased the heat transfer by a factor of forty. In addition, the metal foam with a small porosity and pore density resulted in a better heat transfer performance, but with an increased pressure drop. In their later papers [183–186], the authors examined the influence of the metal foam on the phase change process during the solidification and melting of paraffin. It was found that the additive metal foam significantly increased the heat transfer rate during both solidification and melting. The degree of the heat transfer enhancement depended on the metal foam structure and material used. Table 4 summarises some of recent publications on heat transfer enhancement using filling materials. Parameters such as type of PCM, methods of investigation, charging or discharging processes, validation processes and filling material are used among others to contrast the individual research studies.

4.2.3. Heat transfer intensification using nano-fluid, nano-particles and microencapsulation

4.2.3.1. Nano-particles. Ho and Gao experimentally evaluated the effect of alumina (AL_2O_3) nano-particles on the thermo-physical properties of paraffin (*n-Octadecane*) during the melting/freezing processes [200]. From the results obtained, adding AL_2O_3 nano-particles in paraffin had a small effect on the melting/freezing behaviour of paraffin. A similar result was obtained for the thermal conductivity enhancement using nano-particles. The thermal conductivity of nano-particles in paraffin became considerably higher with the rise of its temperature due to intensification of the Brownian motion. Furthermore, the measured dynamic viscosity and density of pure paraffin were compared with those found in [201] and an excellent agreement was observed. The results also revealed that the dynamic viscosity increased significantly as the amount of AL_2O_3 nano-particles increased. Wu et al. carried out similar work on paraffin saturated with nano-particles [202]. Cu, AL and C/Cu nano-particles were used to improve the heat transfer rate during both freezing and melting processes. It was concluded that the paraffin with nano-particles has a significantly enhanced heat transfer rate compared with pure paraffin, and also that the nano-particles had a little influence on the melting/freezing temperatures. The analysis conducted indicated that Cu nano-particles provided the strongest enhancement compared to Al and C/Cu nano-particles.

Zeng et al. experimentally investigated the influence of Ag nano-particles on the thermal conductivity of PCMs [203]. Tetradecanol (TD) was used as the PCM, and the experiment was carried out using several types of thermal analysis: differential scanning calorimetry (DSC), thermogravimetry (TG), power X-ray diffraction (XRD) and transmission electron microscopy (TEM). It was found from the results that the thermal conductivity of the composite material increased with the rise in the amount of Ag nano-particles.

Numerical simulations using FLUENT software were carried out by Arasu et al. to investigate the effect of AL_2O_3 nano-particles on paraffin wax in a concentric double pipe heat exchanger [204]. The computed thermo-physical properties of paraffin saturated with AL_2O_3 nano-particles were compared with Ho and Gao's measurements in [200] and a good agreement was observed between these two data sets. The results demonstrated that the AL_2O_3 nano-particles in paraffin wax had a significant effect on the charging-discharging rates of the thermal energy compared to the case with pure paraffin. A similar enhancement in the thermal conductivity of the composite materials and in the heat transfer rate was also found. Furthermore, the viscosity of the composite materials increased as the volumetric fraction of AL_2O_3 nano-particles rose, thus improving the natural convection heat transfer effectiveness. The authors' study in [205] repeated this investigation for a square enclosure heated from below and from the vertical side. The results indicated that paraffin wax saturated with nano-particles exhibited increased thermo-physical properties compared to pure paraffin. In [206], the effect of the volume fraction on the solidification and melting processes of paraffin wax was studied for both AL_2O_3 and CuO nano-particles. The authors found that the enhancement in the thermal performance of paraffin wax was greater when AL_2O_3 nano-particles were used compared to the application of CuO nano-particles.

Khodadadi and Fan analytically solved the one-dimensional Stefan problem for the freezing process of nano-particle-enhanced PCM (NEPCM) in a finite slab [207]. Combinations of both water and cyclohexane as a PCM with additions of four types of nano-particles (alumina, copper, copper oxide and titanium) were selected for investigations. The physical model for this investigation is illustrated in Fig. 21. In their next paper [208], the authors investigated the model experimentally. They demonstrated that the freezing process depended

Table 4
Results of studies on heat transfer intensification using filling materials.

No	Authors	Methods	PCM	Filling material	Process	Validation
1.	Pincemin et al. [151]	Experimental	Slat and eutectics	Graphite	Charging process	Yes [187,188]
2.	Zhao and Wu [152]	Experimental	Sodium nitrate $nano_3$	Metal foams and graphite	Charging and discharging	No
3.	Py et al. [153]	Experimental and numerical	Paraffin	Expanded natural graphite	Charging and discharging	No
4.	Zhang and Fang [154]	Experimental	Paraffin	Expanded graphite	Charging and discharging	No
5.	Xiao [155]	Experimental	Paraffin	Thermoplastic elastomer poly graphite	Charging and discharging	No
6.	Sarı and Karaipekli [156]	Experimental	Paraffin (n-docosane)	Expanded graphite	Charging and discharging	No
7.	Karaipekli [157]	Experimental	Static acid	Expanded graphite and carbon fibre	Charging process	Yes [104,155,158–161]
8.	Zhang et al. [162]	Experimental and numerical		Graphite	Charging process	Yes
9.	Mills et al. [163]	Experimental	Paraffin wax	Graphite matrix	Charging and discharging	Yes [153,164,165]
10.	Haillot et al. [189]	Numerical	Paraffin, stearic and other acids	Expanded natural graphite	Charging and discharging	No
11.	Yin et al. [190]	Experimental	Paraffin	Expanded graphite	Charging and discharging	No
12.	Mesalhy [166]	Numerical modelling	N-Octadecane	Metal matrix	Charging process	Yes [81]
13.	Hoogendoorn and Bart [167]	Experimental and numerical	Paraffinic materials	Metal matrix	Charging and discharging	Yes
14.	Phanikumar and Mahajan [168]	Experimental and numerical	–	Metal matrix (aluminium, carbon and nickel)	–	Yes [169]
15	Sasaguchi et al. [170,171]	Experimental and numerical	Pure water	Porous media	Discharging process	Yes
16.	Bhattacharya et al. [172]	Experimental and numerical	Water	Metal foams	–	Yes
17.	Boomsma and Poulikakos [173]	Experimental and numerical	Water	Metal foam	–	Yes [174]
18.	Calmidi and Mahajan [174,175]	Experimental and numerical	–	Metal foam	–	Yes [176]
19.	Erk and Dudukoviċ [177]	Experimental and numerical	N-octadecane	Porous silica support	Charging process	Yes
20.	Weaver and Viskanta [178]	Experimental	Water	Porous (spherical glass balls)	Discharging process	No
21.	Beckermann and Viskanta [179]	Experimental and numerical	Gallium	Porous (spherical glass balls)	Charging and discharging	Yes
22.	Siahpush [191]	Experimental	Eicosane	Copper porous foam	Charging and discharging	Yes
23.	Zhao and Lu [181,182]	Analytical model	–	Metal foam	Charging process	Yes [192]
24.	Zhao and Lu [183]	Experimental	Paraffin RT58	Metal foam	Charging and discharging	Yes
25.	Krishnan [193,194]	Numerical	–	Metal foam	Charging and discharging	Yes [179]
26.	Tong [195]	Numerical	Water	Metal matrix	Charging and discharging	Yes [196–198]
27.	Ettouney et al. [199]	Experimental	Paraffin wax	Metal screens and metal spheres	Charging process	No

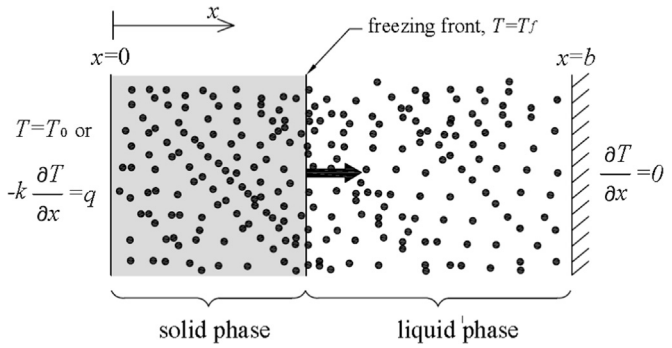

Fig. 21. Schematic diagram for 1-D modelling of the PCM freezing in a finite slab [207,208].

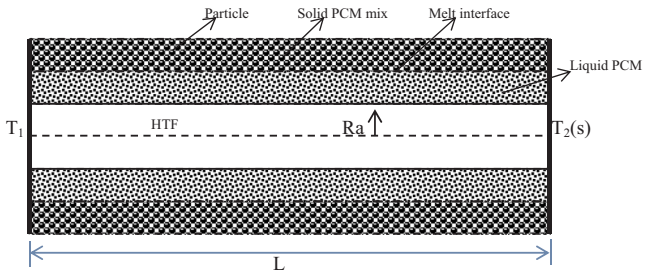

Fig. 22. Schematic of the storage unit containing dispersed particles [219].

only on the volume fraction of nano-particles and was not related to the type of nano-particles. The experimental results indicated that the freezing rate for NEPCM containing 5% of nano-particles was considerably increased. For volume fractions of nano-particles of 1% and 2%, the freezing process was not affected.

Khodadadi and Hosseinizadeh also carried out analytical investigations on the effect of nano-copper particles on natural convection and PCM thermal conductivity in a square storage model [209]. They applied the Boussinesq approximation model in FLUENT to simulate the buoyancy force and density variation. The results obtained from this model were compared with the results by other authors in [210–213], and in general, there was a good agreement between the data sets. It was pointed out that the latent heat of the PCM decreased as the addition of nano-particles increased. The results indicated that the solidification fraction increased rapidly as the mass fraction of suspended particles rose. This is because of the enhanced thermal conductivity and the smaller value of their latent heat. Ranjbar et al. obtained similar results from a numerical study of the solidification process in a 3-D rectangular enclosure filled with PCM with the addition of nano-particles [214]. It was pointed out that the addition of nano-particles suppressed the natural convection, and therefore the heat conduction dominated the heat transfer in both the solid and liquid phases.

Kim and Drzal experimentally investigated the behaviour of exfoliated graphite nano-platelets (xGnP) filled with paraffin wax [215]. The effects of xGnP on the thermal conductivity, melting time, melting temperature and latent heat capacity of paraffin were investigated. Their findings indicated that the thermal conductivity increased with the xGnP content. On the other hand, the use of xGnP did not lead to a decrease in the latent heat of the paraffin/xGnP composite PCM, and therefore, its latent heat storage was not reduced. Liu et al. carried out an experimental study on the solidification/melting of $BaCl_2$ filled with TiO_2 nano-particles [216]. They found that the thermal conductivity and heat transfer were significantly enhanced by adding nano-particles, which also reduced the supercooling of the suspension. Wang et al. used the fractal theory to model the effective thermal conductivity of the PCM liquid with nano-particles [217]. The effects of the particle size and surface adsorption were examined, and when the model results were compared to experimental results [218], a good agreement was observed for particle contents of less than 0.5%.

Seeniraj et al. proposed a theoretical expression for the energy storage and heat flux for cases with and without dispersed particles in the PCM and identified the optimum fraction of dispersed particles to maximise the energy storage and heat flux [219]. The schematic arrangement used in this study is shown in Fig. 22. It was reported that the cumulative energy storage capacity was decreased as the particle fraction was increased, due to the particles reducing the volume occupied within the PCM. However, the addition of particles increased the instantaneous surface heat flux and hence accelerated the energy storage process. The results also revealed that the optimum fraction of dispersed particles to maximise the stored energy depends on the thermal conductivity of the dispersed fraction. Siegel conducted a similar analysis for the planer solidification process [220].

Wang and Choi experimentally evaluated the thermal conductivity of a nano-particle-fluid mixture [221]. They used Al_2O_3 and CuO nano-particles with diameters of 28 nm and 23 nm respectively. Several fluids, such as distilled water, ethylene glycol, engine oil and vacuum pump fluid were dispersed with the two types of nano-particles and examined. The effect of the mixture preparation technique on its thermal conductivity was also investigated. The three different techniques, namely mechanical blending, coating particles with polymers and filtration, were tested and the measured thermal conductivity was compared with the predictions of various theoretical methods [222–227] shown in Table 5. It was reported that the measured thermal conductivity differed from the data reported in the literature, due to the different particle sizes used in the study. The results further indicated that the thermal conductivity of the mixture increased with decreasing particle size and also depended on the dispersion technique used.

Shaikh et al. carried out an experimental and a numerical study of the latent energy storage with a PCM containing dispersed single wall carbon nanotubes (SWCNTs), multiwall CNTs (MWCNTs) and carbon nano-fibres (CNFs) [228]. The results of the numerical model were compared to experimental results and a good agreement was found. Fig. 23 illustrates the physical model and the 2-D arrangement of carbon nanotubes (CNTs) used in the theoretical model. From the experimental results, the maximum value of the latent heat enhancement was found to be in the wax/SWCNTs composite followed by the wax/MWCNTs composite, whilst the minimum enhancement was found in the wax/CNFs composite. The theoretical model also examined the effect of nanoparticle mass fraction, size and type on the intermolecular attraction within the mixture. It was concluded that the molecular density of the SWCNTs was higher compared to that of MWCNTs and CNFs, resulting in the enhanced latent energy. A detailed review of the thermal conductivity enhancement methods in PCM energy storage systems was performed in [229,230]. Liu et al. [229] critically summarised the experimental and numerical methods to enhance the thermal conductivity of phase change materials. They focused on thermal conductivity enhancement using carbon materials as additives/inserts, metal materials or oxides as additives/inserts, and fins enhancement method. Finally, a comparison between the presented methods was discussed and analysed. Karaipekli et al. [230] presented new methods for enhancing the thermal conductivity of the paraffins using carbon nano tubes. The study focused on the preparation, characterization, and implementation of the thermal conductivity using carbon nano tubes as well as the preparation of the composite PCM with (ExP)/n-eicosane (C_2O). The results showed that the mixtures have very good characteristics and physical properties. Furthermore, the carbon nano tubes improved the thermal conductivity with better scale compared to (ExP)/n-eicosane (C_2O). A considerable number of studies were published on the heat transfer enhancement in PCMs using nano-particles, as summarised in Table 8. The studies were classified according to nano-particles type, methods of investigation, PCM materials, charging or discharging processes and validation processes.

Table 5
Effective thermal conductivity of a mixture [221].

Author	Theoretical expressions	Remarks
Maxwell [222]	$\frac{k_e}{k_f} = 1 + \frac{3(\alpha-1)\varnothing}{(\alpha+2)-(\alpha-1)\varnothing}$	Applicable $\varnothing \ll 1$ *or* $\lvert\alpha - 1\rvert \ll 1$
Jeffrey [223]	$\frac{k_e}{k_f} = 1 + 3\beta\varnothing + \varnothing^2\left(3\beta^2 + \frac{3\beta^2}{4} + \frac{9\beta^3}{16}\frac{\alpha+2}{2\alpha+3} + \frac{3\beta^4}{2^6} + ..\right)$	Accurate to order $\varnothing^2$
Davis [224]	$\frac{k_e}{k_f} = 1 + \frac{3(\alpha-1)}{(\alpha+2)-(\alpha-1)\varnothing}[\varnothing + f(\alpha)\varnothing^2 + 0(\varnothing^3)]$	Accurate to order $\varnothing^2$ $f(\alpha) = 2.5$ *for* $\alpha = 10$ $f(\alpha) = 0.5$ *for* $\alpha = \infty$
Lu et al. [225]	$\frac{k_e}{k_f} = 1 + a.\ \varnothing + b.\ \varnothing^2$	For spherical particles a = 2.25, b = 2.27. Forα = 10; a = 3, b = 4.51 for $\alpha = \infty$

4.2.3.2. Nano-fluids. Nano-fluids are dilute liquid suspensions of solid nano-particles or nanofibres with sizes of 1–100 nm [231]. Recent developments in the field of heat transfer have led to a renewed interest in nano-fluids due to of their enhanced thermo-physical properties and heat transfer. Minea [232], summarised the recent numerical studies on the preparation, thermophysical properties, correlations and heat transfer characteristics of hybrid nanofluids and compared between hybrid nanofluids with that of pure water. It can be noticed from the numerical results that hybrid nanofluid significantly improves the conventional heat transfer capacity. This is because the suspension of hybrid nanoparticles highly improved the thermal conductivity of the nanofluid. On the other hand, this study outlined the advantages and disadvantages of using hybrid nanofluids compared to water in term of heat transfer enhancement. Ding et al. reviewed the relevant literature on nano-fluids which covered heat conduction using nano-fluids, convection heat transfer for both natural and forced flow conditions and boiling heat transfer in the nucleate regime [231]. In an extensive study, Godson et al. summarised the results of experimental and theoretical studies on the enhancement of heat transfer using nano-fluids, improvements in thermal conductivity, Brownian motion and free convection in heat transfer [233]. Recent developments in the enhancement of heat transfer using nano-fluids were reviewed by Trisaksri and Wongwises in [234].

Ho et al. numerically examined different models of the effect of the dynamic viscosity and thermal conductivity of nano-fluids on natural convection heat transfer [235]. Numerical 2D modelling was carried out for a vertical square enclosure (Fig. 24), with a water-alumina (AL_2O_3) mixture chosen as the working nano-fluid. Results indicated that the heat transfer across the enclosure was improved with respect to the base fluid. Vajjha et al. experimentally measured the density of three different nano-fluids containing aluminium oxide (AL_2O_3), anti-mony-tin oxide (Sb_2O_5:SnO_2) and zinc oxide (ZnO) nano-particles in a fluid mixture consisting of 60% ethylene glycol and 40% water [236]. The experimental results for density compared favourably with the theoretical results of Pak and Cho [237] and it was demonstrated that the density was increased with the rise of nano-particles content.

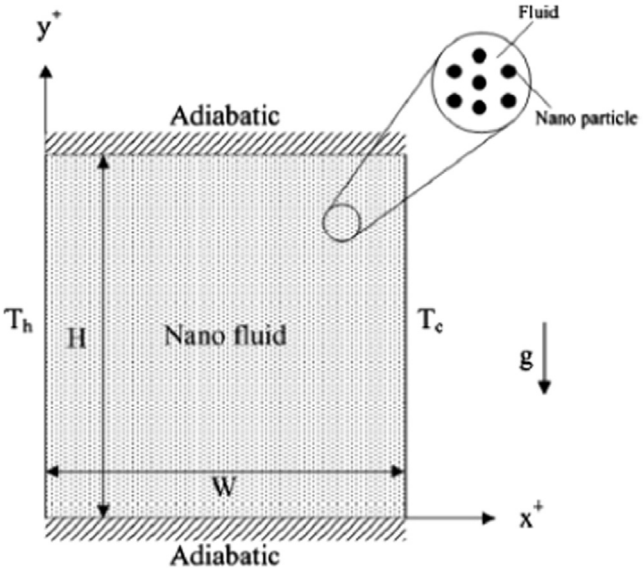

Fig. 24. Schematic of a vertical enclosure system [235].

In another major study, Vajjha and Das experimentally developed a correlation for the thermal conductivity of three nano-fluids over a temperature range of 298–363 K, taking into account the effect of Brownian motion on the thermal conductivity as a function of temperature [238]. They compared their experimental results with those of several existing models [239–247] and found a good agreement. The results indicated that the thermal conductivity of nano-fluids increased with the volume fraction of nano-particles as well as with the increase in the temperature. A subsequent paper examined the impact on heat

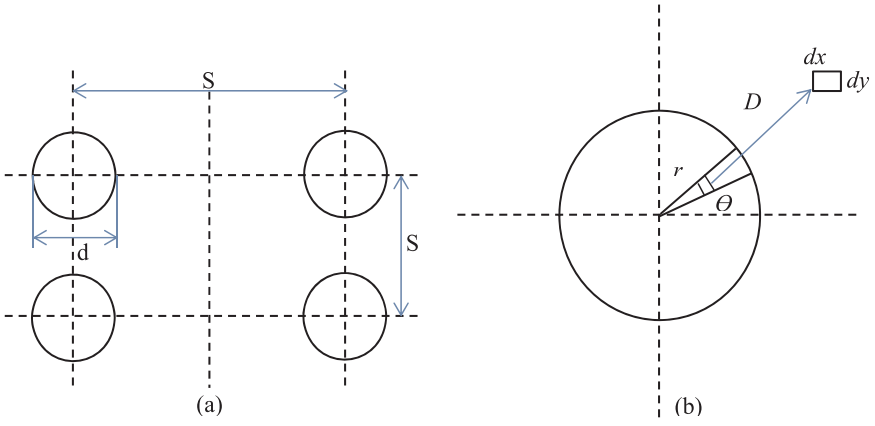

Fig. 23. (a) Physical model and (b) CNT arrangement [228].

transfer of nano-fluid circulating within the flat tubes of an automobile radiator [248]. Using the thermo-physical properties of nano-fluids derived in their previous work [236,238], the problem was solved using the control volume method in FLUENT software. The authors demonstrated that the average heat transfer coefficient significantly increased as the particle volumetric concentration increased. Nevertheless, increasing nano-particles resulted in an increase in the local skin friction, which caused a large pressure drop across the flat tube. Khanafer et al. performed numerical simulations to analyse the heat transfer behaviour of a nano-fluid inside a two-dimensional enclosure for a range of Grashof numbers and volume fractions [210]. The findings seemed to be consistent with those of other researchers [249–252]. The study found that the addition of nano-particles considerably increased the heat transfer rate for any given Grashof number. Furthermore, heat transfer increased with the nanoparticle volume fraction.

A correlation was proposed for the average Nusselt number as a function of the Grashof number ($10^{3<<}G_r^{<<}10^5$) and the nanoparticle volume fraction ($0 \leq \theta \leq 0.25$). Li and Xuan also established a new convective heat transfer correlation for Cu-water nano-fluid under a single-phase fluid model [253]. These correlations are presented below:

$$\overline{Nu} = 0.5163(0.4436 + \varnothing^{1.0809})\, Gr^{0.3123} \quad [210] \tag{27}$$

$$\overline{Nu_{nf}} = 0.4328(1 + 11.285\phi^{0.754} Pe_d^{0.218}) Re_{nf}^{0.333} Pr_{nf}^{0.4} \quad \text{(for laminar Flow)} \quad [253] \tag{28}$$

$$\overline{Nu_{nf}} = 0.0059(1 + 7.6286\varnothing^{0.6886} Pe_d^{0.001}) Re_{nf}^{0.9238} Pr_{nf}^{0.4} \text{ (For turbulent flow)} \quad [253] \tag{29}$$

Abdulhassan et al. experimentally studied the heat transfer performance of nano-fluids circulating through a horizontal tube [254]. Experimental measurements of the nano-fluids thermo-physical properties were compared with results of several studies [221,237,240,255–258] with a deviation not exceeding 3.5%. The results indicated that the presence of nano-particles significantly increased the heat transfer rate as well as the thermo-physical properties of the nano-fluid. The most interesting finding was that circulating nano-fluids through the tube did not result in a large drop in pressure, because nano-particles did not affect the flow behaviour. Gavtash et al. obtained similar results from a numerical study of the nano-fluid in a cylindrical heat pipe [259]. A 2-D model of the heat pipe was created using FLUENT software. The authors found that the nano-fluid improved the heat transfer rate in the heat pipe and reduced its thermal resistance. A preliminary work on heat transfer enhancement was undertaken by Xuan and Roetzel [258]. Two methods were presented to analyse the convective heat transfer with nano-fluids. The first considered the nano-fluid as a single phase fluid, while the other considered it as a multiphase fluid made of the nano-fluid and the particles.

Maïga et al. also reported that nano-particles substantially increase the heat transfer compared to base fluid [260]. They attempted to provide correlations for the Nusselt numbers of nano-fluids in terms of Reynolds and Prandtl numbers. Syam Sundar et al. used FLUENT software to numerically investigate the laminar flow and heat transfer characteristics with three different nano-fluids, namely AL_2O_3, CuO and TiO_2, in a circulating tube [261]. Particle concentrations were in the range from 0.3% to 2%, and the results revealed that the heat transfer coefficient increased with particle concentration. In addition, the highest heat transfer coefficient was provided by AL_2O_3 nano-particles, followed by CuO, with the lowest by TiO_2. Sasmito et al. also studied the laminar flow heat transfer problem in square cross-section tubes with two different nano-fluids, namely AL_2O_3 and CuO in water [262]. The heat transfer was improved with nano-fluids and AL_2O_3 provided a better performance than CuO. According to Wen and Ding [263], particle migration is the reason for the enhancement of the convective heat transfer and results in a non-uniform distribution of the thermal conductivity and the viscosity field as well as a reduction in the thermal boundary layer thickness.

Mahdi et al. [264] developed a numerical model to study the effects of nanoparticles and fins on the solidification enhancement processes of PCM in a triplex-tube thermal energy storage system. The volume for PCM storage, the fin, nanoparticle and total volume fractions were examined and evaluated for several cases of using fins and nano-particles as heat transfer methods. One of the more significant findings to emerge from this study is that the total solidification time has reduced remarkably with fins compared with using either nanoparticles alone or combination nanoparticles with fins. The two-dimensional turbulent flow and heat transfer with three different nano-fluids (AL_2O_3, CuO and SiO_2 in water) circulating through a circular tube under constant heat flux were numerically investigated by Namburu et al. in [265]. The authors developed a new correlation for the Nusselt number and viscosity for nano-fluids with up to 10% volume fraction of nano-particles. They compared their model's results with the correlation presented by Gnielinski in [266] and found a good agreement. Based on their results, they stated that the heat transfer coefficient of nanofluids increased with the volume fraction of nano-particles and Reynolds number. The analysis indicated that CuO nano-fluid had a higher heat transfer performance than AL_2O_3 and SiO_2.. Several methods were used in literature to calculate the dynamic viscosity and thermal conductivity of nano-fluids, as summarised in Tables 6 and 7 respectively.

4.2.3.3. Microencapsulation. A microencapsulated phase change material (MEPCM) is obtained by placing a micro-size solid/liquid PCM core within a solid structure (shell/wall) [273]. A wide range of materials can be used to make the shell, including natural and synthetic polymers [274]. MEPCMs can be prepared by two methods, namely complex coacervation and spray drying, details of which can be found in [274–278]. Xuan et al. experimentally investigated the effect of microencapsulated PCM components on the specific heat capacity and thermal conductivity of a MEPCM suspension [279]. The MEPCM core was paraffin while the shell was made of melamine urea formed from aldehyde resin and iron particles. It was reported that the specific heat of the MEPMC depended on the temperature inside the MEPCM and the volume fraction of the MEPCM particles. In addition, the specific heat capacity of the suspension in the solid region was smaller than that in the liquid region for the same volume of MEPCM. On the other hand, the thermal conductivity increased linearly with the volume fraction of the MEPCM and it also increased with the iron nano-particles inside the MEPCM.

Salaün et al. used microcapsules filled with paraffin and nano-particles of polyvinyl alcohol/hydrated salt to decrease the thermal conductivity of a PCM [280]. They also found that polymer nano-particles did not affect the latent heat, but that the phase change took place over

Table 6
A list of methods used to determine the nano-fluid effective thermal conductivity.

NO	Model	Dynamic viscosity	Remark
1.	Brinkman [267]	$\mu_{nf} = \mu_f(1-\varnothing)^{-2.5}$	$\varnothing$ is nanoparticle volume fraction
2.	Maïga et al. [260]	$\mu_{nf} = \mu_f(1 + 7.3\varnothing + 123\varnothing^2)$	$\varnothing$ is nanoparticle volume fraction
3.	Vajjha [236]	$\mu_{nf} = \mu_f A_2 e^{(C_2\varnothing)}$	$293\ K \leq T \leq 363\ K$ $0.01 \leq \varnothing \leq 0.1$
4.	Ashrae [268]	$\mu_{nf} = \mu_f A_4 e^{\left(\frac{B_4}{T}\right)}$	$293K \leq T \leq 363K$ $B_4 = 2664$
5.	Namburu et al. [269]	$\log \mu_{nf} = Ae^{-BT}$	A and B are cubic polynomial functions of the particles volumetric concentration $T \leq 50^{\circ}C$
6.	Sahoo et al. [270]	$\mu_{nf} = A_1 e^{\left(\frac{B_1}{T} + q_1 C_1 \varnothing\right)}$	$T \geq 90^{\circ}C$

Table 7
List of methods used to determine the nano-fluid dynamic viscosity.

No	Model	Thermal conductivity	Remarks
1.	Maxwell [222]	$\frac{K_{nf}}{K_L} = \frac{K_s + 2K_L + 2(K_s - K_L)\varnothing_s}{K_s + 2K_L - (K_s - K_L)\varnothing_s}$	$\varnothing_s$: solid volume fraction
2.	Charunyakorn et al. [271]	$K_e = K_m\,(1 + b\varnothing Pe_p^{\varnothing})$	
3.	Hamilton and Crosser [256]	$\frac{K_{nf}}{K_L} = \frac{K_s + (n-1)K_L - (n-1)\varnothing_s(K_L - K_s)}{K_s + (n-1)K_f + \varnothing_s(K_L - K_s)}$	n dependent on particle shape and K_s/K_L, $n = 3/\psi$
4.	Jeffrey [223]	$\frac{K_{nf}}{K_L} = 1 + 3\phi_s\left(\frac{K_s/K_L - 1}{K_s/K_L + 2}\right) + 3\phi_s{}^2\left(\frac{K_s/K_L - 1}{K_s/K_L + 2}\right)\cdot\left[1 + \frac{1}{4}\left(\frac{K_s/K_L - 1}{K_s/K_L + 2}\right) + \frac{3}{16}\left(\frac{K_s/K_L - 1}{K_s/K_L + 2}\right)\left(\frac{K_s/K_L - 2}{K_s/K_L + 3}\right) + ..\right]$	
5.	Davis [224]	$\frac{K_{nf}}{K_L} = 1 + \frac{3(K_s/K_L - 1).[\varnothing_s + f.\varnothing_S^2 + O(\varnothing_S^3)]}{(K_s/K_L + 2) - (K_s/K_L - 1)\varnothing_s}$ $f(\alpha) = 2.5\ for\ \alpha = 10, \quad f(\alpha) = 0.5\ for\ \alpha = \infty,$	Accurate to order $\varnothing^2$
6.	Bruggeman [239]	$\frac{K_{nf}}{K_L} = \left[(3\varnothing_s - 1)\frac{K_s}{K_f} + (2 - 3\varnothing_s) + \sqrt{\Delta}\right]/4$ $\Delta = (3\varnothing_s - 1)^2(K_s/K_L)^2 + (2 - 3\varnothing_s)^2 + 2(2 + 9\varnothing_s - 9\varnothing_s^2)\,(K_s/K_L)$	Spherical particles
7.	Yu and Choi [240]	$K_{pe} = \frac{[2(1-\gamma) + (1+\chi)^3(1+2\gamma)]\gamma}{-(1-\gamma) + (1+\chi)^3(1+2\gamma)}K_s\frac{K_{nf}}{K_L} = \frac{K_{pe} + 2K_L + 2(K_{pe} - K_L)(1+\chi)^3\varnothing_s}{K_{pe} + 2K_L - (K_{pe} - K_L)(1+\chi)^3\varnothing_s}$ $\gamma = K_{layer}/K_s,\ \chi = h/r,\ 10K_L < K_{layer} < 100K_L$	h is nano-layer thickness K_{layer} is nanolayer thermal conductivity r is particles radius
8.	Xuan et al. [241]	$\frac{K_{nf}}{K_L} = \frac{K_s + 2K_L + 2(K_s - K_L)\varnothing_s}{K_s + 2K_L - (K_s - K_L)\varnothing_s} + \frac{\rho_s\varnothing C p_s}{2}\sqrt{\frac{KT}{3\pi\mu_L r_c}}$	r_c is the mean radius of gyration of cluster
9.	Koo and Kleinstreuer [242,243]	$\frac{K_{nf}}{K_L} = \frac{K_s + 2K_L + 2(K_s - K_L)\varnothing_s}{K_s + 2K_L - (K_s - K_L)\varnothing_s} + 5\times10^4\beta\varnothing\rho_L Cp_L\sqrt{\frac{KT}{\rho_s d_s}}f(T,\ \varnothing,\ etc.)$	β is fraction of liquid volume
10.	Xue and Xu [244]	$\left(1 - \frac{\varnothing}{\omega}\right)\times\frac{K_{nf} - K_L}{2K_{nf} + K_L} + \frac{\varnothing}{\omega}\frac{\left(K_{nf} - K_2\right)(2K_2 + K_s) - \omega(K_s - K_2)\left(2K_2 + K_{nf}\right)}{\left(2K_{nf} + K_2\right)(2K_2 + K_s) + 2\omega(K_s - K_2)\left(K_2 - K_{nf}\right)} = 0$ $\omega = \left[\frac{r_s}{r_s + t}\right]^3$	K_2: is thermal conductivity of the interfacial shell. T: is the thickness of interfacial shell
11.	Chon et al. [245]	$\frac{K_{nf}}{K_L} = 1 + 64.7\varnothing^{0.7460}\left(\frac{d_L}{d_s}\right)^{0.3690}\left(\frac{K_s}{K_L}\right)^{0.7476}Pr^{0.9955}Re^{1.2321}$ $\mathrm{Pr} = \frac{Cp_L\mu_L}{K_L}, \quad \mathrm{Re} = \frac{\rho_L KT}{3\pi\mu_L^2 l_L}$	l_L is mean-free path for the fluid
12.	Prasher et al. [246]	$\frac{K_{nf}}{K_L} = (1 + A\,\mathrm{Re}^m\,\mathrm{Pr}^{0.333}\varnothing)\left(\frac{[K_s(1+2\alpha) + 2K_m] + 2\varnothing[K_s(1-\alpha) - K_m]}{[K_s(1+2\alpha) + 2K_m] - \varnothing[K_s(1-\alpha) - K_m]}\right)$ $\mathrm{Re} = \frac{1}{\nu}\sqrt{\frac{18KT}{\pi\rho_s d_s}}, \quad K_m = K_L[1 + (1/4)\mathrm{Re.Pr}], \quad \alpha = 2R_bK_m/D_s$	$A = 4\times10^4$ R_b is the interfacial thermal resistance between nano-particles and fluid
13.	Jang and Choi [247]	$\frac{K_{nf}}{K_L} = (1 - \varnothing) + \beta_1 K_p\varnothing + C_1\frac{d_L}{d_s}K_L Re_{dp}^2 Pr\varnothing$ $Re_{dp} = \frac{\overline{C}_{R.M}d_s}{\nu}, \overline{C}_{R.M} = \frac{KT}{3\pi\mu_L d_s l_L}$	$C_1 = 18\times10^6$
14.	Vajjha and Das [238]	$\frac{K_{nf}}{K_L} = \frac{K_s + 2K_L + 2(K_s - K_L)\varnothing_s}{K_s + 2K_L - (K_s - K_L)\varnothing_s} + 5\times10^4\beta\varnothing\rho_L Cp_L\sqrt{\frac{KT}{\rho_s d_s}}f(T,\ \varnothing)$ $f(T,\varnothing) = (2.8217\times10^{-2} + 3.917\times10^{-3})\left(\frac{T}{T_0}\right) + (-3.0669\times10^{-2}\varnothing - 3.91123\times10^{-3})$ for AL_2O_3 particles, $\beta = 8.4407(100\varnothing)^{-1.07304}$, $0.01 \le \varnothing \le 0.1$ for Zno particles, $\beta = 8.4407(100\varnothing)^{-1.07304}$, $0.01 \le \varnothing \le 0.07$ for CuO particles, $\beta = 9.881(100\varnothing)^{-0.9446}$, $0.01 \le \varnothing \le 0.06$	Temperature range $298 \le T \le 363K$
15.	Wang et al. [217]	$\frac{K_{nf}}{K_L} = \frac{(1-\varnothing) + 3\varnothing\int_0^\infty \frac{K_s(r)n(r)}{K_s n(r) + 2K_L}dr}{(1-\varnothing) + 3\varnothing\int_0^\infty \frac{K_s n(r)}{K_s(r) + 2K_L}dr}$	$n(r)$ is the radius distribution function
16.	Keblinski et al. [272]	$\frac{K_{nf}}{K_L} = (1 - \varnothing) + K_s\varnothing + 3C\frac{d_1}{d_s}K_L\,\mathrm{Re}_d^2\mathrm{Pr}\varnothing$ $\mathrm{Re}_{dp} = \frac{\overline{C}_{R.M}d_s}{\nu}$	$\overline{C}_{R.M}$ is the random motion velocity of nano-particles

a wide range of temperatures compared to pure paraffin. Hu and Zhang carried out a numerical investigation of the enhancement of convective heat transfer in a microencapsulated PCM [281]. The model analysed the effect of various factors on the heat transfer enhancement in a laminar flow in a circular tube with a constant wall temperature. These numerical simulations compared favourably with the results of the experimental investigation in [282]. In [283], the authors conducted similar analysis for a circular tube with a constant heat flux, using the effective specific heat capacity model. The numerical simulation results were supported by findings of Alisetti and Roy in [284], namely that the Stefan number, mass flow rate of HTF and volumetric concentration of microcapsules can improve the heat transfer rate.

Alvarado et al. experimentally studied the enhancement of heat transfer in a microencapsulated PCM under constant heat flux and turbulence conditions [285]. The results indicated that the microencapsulated PCM substantially increased the heat transfer even with a low mass fraction. The analysis of results further indicated that the material's melting point was affected by slurry velocity more than heat flux. Su et al. investigated the influence of the core/shell ratio of microPCMs, their average diameter and the thermal conductivity on the phase change behaviour [286] and found that the shell thickness did not have a strong effect. However, higher volume fractions of microPCMs and smaller size enhanced the thermal conductivity of the composite. Özonur et al. used a microencapsulated natural coco fatty

Table 8
Literature on PCM heat transfer intensification using filling materials.

No	Author	Methods	PCM	Enhancement method	Process	Validation
1.	Ho and Gao [200]	Experimental	*N-octadecane*	Nano-particles	Charging and discharging	Yes [201]
2.	Wu et al. [202]	Experimental	Paraffin wax	Nano-particles	Charging and discharging	Yes [200,290–294]
3.	Zeng et al. [203]	Experimental	Tetradecanol (TD)	Nano-particles	Charging process	No
4.	Arasu [204–206]	Numerical	Paraffin wax	Nano-particles	Charging and discharging	Yes [200,209]
5.	Khodadadi and Fan [207]	Numerical	Cyclohexane and water	Nano-particles	Discharging process	Yes
6.	Fan and Khodadadi [208]	Experimental	Cyclohexane and water	Nano-particles	Discharging process	Yes
7.	Khodadadi and Hosseinizadeh [209]	Numerical	Water	Nano-particles	Discharging process	Yes [210–213]
8.	Putnam et al. [295]	Numerical	Polymethylmethacrylate	Nano-particles	–	No
9.	Ranjbar et al. [214]	Numerical	–	Nano-particles	Discharging process	Yes [33,209–211]
10.	Kim and Drzal [215]	Experimental	Paraffin	Nano-platelets of exfoliated graphite (xgnp)	Charging process	No [218]
11.	Liu et al. [216]	Experimental	$Bacl_2$	Nano-particles	Charging and discharging	No
12.	Wang [217]	Numerical modelling	Water	Nano-particles	Charging (melting) process	Yes
13.	Seeniraj [219]	Numerical	*N-Octadecane*	Dispersed particles	Charging process	No
14.	Siegel [220]	Numerical	*N-Octadecane*	Dispersed particles	Discharging process	No
15.	Wang and Choi [221]	Experimental and Numerical	Distilled water, ethylene glycol, engine oil, and vacuum pump fluid	Nano-particles		Yes [222–227]
16.	Shaikh [228]	Experimental and Numerical	Paraffin wax	Nano-particles	Charging process	Yes
17.	Halte et al. [296]	Experimental	–	Nano-particles	–	No
18.	Elgafy and Lafdi [297]	Experimental and Numerical	Paraffin wax	Nano-particles	Discharging process	Yes
19.	Zeng et al. [298]	Experimental	Nitric acid	Nano-particles	Charging process	No
20.	Zeng et al. [299]	Experimental	Tetradecanol	Nano-particles	Charging process	No
21.	Wu et al. [300]	Experimental	Water	Nano-particles	Discharging process	Yes [301,302]
22.	Ho [235]	Numerical	Water	Nano-fluids	Charging process	Yes [251,252]
23.	Vajjha [236]	Experimental	Ethylene glycol and water	Nano-fluid	Charging process	Yes [237]
24.	Vajjha and Das [238,248]	Experimental and Numerical	Ethylene glycol and water	Nano-fluid	Charging process	Yes models [239–247]
25.	Khanafer [210]	Numerical	–	Nano-fluid	Charging process	Yes [249–252]
26.	Abdulhassan [254]	Experimental	Water	Nano-fluid	Charging process	Yes [221,237,240,255–258]
27.	Gavtash et al. [259]	Numerical	Water	Nano-fluid	Charging process	No
28.	Maïga et al. [260]	Numerical	Water and ethylene glycol	Nano-fluid	Charging process	Yes [303]
29.	Syam Sundar et al. [261]	Numerical	Water	Nano-fluid	Charging process	Yes [304]
30.	Sasmito [262]	Numerical	Water	Nano-fluid	Discharging process	Yes [305]
31.	Wen and Ding [263]	Experimental	Water	Nano-fluid	Charging process	Yes [304]
32.	Namburu et al. [265]	Numerical	Water	Nano-fluid	Charging process	Yes [266]
33.	Xuan and Roetzel [258]	Numerical	Water	Nano-fluid	Charging process	Yes
34.	Li and Xuan [253]	Experimental	Water	Nano-fluid	Charging process	Yes
35.	Keblinski et al. [272]	Numerical	–	Nano-fluid	Charging process	No
36.	Wang [306]	Experimental	Water	Nano-fluid	Charging process	No
37.	Bönnemann et al. [307]	Experimental	Water	Nano-fluid	Charging process	No
38.	Gao et al. [308]	Experimental	Water	Nano-fluid	Charging and discharging process	No
39.	Chein and Huang [309]	Numerical	Water	Nano-fluid	Discharging process	Yes [310]
40.	Xuan [279]	Experimental	Paraffin	Microcapsules	Charging process	No
41.	Salaün et al. [280]	Experimental	Paraffin	Microcapsules	Charging process	No
42.	Hu and Zhang [281]	Numerical	Water	Microcapsules	Charging process	Yes [282]
43.	Zhang [283]	Numerical	Water	Microcapsules	Charging process	Yes [284]
44.	Alvarado et al. [285]	Experimental	Water	Microcapsules	Charging and discharging	No
45.	Su et al. [286]	Experimental	Paraffin	Microcapsules	Charging process	No
46.	Özonur et al. [287]	Experimental	Natural coco a fatty acid mixture	Microcapsules	Charging and discharging	No
47.	Rao et al. [288]	Experimental	*N-Octadecane*	Microcapsules	Charging and discharging	No
48.	Brown [289]	Experimental	Octadecane and paraffin	Microcapsules	Charging process	No

acid mixture as a PCM for a thermal storage system [287]. The transition temperature and the stability of the thermal energy storage of the PCM were investigated during both the charging and discharging processes. It was demonstrated that the thermal properties of the microencapsulated PCM were stable after 50 cycles. Rao et al. experimentally investigated the enhancement of the convective heat transfer in microencapsulated PCM-water additives flowing through rectangular mini channels [288]. It was found that an increase in the mass flow rate and MEPCM volume substantially increased the heat transfer rate. The analysis also indicated that the thermal performance of the suspensions

with a higher mass concentration was less effective at high mass flow rates due to the shorter residence time of the MEPCM additives.

The effects of several microencapsulated products on the heat transfer in gas-fluidized beds were examined by Brown et al. [289]. Paraffin and octadecane were used as MEPCM cores, while the shells were made of polymethylene-urea, cross-linked nylon and gelatine. The results revealed that the octadecane/gelatine MEPCM exhibited better heat transfer performance. Furthermore, the heat transfer was enhanced by 85% during the phase transition compared to that of the single phase. A considerable number of research studies were published on heat transfer enhancement in PCMs using nanoparticles, as summarised in Table 8. The studies were classified according to several metrics and parameters similar to those used in previously presented tables.

5. Conclusions

This paper presents an extensive review of a number of significant studies relevant to the topic of thermal storage systems. The techniques deployed to enhance the energy performance of thermal storage systems and the methods used to improve heat transfer in phase change materials were analysed. From the review, it can be seen that encapsulation and packed beds technologies have been well investigated, both analytically and experimentally, in a large volume of published papers. Parameters such as designs and configurations, PCM materials, and heat transfer enhancement methods are used among others to contrast the individual research studies. However, a limited number of studies have been devoted to assessing the pressure drops observed in packed bed thermal storage systems and determining the friction factor as a function of the size, shape, and geometry of the packed bed system.

Different geometries and configurations of fins and other types of extended surfaces, porous media, metal foams, matrix materials and graphite materials have been extensively studied as means to enhance the heat transfer process in thermal storage systems by increasing the effective thermal conductivity in the mixture of phase change materials and additive components. The key disadvantage with the above methods is that it is necessary to increase the system volume in order to provide the same amount of stored energy. A considerable number of studies have been devoted to investigating the effect of nano-fluids, nano-particles, and microencapsulation on the thermal performance of LHTSs. The results of these studies indicate that the higher heat transfer rates in PCMs with filling materials were due to the PCM's increased thermal conductivity

One of the important outcomes of this literature review is highlighting the significant role that the natural convection plays during the PCM solidification and melting processes. The natural convection flows are extremely sensitive to the geometry and size of the enclosures and depend on the density, viscosity and thermal conductivity of the phase change materials used. Therefore, a detailed study of the natural convection inside storage systems with liquid PCMs is very important for the storage system design process.

References

[1] Boden TA, Marland G, Andres RJ. Global, regional, and national fossil fuel CO_2 Emissions. Carbon Dioxide Information Analysis Center, Environmental Sciences Division , Oak Ridge National Laboratory; 2011http://cdiac.ess-dive.lbl.gov/trends/emis/overview_2011.html.

[2] IEA. Technology roadmaps solar photovoltaic energy.

[3] Goswami DY, Kreith F, Kreider JF. Principles of solar engineering. Second edition Taylor & Francis; 2000.

[4] Abhat A. Low temperature latent heat thermal energy storage: heat storage materials. Sol Energy 1983;30:313–32.

[5] Castell A, Solé C. An overview on design methodologies for liquid–solid PCM storage systems. Renew Sustain Energy Rev 2015;52:289–307. [12/01/ 2015].

[6] Ibrahim NI, Al-Sulaiman FA, Rahman S, Yilbas BS, Sahin AZ. Heat transfer enhancement of phase change materials for thermal energy storage applications: a critical review. Renew Sustain Energy Rev 2017;74:26–50. [2017/07/01/].

[7] Khan MMA, Saidur R, Al-Sulaiman FA. A review for phase change materials (PCMs) in solar absorption refrigeration systems. Renew Sustain Energy Rev 2017;76:105–37. [2017/09/01/].

[8] Safari A, Saidur R, Sulaiman FA, Xu Y, Dong J. A review on supercooling of phase change materials in thermal energy storage systems. Renew Sustain Energy Rev 2017;70:905–19. [2017/04/01/].

[9] Pereira J, da Cunha, Eames P. Thermal energy storage for low and medium temperature applications using phase change materials – A review. Appl Energy 2016;177:227–38. [2016/09/01/].

[10] Tay NHS, Liu M, Belusko M, Bruno F. Review on transportable phase change material in thermal energy storage systems. Renew Sustain Energy Rev 2017;75:264–77. [2017/08/01/].

[11] Zhou Z, Zhang Z, Zuo J, Huang K, Zhang L. Phase change materials for solar thermal energy storage in residential buildings in cold climate. Renew Sustain Energy Rev 2015;48:692–703. [2015/08/01/].

[12] Muhammad M. Review of PCMS and heat transfer enhancement methods applied in parabolic trough solar plants thermal storage systems. Niger J Technol 2018;37.

[13] Kenisarin M, Mahkamov K. Solar energy storage using phase change materials. Renew Sustain Energy Rev 2007;11:1913–65.

[14] Farid MM, Khudhair AM, Razack SAK, Al-Hallaj S. A review on phase change energy storage: materials and applications. Energy Convers Manag 2004;45:1597–615.

[15] Agyenim F, Hewitt N, Eames P, Smyth M. A review of materials, heat transfer and phase change problem formulation for latent heat thermal energy storage systems (LHTESS). Renew Sustain Energy Rev 2010;14:615–28.

[16] Zalba B, Marín JM, Cabeza LF, Mehling H. Review on thermal energy storage with phase change: materials, heat transfer analysis and applications. Appl Therm Eng 2003;23:251–83.

[17] Regin AF, Solanki SC, Saini JS. Heat transfer characteristics of thermal energy storage system using PCM capsules: a review. Renew Sustain Energy Rev 2008;12:2438–58.

[18] de Gracia A, Cabeza LF. Numerical simulation of a PCM packed bed system: a review. Renew Sustain Energy Rev 2017;69:1055–63. [2017/03/01/].

[19] Jacob R, Bruno F. Review on shell materials used in the encapsulation of phase change materials for high temperature thermal energy storage. Renew Sustain Energy Rev 2015;48:79–87. [2015/08/01/].

[20] Abokersh MH, Osman M, El-Baz O, El-Morsi M, Sharaf O. Review of the phase change material (PCM) usage for solar domestic water heating systems (SDWHS). Int J Energy Res 2018;42:329–57.

[21] Milián YE, Gutiérrez A, Grágeda M, Ushak S. A review on encapsulation techniques for inorganic phase change materials and the influence on their thermophysical properties. Renew Sustain Energy Rev 2017;73:983–99. [2017/06/01/].

[22] Felix Regin A, Solanki SC, Saini JS. An analysis of a packed bed latent heat thermal energy storage system using PCM capsules: numerical investigation. Renew Energy 2009;34:1765–73.

[23] Abdel-Rehim Zeinab S, Lashine A. Packed bed-PCM material latent heat thermal energy storage system. ESRJ– Fac Eng Shoubra 2011;14:23.

[24] Cho K, Choi SH. Thermal characteristics of paraffin in a spherical capsule during freezing and melting processes. Int J Heat Mass Transf 2000;43:3183–96.

[25] Bédécarrats JP, Strub F, Falcon B, Dumas JP. Phase-change thermal energy storage using spherical capsules: performance of a test plant. Int J Refrig 1996;19:187–96.

[26] Dumas JP, Bedecarrats JP, Strub F, Falcon B. "Modelization of a tank filled with spherical nodules containing a phase change material," In: Proceedings of the 10th international heat transfer conference, Brighton; 1994.

[27] Ismail KAR, Henríquez JR. Numerical and experimental study of spherical capsules packed bed latent heat storage system. Appl Therm Eng 2002;22:1705–16.

[28] Singh R, Saini RP, Saini JS. Simulated performance of packed bed solar energy storage system having storage material elements of large size - Part I. Open Fuels Energy Sci J 2008:91–6.

[29] Singh R, Saini RP, Saini JS. Simulated performance of packed bed solar energy storage system having storage material elements of large size - Part II. Open Fuels Energy Sci J 2008:97–101.

[30] Singh R, Saini RP, Saini JS. Simulated performance of packed bed solar energy storage system having storage material elements of large size - Part III. Open Fuels Energy Sci J 2008:102–6.

[31] Singh R, Saini RP, Saini JS. Models for predicting thermal performance of packed bed energy storage for solar air heaters- A review. Open Fuels Energy Sci J 2009;2:47–53.

[32] Wang J, Ouyang Y, Chen G. Experimental study on charging processes of a cylindrical heat storage capsule employing multiple-phase-change materials. Int J Energy Res 2001;25:439–47.

[33] Zivkovic B, Fujii I. An analysis of isothermal phase change of phase change material within rectangular and cylindrical containers. Sol Energy 2001;70:51–61.

[34] Tan FL, Hosseinizadeh SF, Khodadadi JM, Fan L. Experimental and computational study of constrained melting of phase change materials (PCM) inside a spherical capsule. Int J Heat Mass Transf 2009;52:3464–72.

[35] Tan FL, Chan CW. Solidification inside a sphere—an experimental study. Int Commun Heat Mass Transf 2006;33:335–41.

[36] Tan FL. Constrained and unconstrained melting inside a sphere. Int Commun Heat Mass Transf 2008;35:466–75.

[37] Koizumi H. Time and spatial heat transfer performance around an isothermally heated sphere placed in a uniform, downwardly directed flow (in relation to the enhancement of latent heat storage rate in a spherical capsule). Appl Therm Eng 2004;24:2583–600.

[38] Yuge T. Experiments on heat transfer from spheres including combined natural and forced convection. J Heat Transf 1960;82:214–20.

[39] Jia H, Gogos G. Laminar natural convection heat transfer from isothermal spheres.

Int J Heat Mass Transf 1996;39:1603–15.
[40] Beasley DE, Ramanarayanan C. Thermal response of a packed bed of spheres containing a phase-change material. Int J Energy Res 1989;13:253–65.
[41] Khalil A, Kassem MAEW, Salama M. Experimental evaluation of packed bed heat transfer relations. J Eng Comput Sci 2008;1:43–55.
[42] Nsofor EC, Adebiyi GA. Measurements of the gas-particle convective heat transfer coefficient in a packed bed for high-temperature energy storage. Exp Therm Fluid Sci 2001;24:1–9.
[43] Varun F, Singh SK, Tyagi, Nautiyal H. Experimental investigation of packed bed solar thermal energy system with cylindrical elements. Int J Sci Technol 2010;1:43–50.
[44] Shiina Y, Inagaki T. Study on the efficiency of effective thermal conductivities on melting characteristics of latent heat storage capsules. Int J Heat Mass Transf 2005;48:373–83.
[45] Hawlader MNA, Uddin MS, Zhu HJ. Encapsulated phase change materials for thermal energy storage: experiments and simulation. Int J Energy Res 2002;26:159–71.
[46] Chen SL. One-dimensional analysis of energy storage in packed capsules. Trans ASAE (United States) 1992;114:127–30.
[47] Chen SL, Yue JS. A simplified analysis for cold storage in porous capsules with solidification. J Energy Resour Technol (United States) 1991;113(2):108–16.
[48] Silva PD, Gonçalves LC, Pires L. Transient behaviour of a latent-heat thermal-energy store: numerical and experimental studies. Appl Energy 2002;73:83–98.
[49] Bilir L, İlken Z. Total solidification time of a liquid phase change material enclosed in cylindrical/spherical containers. Appl Therm Eng 2005;25:1488–502.
[50] Ismail KAR, Henríquez JR. Solidification of pcm inside a spherical capsule. Energy Convers Manag 2000;41:173–87.
[51] Ismail KAR, Stuginsky Jr R. A parametric study on possible fixed bed models for pcm and sensible heat storage. Appl Therm Eng 1999;19:757–88.
[52] Farid MM, Husian RM. An electrical storage heater using the phase-change method of heat storage. Energy Convers Manag 1990;30:219–30.
[53] Kousksou T, Bédécarrats JP, Dumas JP, Mimet A. Dynamic modelling of the storage of an encapsulated ice tank. Appl Therm Eng 2005;25:1534–48.
[54] Eames IW, Adref KT. Freezing and melting of water in spherical enclosures of the type used in thermal (ice) storage systems. Appl Therm Eng 2002;22:733–45.
[55] Hirata T, Makino Y, Kaneko Y. Analysis of close-contact melting for octadecane and ice inside isothermally heated horizontal rectangular capsule. Int J Heat Mass Transf 1991;34:3097–106.
[56] Khodadadi JM, Zhang Y. Effects of buoyancy-driven convection on melting within spherical containers. Int J Heat Mass Transf 2001;44:1605–18.
[57] Fomin SA, Saitoh TS. Melting of unfixed material in spherical capsule with non-isothermal wall. Int J Heat Mass Transf 1999;42:4197–205.
[58] Saito A, Okawa S, Shintani T, Iwamoto R. On the heat removal characteristics and the analytical model of a thermal energy storage capsule using gelled Glauber's salt as the PCM. Int J Heat Mass Transf 2001;44:4693–701.
[59] Yagi J, Akiyama T. Storage of thermal energy for effective use of waste heat from industries. J Mater Process Technol 1995;48:793–804.
[60] Benmansour A, Hamdan MA, Bengeuddach A. Experimental and numerical investigation of solid particles thermal energy storage unit. Appl Therm Eng 2006;26:513–8.
[61] Katayama K, Saito A, Utaka Y, Saito A, Matsui H, Maekawa H, et al. Heat transfer characteristics of the latent heat thermal energy storage capsule. Sol Energy 1981;27:91–7.
[62] Wei J, Kawaguchi Y, Hirano S, Takeuchi H. Study on a PCM heat storage system for rapid heat supply. Appl Therm Eng 2005;25:2903–20.
[63] Arkar C, Medved S. Influence of accuracy of thermal property data of a phase change material on the result of a numerical model of a packed bed latent heat storage with spheres. Thermochim Acta 2005;438:192–201.
[64] Lacroix M. Contact melting of a phase change material inside a heated parallelepedic capsule. Energy Convers Manag 2001;42:35–47.
[65] Assis E, Katsman L, Ziskind G, Letan R. Numerical and experimental study of melting in a spherical shell. Int J Heat Mass Transf 2007;50:1790–804.
[66] Jian-you L. Numerical and experimental investigation for heat transfer in triplex concentric tube with phase change material for thermal energy storage. Sol Energy 2008;82:977–85.
[67] Mellouli S, Askri F, Abhilash E, Nasrallah S Ben. Impact of using a heat transfer fluid pipe in a metal hydride-phase change material tank. Appl Therm Eng 2017;113:554–65. [2017/02/25/].
[68] Ho CJ, Chen S. Numerical simulation of melting of ice around a horizontal cylinder. Int J Heat Mass Transf 1986;29:1359–69.
[69] White DA. Melting of ice and freezing of water around a horizontal cylinder. Indiana: M.S Purdue University; 1984.
[70] Rieger H, Projahn U, Beer H. Analysis of the heat transport mechanisms during melting around a horizontal circular cylinder. Int J Heat Mass Transf 1982;25:137–47.
[71] Dimaano MNR, Watanabe T. Performance investigation of the capric and lauric acid mixture as latent heat energy storage for a cooling system. Sol Energy 2002;72:205–15.
[72] Bareiss M, Beer H. An analytical solution of the heat transfer process during melting of an unfixed solid phase change material inside a horizontal tube. Int J Heat Mass Transf 1984;27:739–46.
[73] Ismail KAR, Abugderah MM. Performance of a thermal storage system of the vertical tube type. Energy Convers Manag 2000;41:1165–90.
[74] Al-Maghalseh MM. Investigate the natural convection heat transfer in a PCM thermal storage system using ANSYS/FLUENT. JJMIE 2017;11.
[75] Sari A, Kaygusuz K. Thermal performance of a eutectic mixture of lauric and stearic acids as PCM encapsulated in the annulus of two concentric pipes. Sol Energy 2002;72:493–504.
[76] Sari A, Kaygusuz K. Thermal energy storage system using stearic acid as a phase change material. Sol Energy 2001;71:365–76.
[77] Sari A, Kaygusuz K. Thermal performance of palmitic acid as a phase change energy storage material. Energy Convers Manag 2002;43:863–76.
[78] Sarı A, Kaygusuz K. Thermal and heat transfer characteristics in a latent heat storage system using lauric acid. Energy Convers Manag 2002;43:2493–507.
[79] Kaygusuz ASK. Thermal energy storage system using Some fatty acids as latent heat energy storage materials. Energy Sources 2001;23:275–85. [2001/04/01].
[80] Sarı A, Kaygusuz K. Thermal performance of myristic acid as a phase change material for energy storage application. Renew Energy 2001;24:303–17.
[81] Khillarkar DB, Gong ZX, Mujumdar AS. Melting of a phase change material in concentric horizontal annuli of arbitrary cross-section. Appl Therm Eng 2000;20:893–912.
[82] Shmueli H, Ziskind G, Letan R. Melting in a vertical cylindrical tube: numerical investigation and comparison with experiments. Int J Heat Mass Transf 2010;53:4082–91.
[83] Jones BJ, Sun D, Krishnan S, Garimella SV. Experimental and numerical study of melting in a cylinder. Int J Heat Mass Transf 2006;49:2724–38.
[84] Fang Y, Niu J, Deng S. Numerical analysis for maximizing effective energy storage capacity of thermal energy storage systems by enhancing heat transfer in PCM. Energy Build 2018;160:10–8. [2018/02/01/].
[85] Regin AF, Solanki SC, Saini JS. Latent heat thermal energy storage using cylindrical capsule: numerical and experimental investigations. Renew Energy 2006;31:2025–41.
[86] Sun D, Annapragada SR, Garimella SV. Experimental and numerical study of melting of particle-laden materials in a cylinder. Int J Heat Mass Transf 2009;52:2966–78.
[87] Zhang Y, Faghri A. Semi-analytical solution of thermal energy storage system with conjugate laminar forced convection. Int J Heat Mass Transf 1996;39:717–24.
[88] Zhang Y, Faghri A. Heat transfer enhancement in latent heat thermal energy storage system by using an external radial finned tube. J Enhanc Heat Transf 1996;3:119–27.
[89] Pahamli Y, Hosseini MJ, Ranjbar AA, Bahrampoury R. Inner pipe downward movement effect on melting of PCM in a double pipe heat exchanger. Appl Math Comput 2018;316:30–42. [2018/01/01/].
[90] Hosseini MJ, Ranjbar AA, Sedighi K, Rahimi M. A combined experimental and computational study on the melting behavior of a medium temperature phase change storage material inside shell and tube heat exchanger. IntCommun Heat Mass Transf 2012;39:1416–24. [2012/11/01/].
[91] Cabeza LF, Ibáñez M, Solé C, Roca J, Nogués M. Experimentation with a water tank including a PCM module. Sol Energy Mater Sol Cells 2006;90:1273–82.
[92] Wu YK, Lacroix M. Melting of a PCM inside a vertical cylindrical capsule. Int J Numer Methods Fluids 1995;20:559–72.
[93] Wu YK. Numerical studies of melting process in a cylindrical enclosure [Ph.D.]. École Polytechnique de Montréal; 1990.
[94] Prud'homme M, Nguyen TH, Wu YK. Simulation numérique de la fusion à l'intérieur d'un cylindre adiabatique chauffé par le bas. Int J Heat Mass Transf 1991;34:2275–86.
[95] Wu YK, Prud'homme M, Nguyen TH. Étude numérique de la fusion autour d'un cylindre vertical soumis à deux types de conditions limites. Int J Heat Mass Transf 1989;32:1927–38.
[96] Rieger H, Beer H. The melting process of ice inside a horizontal cylinder: effects of density anomaly. J Heat Transf 1986;108:166–73.
[97] Rieger H, Projahn U, Bareiss M, Beer H. Heat transfer during melting inside a horizontal tube. J Heat Transf 1983;105:226–34.
[98] Tay NHS, Belusko M, Bruno F. Experimental investigation of tubes in a phase change thermal energy storage system. Appl Energy 2012;90:288–97.
[99] Tay NHS, Bruno F, Belusko M. Experimental validation of a CFD model for tubes in a phase change thermal energy storage system. Int J Heat Mass Transf 2012;55:574–85.
[100] Saraswat A, Bhattacharjee R, Verma A, Das MK, Khandekar S. Investigation of diffusional transport of heat and its enhancement in phase-change thermal energy storage systems. Appl Therm Eng 2017;111:1611–21. [2017/01/25/].
[101] Saitoh T, Hirose K. High rayleigh number solutions to problems of latent heat thermal energy storage in a horizontal cylinder capsule. J Heat Transf 1982;104:545–53.
[102] Pannu J, Joglekar G, Rice PA. Natural convection heat transfer to cylinders of phase change material used for thermal storage. Am Inst Chem Eng 1980;76:47–55.
[103] Sparrow EM, Broadbent JA. Inward melting in a vertical tube which allows free expansion of the phase-change medium. J Heat Transf 1982;104:309–15.
[104] Fukai J, Kanou M, Kodama Y, Miyatake O. Thermal conductivity enhancement of energy storage media using carbon fibers. Energy Convers Manag 2000;41:1543–56.
[105] Fukai J, Hamada Y, Morozumi Y, Miyatake O. Effect of carbon-fiber brushes on conductive heat transfer in phase change materials. Int J Heat Mass Transf 2002;45:4781–92.
[106] Fukai J, Hamada Y, Morozumi Y, Miyatake O. Improvement of thermal characteristics of latent heat thermal energy storage units using carbon-fiber brushes: experiments and modeling. Int J Heat Mass Transf 2003;46:4513–25.
[107] Hamada Y, Ohtsu W, Fukai J. Thermal response in thermal energy storage material around heat transfer tubes: effect of additives on heat transfer rates. Sol Energy 2003;75:317–28.
[108] Trp A. "A numerical and experimental study of transient heat transfer in a shell-

and-tube latent heat storage unit with paraffin as a phase change material," presented at the Energy and the Environment; 2002.
[109] Trp A. An experimental and numerical investigation of heat transfer during technical grade paraffin melting and solidification in a shell-and-tube latent thermal energy storage unit. Sol Energy 2005;79:648–60.
[110] Trp A, Lenic K, Frankovic B. Analysis of the influence of operating conditions and geometric parameters on heat transfer in water-paraffin shell-and-tube latent thermal energy storage unit. Appl Therm Eng 2006;26:1830–9.
[111] Gasia J, Tay NHS, Belusko M, Cabeza LF, Bruno F. Experimental investigation of the effect of dynamic melting in a cylindrical shell-and-tube heat exchanger using water as PCM [2017/01/01/]. Appl Energy 2017;185:136–45. [2017/01/01/].
[112] Lacroix M. Numerical simulation of a shell-and-tube latent heat thermal energy storage unit. Sol Energy 1993;50:357–67.
[113] Morcos VH. Investigation of a latent heat thermal energy storage system. Sol amp; Wind Technol 1990;7:197–202.
[114] Ezan MA, Ozdogan M, Erek A. Experimental study on charging and discharging periods of water in a latent heat storage unit. Int J Therm Sci 2011;50:2205–19.
[115] Jin X, Hu H, Shi X, Zhou X, Yang L, Yin Y, et al. A new heat transfer model of phase change material based on energy asymmetry. Appl Energy 2018;212:1409–16. [2018/02/15/].
[116] Akgün M, Aydın O, Kaygusuz K. Experimental study on melting/solidification characteristics of a paraffin as PCM. Energy Convers Manag 2007;48:669–78.
[117] Akgün M, Aydın O, Kaygusuz K. Thermal energy storage performance of paraffin in a novel tube-in-shell system. Appl Therm Eng 2008;28:405–13.
[118] Lu J, Ding J, Yang J. Solidification and melting behaviors and characteristics of molten salt in cold filling pipe. Int J Heat Mass Transf 2010;53:1628–35.
[119] Hasan A. Phase change material energy storage system employing palmitic acid. Sol Energy 1994;52:143–54.
[120] Yang M, Tao WQ. Numerical study of natural convection heat transfer in a cylindrical envelope with internal concentric slotted hollow cylinder. Numer Heat Transf, Part A: Appl 1992;22:289–305. [1992/10/01].
[121] Hendra R, Hamdani, Mahlia TMI, Masjuki HH. Thermal and melting heat transfer characteristics in a latent heat storage system using mikro. Appl Therm Eng 2005;25:1503–15.
[122] Ismail KAR, Gonçalves MM. Thermal performance of a pcm storage unit. Energy Convers Manag 1999;40:115–38.
[123] Castell A, Belusko M, Bruno F, Cabeza LF. Maximisation of heat transfer in a coil in tank PCM cold storage system. Appl Energy 2011;88:4120–7.
[124] Abdulateef AM, Mat S, Abdulateef J, Sopian K, Al-Abidi AA. Geometric and design parameters of fins employed for enhancing thermal energy storage systems: a review. Renew Sustain Energy Rev 2018.
[125] Liu Z, Sun X, Ma C. Experimental investigations on the characteristics of melting processes of stearic acid in an annulus and its thermal conductivity enhancement by fins. Energy Convers Manag 2005;46:959–69.
[126] Stritih U. An experimental study of enhanced heat transfer in rectangular PCM thermal storage. Int J Heat Mass Transf 2004;47:2841–7.
[127] Velraj R, Seeniraj RV, Hafner B, Faber C, Schwarzer K. Experimental analysis and numerical modelling of inward solidification on a finned vertical tube for a latent heat storage unit. Sol Energy 1997;60:281–90.
[128] Velraj R, Seeniraj RV, Hafner B, Faber C, Schwarzer K. Heat transfer enhancement in a latent heat storage system. Sol Energy 1999;65:171–80.
[129] Kayansayan N, Acar M Ali. Ice formation around a finned-tube heat exchanger for cold thermal energy storage. Int J Therm Sci 2006;45:405–18.
[130] Lacroix M. Study of the heat transfer behavior of a latent heat thermal energy storage unit with a finned tube. Int J Heat Mass Transf 1993;36:2083–92.
[131] Ismail KAR, Alves CLF, Modesto MS. Numerical and experimental study on the solidification of PCM around a vertical axially finned isothermal cylinder. Appl Therm Eng 2001;21:53–77.
[132] Zhang Y, Faghri A. Heat transfer enhancement in latent heat thermal energy storage system by using the internally finned tube. Int J Heat Mass Transf 1996;39:3165–73.
[133] Youssef W, Ge YT, Tassou SA. CFD modelling development and experimental validation of a phase change material (PCM) heat exchanger with spiral-wired tubes. Energy Convers Manag 2018;157:498–510. [2018/02/01/].
[134] Castell A, Solé C, Medrano M, Roca J, Cabeza LF, García D. Natural convection heat transfer coefficients in phase change material (PCM) modules with external vertical fins. Appl Therm Eng 2008;28:1676–86.
[135] Agyenim F, Eames P, Smyth M. A comparison of heat transfer enhancement in a medium temperature thermal energy storage heat exchanger using fins. Sol Energy 2009;83:1509–20.
[136] Abdulateef AM, Mat S, Sopian K, Abdulateef J, Gitan AA. Experimental and computational study of melting phase-change material in a triplex tube heat exchanger with longitudinal/triangular fins. Sol Energy 2017;155:142–53. [2017/10/01/].
[137] Shatikian V, Ziskind G, Letan R. Numerical investigation of a PCM-based heat sink with internal fins: constant heat flux. Int J Heat Mass Transf 2008;51:1488–93.
[138] Shatikian V, Ziskind G, Letan R. Numerical investigation of a PCM-based heat sink with internal fins. Int J Heat Mass Transf 2005;48:3689–706.
[139] Sparrow EM, Larson ED, Ramsey JW. Freezing on a finned tube for either conduction-controlled or natural-convection-controlled heat transfer. Int J Heat Mass Transf 1981;24:273–84.
[140] Ermis K, Erek A, Dincer I. Heat transfer analysis of phase change process in a finned-tube thermal energy storage system using artificial neural network. Int J Heat Mass Transf 2007;50:3163–75.
[141] Kazemi M, Hosseini MJ, Ranjbar AA, Bahrampoury R. Improvement of longitudinal fins configuration in latent heat storage systems. Renew Energy 2018;116:447–57. [2018/02/01/].
[142] Eftekhar J, Haji-Sheikh A, Lou DYS. Heat Transfer Enhancement in a Paraffin Wax Thermal Storage System. J Sol Energy Eng 1984;106:299–306.
[143] Bathelt AG, Viskanta R. Heat transfer at the solid-liquid interface during melting from a horizontal cylinder. Int J Heat Mass Transf 1980;23:1493–503.
[144] Padmanabhan PV, Murthy MV Krishna. Outward phase change in a cylindrical annulus with axial fins on the inner tube. Int J Heat Mass Transf 1986;29:1855–68.
[145] Tan L, Kwok Y, Date A, Akbarzadeh A. Numerical study of natural convection effects in latent heat storage using aluminum fins and spiral fillers. Int J Mech Aerosp Eng 2012;6:238–45.
[146] Agyenim F, Eames P, Smyth M. Experimental study on the melting and solidification behaviour of a medium temperature phase change storage material (Erythritol) system augmented with fins to power a LiBr/H_2O absorption cooling system. Renew Energy 2011;36:108–17.
[147] Choi JC, Kim SD. Heat transfer in a latent heat-storage system using MgCl2·6H2O at the melting point. Energy 1995;20:13–25.
[148] Abdulateef AM, Abdulateef J, Mat S, Sopian K, Elhub B, Mussa MA. Experimental and numerical study of solidifying phase-change material in a triplex-tube heat exchanger with longitudinal/triangular fins. Int Commun Heat Mass Transf 2018;90:73–84. [2018/01/01/].
[149] Ismail KAR, Lino FAM. Fins and turbulence promoters for heat transfer enhancement in latent heat storage systems. Exp Therm Fluid Sci 2011;35:1010–8.
[150] Saha SK, Dutta P. Heat transfer correlations for PCM-based heat sinks with plate fins. Appl Therm Eng 2010;30:2485–91.
[151] Pincemin S, Olives R, Py X, Christ M. Highly conductive composites made of phase change materials and graphite for thermal storage. Sol Energy Mater Sol Cells 2008;92:603–13.
[152] Zhao CY, Wu ZG. Heat transfer enhancement of high temperature thermal energy storage using metal foams and expanded graphite. Sol Energy Mater Sol Cells 2011;95:636–43.
[153] Py X, Olives R, Mauran S. Paraffin/porous-graphite-matrix composite as a high and constant power thermal storage material. Int J Heat Mass Transf 2001;44:2727–37.
[154] Zhang Z, Fang X. Study on paraffin/expanded graphite composite phase change thermal energy storage material. Energy Convers Manag 2006;47:303–10.
[155] Xiao M, Feng B, Gong K. Preparation and performance of shape stabilized phase change thermal storage materials with high thermal conductivity. Energy Convers Manag 2002;43:103–8.
[156] Sarı A, Karaipekli A. Thermal conductivity and latent heat thermal energy storage characteristics of paraffin/expanded graphite composite as phase change material. Appl Therm Eng 2007;27:1271–7.
[157] Karaipekli A, Sarı A, Kaygusuz K. Thermal conductivity improvement of stearic acid using expanded graphite and carbon fiber for energy storage applications. Renew Energy 2007;32:2201–10.
[158] Frusteri F, Leonardi V, Vasta S, Restuccia G. Thermal conductivity measurement of a PCM based storage system containing carbon fibers. Appl Therm Eng 2005;25:1623–33.
[159] Marín JM, Zalba B, Cabeza LF, Mehling H. Improvement of a thermal energy storage using plates with paraffin–graphite composite. Int J Heat Mass Transf 2005;48:2561–70.
[160] Sarı A. Form-stable paraffin/high density polyethylene composites as solid–liquid phase change material for thermal energy storage: preparation and thermal properties. Energy Convers Manag 2004;45:2033–42.
[161] Bansal NK, Buddhi D. An analytical study of a latent heat storage system in a cylinder. Energy Convers Manag 1992;33:235–42.
[162] Zhang Y, Ding J, Wang X, Yang R, Lin K. Influence of additives on thermal conductivity of shape-stabilized phase change material. Sol Energy Mater Sol Cells 2006;90:1692–702.
[163] Mills A, Farid M, Selman JR, Al-Hallaj S. Thermal conductivity enhancement of phase change materials using a graphite matrix. Appl Therm Eng 2006;26:1652–61.
[164] Han JH, Cho KW, Lee KH, Kim H. Porous graphite matrix for chemical heat pumps. Carbon 1998;36:1801–10.
[165] Bonnissel M, Luo L, Tondeur D. Compacted exfoliated natural graphite as heat conduction medium. Carbon 2001;39:2151–61.
[166] Mesalhy O, Lafdi K, Elgafy A, Bowman K. Numerical study for enhancing the thermal conductivity of phase change material (PCM) storage using high thermal conductivity porous matrix. Energy Convers Manag 2005;46:847–67.
[167] Hoogendoorn CJ, Bart GCJ. Performance and modelling of latent heat stores. Sol Energy 1992;48:53–8.
[168] Phanikumar MS, Mahajan RL. Non-Darcy natural convection in high porosity metal foams. Int J Heat Mass Transf 2002;45:3781–93.
[169] Beckermann C, Ramadhyani S, Viskanta R. Natural convection flow and heat transfer between a fluid layer and a porous layer inside a rectangular enclosure. J Heat Transf 1987;109:363–70.
[170] Sasaguchi K, Kusano K, Viskanta R. A numerical analysis of solid-liquid phase change heat transfer around a single and two horizontal, vertically spaced cylinders in a rectangular cavity. Int J Heat Mass Transf 1997;40:1343–54.
[171] Sasaguchi K, Kuwabara K, Kusano K, Kitagawa H. Transient cooling of water around a cylinder in a rectangular cavity—a numerical analysis of the effect of the position of the cylinder. Int J Heat Mass Transf 1998;41:3149–56.
[172] Bhattacharya A, Calmidi VV, Mahajan RL. Thermophysical properties of high porosity metal foams. Int J Heat Mass Transf 2002;45:1017–31.
[173] Boomsma K, Poulikakos D. On the effective thermal conductivity of a three-dimensionally structured fluid-saturated metal foam. Int J Heat Mass Transf 2001;44:827–36.

[174] Calmidi VV, Mahajan RL. The effective thermal conductivity of high porosity fibrous metal foams. J Heat Transf 1999;121:466–71.
[175] Calmidi VV, Mahajan RL. Forced convection in high porosity metal foams. J Heat Transf 2000;122:557–65.
[176] Hunt ML, Tien CL. Effects of thermal dispersion on forced convection in fibrous media. Int J Heat Mass Transf 1988;31:301–9.
[177] Erk HF, Dudukoviæ MP. Phase-change heat regenerators: modeling and experimental studies. AIChE J 1996;42:791–808.
[178] Weaver JA, Viskanta R. Freezing of water saturated porous media in a rectangular cavity. J Int Commun Heat Mass Transf 1986;13(3):245–52.
[179] Beckermann C, Viskanta R. Natural convection solid/liquid phase change in porous media. Int J Heat Mass Transf 1988;31:35–46.
[180] Ji C, Qin Z, Low Z, Dubey S, Choo FH, Duan F. Non-uniform heat transfer suppression to enhance PCM melting by angled fins. Appl Therm Eng 2018;129:269–79. [2018/01/25/].
[181] Lu W, Zhao CY, Tassou SA. Thermal analysis on metal-foam filled heat exchangers. Part I: metal-foam filled pipes. Int J Heat Mass Transf 2006;49:2751–61.
[182] Zhao CY, Lu W, Tassou SA. Thermal analysis on metal-foam filled heat exchangers. Part II: tube heat exchangers. Int J Heat Mass Transf 2006;49:2762–70.
[183] Zhao CY, Lu W, Tian Y. Heat transfer enhancement for thermal energy storage using metal foams embedded within phase change materials (PCMs). Sol Energy 2010;84:1402–12.
[184] Wu ZG, Zhao CY. Experimental investigations of porous materials in high temperature thermal energy storage systems. Sol Energy 2011;85:1371–80.
[185] Tian YY, Zhao C-Y. Heat transfer analysis for phase change materials (PCMs),In: Proceedings of the 11th international conference on energy storage (Effstock 2009), Stockholm, Sweden; 2009.
[186] Tian YY, Zhao C-Y. Numerical investigation of heat transfer in phase change materials using non-equilibrium model, Proceedings of the 11th UK national heat transfer conference, London, UK; 2009.
[187] Kramer CM, Wilson CJ. The phase diagram of NaNO3–KNO3. Thermochim Acta 1980;42:253–64.
[188] Rogers DJ, Janz GJ. Melting-crystallization and premelting properties of sodium nitrate-potassium nitrate. enthalpies and heat capacities. J Chem Eng Data 1982;27:424–8. [1982/10/01].
[189] Haillot D, Py X, Goetz V, Benabdelkarim M. Storage composites for the optimisation of solar water heating systems. Chem Eng Res Des 2008;86:612–7.
[190] Yin H, Gao X, Ding J, Zhang Z. Experimental research on heat transfer mechanism of heat sink with composite phase change materials. Energy Convers Manag 2008;49:1740–6.
[191] Siahpush A, O'Brien J, Crepeau J. Phase change heat transfer enhancement using copper porous foam. J Heat Transf 2008;130. [pp. 082301-11].
[192] Zhao CY, Kim T, Lu TJ, Hodson HP. Thermal transport in high porosity cellular metal foams. J Thermophys Heat Transf 2004;18:309–17. [2004/07/01].
[193] Krishnan S, Murthy JY, Garimella SV. A two-temperature model for solid-liquid phase change in metal foams. J Heat Transf 2005;127:995–1004.
[194] Krishnan S, Murthy J Y, Garimella S V. A two-temperature model for solid/liquid phase change in metal foams, In: Proceedings of the ASME conference, 2004, pp. 609–619.
[195] Tong X, Khan JA, RuhulAmin M. Enhancement of heat transfer by inserting a metal matrix into a phase change material. Numer Heat Transf, Part A: Appl 1996;30:125–41. [1996/08/01].
[196] Sparrow EM, Patankar SV, Ramadhyani S. Analysis of melting in the presence of natural convection in the melt region. J Heat Transf 1977;99:520–6.
[197] Lin DS, Nansteel MW. Natural convection in a vertical annulus containing water near the density maximum. J Heat Transf 1987;109:899–905.
[198] Charn-Jung K, Sung Tack R, Sik L Joon. An efficient computational technique to solve the moving boundary problems in the axisymmetric geometries. Int J Heat Mass Transf 1993;36:3759–64.
[199] Ettouney HM, Alatiqi I, Al-Sahali M, Ahmad Al-Ali S. Heat transfer enhancement by metal screens and metal spheres in phase change energy storage systems. Renew Energy 2004;29:841–60.
[200] Ho CJ, Gao JY. Preparation and thermophysical properties of nanoparticle-in-paraffin emulsion as phase change material. Int Commun Heat Mass Transf 2009;36:467–70.
[201] Humphries WR, Griggs EI. A design for phase change thermal control and energy storage devices. USA: National Aeronautics and Space Administration (NASA); 1977.
[202] Wu S, Zhu D, Zhang X, Huang J. Preparation and melting/freezing characteristics of Cu/paraffin nanofluid as phase-change material (PCM). Energy Fuels 2010;24:1894–8. [2010/03/18].
[203] Zeng J, Sun L, Xu F, Tan Z, Zhang Z, Zhang J, et al. Study of a PCM based energy storage system containing Ag nanoparticles. J Therm Anal Calorim 2007;87:371–5.
[204] Arasu AV, Sasmito AP, Mujumdar AS. Numerical performance study of paraffin wax dispersed with alumina in a concentric pipe latent heat storage system. Therm Sci 2012;2012. [*OnLine, pp.* 4-4].
[205] Arasu AV, Mujumdar AS. Numerical study on melting of paraffin wax with Al_2O_3 in a square enclosure. Int Commun Heat Mass Transf 2012;39:8–16.
[206] Arasu AV, Sasmito AP, Mujumdar AS. Thermal performance enhancement of paraffin wax with AL2O3 and CuO nanoparticles – a numerical study. Front Heat Mass Transf (FHMT) 2011.
[207] Khodadadi JM, Fan L. Expedited freezing of nanoparticle-Enhanced phase change materials (NEPCM) exhibited Through a simple 1-D Stefan problem formulation. ASME Conf Proc 2009;2009:345–51.
[208] Fan L, Khodadadi JM. Experimental verification of expedited freezing of nanoparticle-enhanced phase change materials (NEPCM), In: Proceedings of the ASME conference, vol. 2011, 2011, pp. T10221-T10221-7.
[209] Khodadadi JM, Hosseinizadeh SF. Nanoparticle-enhanced phase change materials (NEPCM) with great potential for improved thermal energy storage. Int Commun Heat Mass Transf 2007;34:534–43.
[210] Khanafer K, Vafai K, Lightstone M. Buoyancy-driven heat transfer enhancement in a two-dimensional enclosure utilizing nanofluids. Int J Heat Mass Transf 2003;46:3639–53.
[211] Brent AD, Voller VR, Reid KJ. Enthalpy-porosity technique for modeling convection-diffusion phase change: application to the melting of a pure metal. Numer Heat Transf 1988;13:297–318. [1988/04/01].
[212] Gau C, Viskanta R. Melting and solidification of a pure metal on a vertical wall. J Heat Transf 1986;108:174–81.
[213] Banaszek YJTAKMRJ. Semi-implicit FEM analysis of natural convection in freezing water. Numer Heat Transf, Part A: Appl 1999;36:449–72. [1999/10/01].
[214] Ranjbar AA, Kashani S, Hosseinizadeh SF, Ghanbarpour M. Numerical heat transfer studies of a latent heat storage system containing nano-enhanced phase change material. Therm Sci 2011;15:169–81.
[215] Kim S, Drzal LT. High latent heat storage and high thermal conductive phase change materials using exfoliated graphite nanoplatelets. Sol Energy Mater Sol Cells 2009;93:136–42.
[216] Liu Y-D, Zhou Y-G, Tong M-W, Zhou X-S. Experimental study of thermal conductivity and phase change performance of nanofluids PCMs. Microfluid Nanofluid 2009;7:579–84. [2009/10/01].
[217] Wang B-X, Zhou L-P, Peng X-F. A fractal model for predicting the effective thermal conductivity of liquid with suspension of nanoparticles. Int J Heat Mass Transf 2003;46:2665–72.
[218] Zhou LP, Wang BX. Experimental research on the thermophysical properties of nanoparticle suspensions using the quasi-steady state method. Ann Proc Chin Eng Thermophys 2002:889–92.
[219] Seeniraj RV, Velraj R, Narasimhan NL. Heat transfer enhancement study of a lhts unit containing dispersed high conductivity particles. J Sol Energy Eng 2002;124:243–9.
[220] Siegel R. Solidification of low conductivity material containing dispersed high conductivity particles. Int J Heat Mass Transf 1977;20:1087–9.
[221] Wang X, Xu X, Choi SUS. Thermal conductivity of nanoparticle - fluid mixture. J Thermophys Heat Transf 1999;13:474–80. [1999/10/01].
[222] Maxwell JC. Electricity and magnetism, Part II. 3 ed. Clarendon: Oxford; 1904.
[223] Jeffrey DJ. Conduction through a random suspension of spheres. Proc R Soc Lond 1973;335:355–67. [November 27, 1973].
[224] Davis RH. The effective thermal conductivity of a composite material with spherical inclusions [1986/05/01]. Int J Thermophys 1986;7:609–20. [1986/05/01].
[225] Lu S, Yuan x, Lin H, Chi. Effective conductivity of composites containing aligned spheroidal inclusions of finite conductivity. J Appl Phys 1996;79:6761–9.
[226] Bonnecaze RT, Brady JF. A method for determining the effective conductivity of dispersions of particles. Proc R Soc Lond 1990;430:285–313. [August 1990].
[227] Bonnecaze RT, Brady JF. The effective conductivity of random suspensions of spherical particles. Proc R Soc Lond 1991;432:445–65. [March 1991].
[228] Shaikh S, Lafdi K, Hallinan K. Carbon nanoadditives to enhance latent energy storage of phase change materials. J Appl Phys 2008;103. [pp. 094302-094302-6].
[229] Liu L, Su D, Tang Y, Fang G. Thermal conductivity enhancement of phase change materials for thermal energy storage: a review. Renew Sustain Energy Rev 2016;62:305–17. [2016/09/01/].
[230] Karaipekli A, Biçer A, Sarı A, Tyagi VV. Thermal characteristics of expanded perlite/paraffin composite phase change material with enhanced thermal conductivity using carbon nanotubes. Energy Convers Manag 2017;134:373–81. [2017/02/15/].
[231] Ding Y, Chen H, Wang L, Yang C, He Y, Yang W, et al. Heat transfer intensification using nanofluids. Kona-Powder Part 2007;25:23–38.
[232] Minea AA. Challenges in hybrid nanofluids behavior in turbulent flow: recent research and numerical comparison. Renew Sustain Energy Rev 2017;71:426–34. [2017/05/01/].
[233] Godson L, Raja B, Mohan Lal D, Wongwises S. Enhancement of heat transfer using nanofluids—An overview. Renew Sustain Energy Rev 2010;14:629–41.
[234] Trisaksri V, Wongwises S. Critical review of heat transfer characteristics of nanofluids. Renew Sustain Energy Rev 2007;11:512–23.
[235] Ho CJ, Chen MW, Li ZW. Numerical simulation of natural convection of nanofluid in a square enclosure: effects due to uncertainties of viscosity and thermal conductivity. Int J Heat Mass Transf 2008;51:4506–16.
[236] Vajjha RS, Das DK, Mahagaonkar BM. Density measurement of different nanofluids and their comparison with theory. Pet Sci Technol 2009;27:612–24.
[237] Pak BC, Cho YI. Hydrodynamic and heat transfer study of dispersed fluids with submicron metallic oxide particles. Exp Heat Transf 1998;11:151–70. [1998/04/01].
[238] Vajjha RS, Das DK. Experimental determination of thermal conductivity of three nanofluids and development of new correlations. Int J Heat Mass Transf 2009;52:4675–82.
[239] Bruggeman DAG. Berechnung verschiedener physikalischer Konstanten von heterogenen Substanzen. I. Dielektrizitätskonstanten und Leitfähigkeiten der Mischkörper aus isotropen Substanzen. Ann der Phys 1935;416:636–64.
[240] Yu W, Choi SUS. The role of interfacial layers in the Enhanced thermal conductivity of nanofluids: a Renovated Maxwell model. J Nanopart Res 2003;5:167–71. [2003/04/01].
[241] Xuan Y, Li Q, Hu W. Aggregation structure and thermal conductivity of nanofluids. AIChE J 2003;49:1038–43.
[242] Koo J, Kleinstreuer C. A new thermal conductivity model for nanofluids. J

Nanopart Res 2004;6:577–88. [2004/12/01].
[243] Koo J, Kleinstreuer C. Laminar nanofluid flow in microheat-sinks. Int J Heat Mass Transf 2005;48:2652–61.
[244] Xue Q, Xu W-M. A model of thermal conductivity of nanofluids with interfacial shells. Mater Chem Phys 2005;90:298–301.
[245] Chon CH, Kihm KD, Lee SP, Choi SUS. Empirical correlation finding the role of temperature and particle size for nanofluid (Al[sub 2]O[sub 3]) thermal conductivity enhancement. Appl Phys Lett 2005;87:153107–17.
[246] Prasher R, Bhattacharya P, Phelan PE. Brownian-motion-based convective-conductive model for the effective thermal conductivity of nanofluids. J Heat Transf 2006;128:588–95.
[247] Jang SP, Choi SUS. Effects of various parameters on nanofluid thermal conductivity. J Heat Transf 2007;129:617–23.
[248] Vajjha RS, Das DK, Namburu PK. Numerical study of fluid dynamic and heat transfer performance of Al_2O_3 and CuO nanofluids in the flat tubes of a radiator. Int J Heat Fluid Flow 2010;31:613–21.
[249] Barakos G, Mitsoulis E, Assimacopoulos D. Natural convection flow in a square cavity revisited: laminar and turbulent models with wall functions. Int J Numer Methods Fluids 1994;18:695–719.
[250] Markatos NC, Pericleous KA. Laminar and turbulent natural convection in an enclosed cavity. Int J Heat Mass Transf 1984;27:755–72.
[251] Davis G De Vahl. Natural convection of air in a square cavity: a bench mark numerical solution. Int J Numer Methods Fluids 1983;3:249–64.
[252] Fusegi T, Hyun JM, Kuwahara K, Farouk B. A numerical study of three-dimensional natural convection in a differentially heated cubical enclosure. Int J Heat Mass Transf 1991;34:1543–57.
[253] Li Q, Xuan Y. Convective heat transfer and flow characteristics of Cu-water nanofluid. Sci China Ser E: Technol Sci 2002;45:408–16. [2002/08/01].
[254] Abd. K Abdulhassan, Al-Jabair Sattar, Sultan K. Experimental investigation of heat transfer and flow of nano fluids in horizontal circular tube. Int J Mech Aerosp Eng 2012;6.
[255] Batchelor GK. The effect of Brownian motion on the bulk stress in a suspension of spherical particles. J Fluid Mech 1977;83:97–117.
[256] Hamilton RL, Crosser OK. Thermal conductivity of heterogeneous two-component systems. Ind Eng Chem Fundam 1962;1:187–91. [1962/08/01].
[257] Timofeeva EV, Gavrilov AN, McCloskey JM, Tolmachev YV, Sprunt S, Lopatina LM, et al. Thermal conductivity and particle agglomeration in alumina nanofluids: experiment and theory. Phys Rev E 2007;76:061203.
[258] Xuan Y, Roetzel W. Conceptions for heat transfer correlation of nanofluids. Int J Heat Mass Transf 2000;43:3701–7.
[259] Gavtash B, Hussain K, Layeghi M, Lafmejani SS. Numerical simulation of the effects of nanofluid on a heat pipe thermal performance. Int J Mech Aerosp Eng 2012;6.
[260] Maïga SEB, Nguyen CT, Galanis N, Roy G. "Heat transfer enhancement in forced convection laminar tube flow by using nanofluids," In: Proceedings of international symposium on advances in computational heat transfer III, vol. Paper CHT-040101, 2004, p. 24.
[261] Syam Sundar L, Sharma KV, Parveen S, Gaffar MA. Laminar convective heat transfer of nanofluids in a circular tube under constant heat flux. Int J Nanopart 2009;2:314–20.
[262] Sasmito AP, Kurnia JC, Mujumdar AS. Numerical evaluation of laminar heat transfer enhancement in nanofluid flow in coiled square tubes. Nanoscale Res Lett 2011;6:376.
[263] Wen D, Ding Y. Experimental investigation into convective heat transfer of nanofluids at the entrance region under laminar flow conditions. Int J Heat Mass Transf 2004;47:5181–8.
[264] Mahdi JM, Nsofor EC. Solidification enhancement of PCM in a triplex-tube thermal energy storage system with nanoparticles and fins. Appl Energy 2018;211:975–86. [2018/02/01/].
[265] Namburu PK, Das DK, Tanguturi KM, Vajjha RS. Numerical study of turbulent flow and heat transfer characteristics of nanofluids considering variable properties. Int J Therm Sci 2009;48:290–302.
[266] Gnielinski V. New equations for heat and mass transfer in turbulent pipe and channel flow. Int Chem Eng 1976;16:359–68.
[267] Brinkman HC. The viscosity of concentrated suspensions and solutions. J Chem Phys 1952;20:571.
[268]. "2009 ASHRAE Handbook - Fundamentals (I-P Edition),"ed: American Society of Heating, Refrigerating and Air-Conditioning Engineers, Inc.
[269] Namburu PK, Kulkarni DP, Misra D, Das DK. Viscosity of copper oxide nanoparticles dispersed in ethylene glycol and water mixture. Exp Therm Fluid Sci 2007;32:397–402.
[270] Sahoo BC, Vajjha RS, Ganguli R, Chukwu GA, Das DK. Determination of rheological behavior of aluminum oxide nanofluid and development of new viscosity correlations. Pet Sci Technol 2009;27:1757–70. [2009/10/21].
[271] Charunyakorn P, Sengupta S, Roy SK. Forced convection heat transfer in microencapsulated phase change material slurries: flow in circular ducts. Int J Heat Mass Transf 1991;34:819–33.
[272] Keblinski P, Phillpot SR, Choi SUS, Eastman JA. Mechanisms of heat flow in suspensions of nano-sized particles (nanofluids). Int J Heat Mass Transf 2002;45:855–63.
[273] Jegadheeswaran S, Pohekar SD. Performance enhancement in latent heat thermal storage system: a review. Renew Sustain Energy Rev 2009;13:2225–44.
[274] Hawlader MNA, Uddin MS, Khin MM. Microencapsulated PCM thermal-energy storage system. Appl Energy 2003;74:195–202.
[275] Chen B, Wang X, Zeng R, Zhang Y, Wang X, Niu J, et al. An experimental study of convective heat transfer with microencapsulated phase change material suspension: laminar flow in a circular tube under constant heat flux. Exp Therm Fluid Sci 2008;32:1638–46.
[276] Alkan C, Sarı A, Karaipekli A, Uzun O. Preparation, characterization, and thermal properties of microencapsulated phase change material for thermal energy storage. Sol Energy Mater Sol Cells 2009;93:143–7.
[277] Cho J-S, Kwon A, Cho C-G. Microencapsulation of octadecane as a phase-change material by interfacial polymerization in an emulsion system. Colloid Polym Sci 2002;280:260–6. [2002/03/01].
[278] Bayés-García L, Ventolà L, Cordobilla R, Benages R, Calvet T, Cuevas-Diarte MA. Phase Change Materials (PCM) microcapsules with different shell compositions: preparation, characterization and thermal stability. Sol Energy Mater Sol Cells 2010;94:1235–40.
[279] Xuan Y, Huang Y, Li Q. Experimental investigation on thermal conductivity and specific heat capacity of magnetic microencapsulated phase change material suspension. Chem Phys Lett 2009;479:264–9.
[280] Salaün F, Devaux E, Bourbigot S, Rumeau P, Chapuis P-O, Saha SK, et al. Polymer nanoparticles to decrease thermal conductivity of phase change materials. Thermochim Acta 2008;477:25–31.
[281] Hu X, Zhang Y. Novel insight and numerical analysis of convective heat transfer enhancement with microencapsulated phase change material slurries: laminar flow in a circular tube with constant heat flux. Int J Heat Mass Transf 2002;45:3163–72.
[282] Goel M, Roy SK, Sengupta S. Laminar forced convection heat transfer in microcapsulated phase change material suspensions. Int J Heat Mass Transf 1994;37:593–604.
[283] Zhang Y, Hu X, Wang X. Theoretical analysis of convective heat transfer enhancement of microencapsulated phase change material slurries. Heat Mass Transf 2003;40:59–66. [2003/12/01].
[284] Alisetti EL, Roy SK. Forced convection heat transfer to phase change material slurries in circular ducts. *Journal Thermophys Heat Transf* 2000;14:115–8. [2000/01/01].
[285] Alvarado JL, Marsh C, Sohn C, Phetteplace G, Newell T. Thermal performance of microencapsulated phase change material slurry in turbulent flow under constant heat flux. Int J Heat Mass Transf 2007;50:1938–52.
[286] Su J-F, Wang X-Y, Huang Z, Zhao Y-H, Yuan X-Y. Thermal conductivity of microPCMs-filled epoxy matrix composites [2011/09/01]. *Colloid Polym Sci* 2011;289:1535–42. [2011/09/01].
[287] Özonur Y, Mazman M, Paksoy HÖ, Evliya H. Microencapsulation of coco fatty acid mixture for thermal energy storage with phase change material. Int J Energy Res 2006;30:741–9.
[288] Rao Y, Dammel F, Stephan P, Lin G. Convective heat transfer characteristics of microencapsulated phase change material suspensions in minichannels [2007/12/01]. Heat Mass Transf 2007;44:175–86. [2007/12/01].
[289] Brown RC, Rasberry JD, Overmann SP. Microencapsulated phase-change materials as heat transfer media in gas-fluidized beds. Powder Technol 1998;98:217–22.
[290] Sarı A, Karaipekli A. Preparation, thermal properties and thermal reliability of capric acid/expanded perlite composite for thermal energy storage. Mater Chem Phys 2008;109:459–64.
[291] Karaipekli A, Sarı A. Capric–myristic acid/expanded perlite composite as form-stable phase change material for latent heat thermal energy storage. Renew Energy 2008;33:2599–605.
[292] Sarı A, Karaipekli A, Alkan C. Preparation, characterization and thermal properties of lauric acid/expanded perlite as novel form-stable composite phase change material. Chem Eng J 2009;155:899–904.
[293] Wang J, Xie H, Xin Z. Thermal properties of paraffin based composites containing multi-walled carbon nanotubes. Thermochim Acta 2009;488:39–42.
[294] Karaipekli A, Sarı A. Capric–myristic acid/vermiculite composite as form-stable phase change material for thermal energy storage. Sol Energy 2009;83:323–32.
[295] Putnam SA, Cahill DG, Ash BJ, Schadler LS. High-precision thermal conductivity measurements as a probe of polymer/nanoparticle interfaces. J Appl Phys 2003;94:6785–8.
[296] Halte V, Bigot J-Y, Palpant B, Broyer M, Prevel B, Perez A. Size dependence of the energy relaxation in silver nanoparticles embedded in dielectric matrices. Appl Phys Lett 1999;75:3799–801.
[297] Elgafy A, Lafdi K. Effect of carbon nanofiber additives on thermal behavior of phase change materials. Carbon 2005;43:3067–74.
[298] Zeng JL, Cao Z, Yang DW, Xu F, Sun LX, Zhang XF, et al. Effects of MWNTs on phase change enthalpy and thermal conductivity of a solid-liquid organic PCM. J Therm Anal Calorim 2009;95:507–12. [2009/02/01].
[299] Zeng JL, Cao Z, Yang DW, Sun LX, Zhang L. Thermal conductivity enhancement of Ag nanowires on an organic phase change material. J Therm Anal Calorim 2010;101:385–9. [2010/07/01].
[300] Wu S, Zhu D, Li X, Li H, Lei J. Thermal energy storage behavior of Al_2O_3–H_2O nanofluids. Thermochim Acta 2009;483:73–7.
[301] Liu YD. Study On preparation and thermal properties of phase change nanocomposites for cool storage [Ph.D.]. Engineering & Technology, Chongqing University, China; 2005.
[302] Alvarado JL, Marsh C, Sohn C, Vilceus M, Hock V, Phetteplace G, et al. Characterization of supercooling suppression of microencapsulated phase change material by using DSC. J Therm Anal Calorim 2006;86:505–9. [2006/11/01].
[303] Eckert ERG, Drake Jr RM. Analysis of heat and mass transfer. New York: USA Hemisphere Publishing, New York, NY; 1972.
[304] Shah RK. Thermal entry lrnght solution for the circular tube and parallel plates, In: Proceedings of the 3rd national heat and mass transfer conference III, Bombay, 1975, pp. 314–320.
[305] Anoop KB, Sundararajan T, Das SK. Effect of particle size on the convective heat

transfer in nanofluid in the developing region. Int J Heat Mass Transf 2009;52:2189–95.
[306] Wang X-j, Li X, Yang S. Influence of pH and SDBS on the stability and thermal conductivity of nanofluids. Energy Fuels 2009;23:2684–9. [2009/05/21].
[307] Bönnemann H, Botha SS, Bladergroen B, Linkov VM. Monodisperse copper- and silver-nanocolloids suitable for heat-conductive fluids. Appl Organomet Chem 2005;19:768–73.
[308] Gao JW, Zheng RT, Ohtani H, Zhu DS, Chen G. Experimental investigation of heat conduction mechanisms in nanofluids. clue on clustering [2009/12/09]. Nano Lett 2009;9:4128–32. [2009/12/09].
[309] Chein R, Huang G. Analysis of microchannel heat sink performance using nanofluids. Appl Therm Eng 2005;25:3104–14.
[310] Lee S, Choi SUS. Application of metallic nanoparticle suspensions in advanced cooling systems, In: Proceedings of recent advances in solids/structures and application of metallic materials; 1996.